# UNIVERSITÉ DE FRANCHE-COMTÉ
## ÉCOLE DOCTORALE « LOUIS PASTEUR »

A dissertation submitted in partial fulfilment of the requirements for the Ph.D. degree in
**CHEMISTRY**

# SPACE RADIATION-INDUCED BYSTANDER EFFECT: KINETICS OF BIOLOGIC RESPONSES, MECHANISMS, AND SIGNIFICANCE OF SECONDARY RADIATIONS

by

**Géraldine GONON**

12 December, 2011

**Mentors**

| | |
|---|---|
| Michel Fromm | Professor, Laboratoire de Chimie Physique et Rayonnements Alain Chambaudet, Unité Mixte de Recherche (UMR)- Commissariat à l'Énergie Atomique (CEA) E4, Université de Franche-Comté, Besançon, France |
| Edouard I. Azzam | Professor, Department of Radiology, Division of Radiation Research, University of Medicine and Dentistry of New Jersey, New Jersey Medical School, Cancer Center, Newark, NJ, USA |

**Referees**

| | |
|---|---|
| Jaime F. Angulo-Mora | Research Manager, Laboratoire de RadioToxicologie, CEA, Direction des Sciences du Vivant, Bruyères-le-Châtel, France |
| Nicolas Foray | Research Manager, Institut National de la Santé et de la Recherche Médicale (INSERM) CR-U1052, Centre de Recherche en Cancérologie de Lyon, Groupe de Radiobiologie, France |

**Examiners**

| | |
|---|---|
| Roger W. Howell | Professor, Department of Radiology, Division of Radiation Research, University of Medicine and Dentistry of New Jersey, New Jersey Medical School, Cancer Center, Newark, NJ, USA |
| Jean-Emmanuel Groetz | Maître de Conférence, Laboratoire de Chimie Physique et Rayonnements Alain Chambaudet, UMR-CEA E4, Université de Franche-Comté, Besançon, France |
| Hicham Khodja | Research Engineer, Laboratoire d'Étude des Éléments Légers, UMR 3299-CEA/Centre National de la Recherche Scientifique (CNRS), Gif-sur-Yvette, France |

*To Laurent and Théophile*

*To my parents and grandparents*

# ACKNOLEDGEMENTS

I also thank Peter Guida and his NASA Space Radiation Laboratory team for their support during the experiments. I am grateful to Drs. Adam Rusek, Michael Sivertz, I-Hung-Chang for their help in dosimetry. I also thank Gary Moss from Track Analysis Systems Ltd for his involvement in the development of cell culture dishes with the CR-39.

I also express my full sympathy to all members or ex-members of the laboratory Sylvain Gaillard, Mironel Enescu, Manuel Grivet, Christelle Brun-Bergeon, Sarah Foley, Christopher Mavon, Franck Berger, and Jean-Baptiste Sanchez.

I thank all of my friends Céline, Géraldine, Amélie, Stéphanie, Cécilia, Yacine, Annaïg, Charlotte, Sylvie, Hillary… ... for their sincere friendship and encouragement.

I would also like to thank my family, for their constant support and love throughout my studies and my PhD. To my parents, who brought me into this world and who gave me the desire to always move forward, along with their beautiful model of perseverance. I thank my sister Charlotte and my brothers Thomas and Clovis for their encouragement. To Laurent, my other half, who has always supported me and who accompanied me on this journey to the other side of the Atlantic. The questioning, the misunderstanding, and the laughs! We returned with a "mini-us" named Théophile, love of our life...

Finally, thank you to everyone that I have not mentioned here who will recognize themselves in these lines.

# REMERCIEMENTS

# ABSTRACT

Widespread evidence indicates that exposure of cell cultures to α particles results in significant biological changes in both the irradiated and non-irradiated *bystander* cells in the population. The induction of non-targeted biological responses in cell cultures exposed to low fluences of high charge (Z) and high energy (E) particles is relevant to estimates of the health risks of space radiation and to radiotherapy. Here, we investigated the mechanisms underlying the induction of stressful effects in confluent normal human fibroblast cultures exposed to low fluences of 1000 MeV/u iron ions (linear energy transfer (LET) ~151 keV/μm), 600 MeV/u silicon ions (LET ~50 keV/μm) or 290 MeV/u carbon ions (LET ~13 keV/μm). We compared the results with those obtained in cell cultures exposed, in parallel, to low fluences of 0.92 MeV/u α particles (LET ~109 keV/μm).

Induction of DNA damage, changes in gene expression, protein carbonylation and lipid peroxidation during 24 h after exposure of confluent cultures to mean doses as low as 0.2 cGy of iron or silicon ions strongly supported the propagation of stressful effects from irradiated to bystander cells. At a mean dose of 0.2 cGy, only ~1 and 3 % of the cells would be targeted through the nucleus by an iron or silicon ion, respectively. Within 24 h post-irradiation, immunoblot analyses revealed significant increases in the levels of phospho-TP53 (serine 15), p21$^{Waf1}$ (also known as CDKN1A), HDM2, phospho-ERK1/2, protein carbonylation and lipid peroxidation. The magnitude of the responses suggested participation of non-targeted cells in the response. Furthermore, when the irradiated cell populations were subcultured in fresh medium shortly after irradiation, greater than expected increases in the levels of these markers were also observed during 24 h. Together, the results imply a rapidly propagated and persistent bystander effect. *In situ* analyses in confluent cultures showed 53BP1 foci formation, a marker of DNA damage, in more cells than expected based on the fraction of cells traversed through the nucleus by an iron or silicon ion. The effect was

expressed as early as 15 min after exposure, peaked at 1 h and decreased by 24 h. A similar tendency occurred after exposure to a mean absorbed dose of 0.2 cGy of 3.7 MeV α particles, but not after 0.2 cGy of 290 MeV/u carbon ions.

Analyses in dishes that incorporate a CR-39 solid state nuclear track detector bottom identified the cells irradiated with iron or silicon ions and further supported the participation of bystander cells in the stress response. Mechanistic studies indicated that gap junction intercellular communication, DNA repair, and oxidative metabolism participate in the propagation of the induced effects.

We also considered the possible contribution of secondary particles produced along the primary particle tracks to the biological responses. Simulations with the FLUKA multi-particle transport code revealed that fragmentation products, other than electrons, in cells cultures exposed to HZE particles comprise <1 % of the absorbed dose. Further, the radial spread of dose due to secondary heavy ion fragments is confined to approximately 10-20 µm Thus, the latter are unlikely to significantly contribute to the stressful effects in cells not targeted by primary HZE particles.

# RÉSUMÉ

De nombreuses études ont montré que l'exposition de cultures cellulaires à des particules α conduit à des changements biologiques importants autant dans les cellules irradiées que dans les cellules *bystander* non-irradiées. L'étude des réponses biologiques non-ciblées dans des cultures cellulaires exposées à de faibles fluences d'ions lourds permet d'estimer les risques pour la santé du rayonnement spatial et de la radiothérapie. Nous avons caractérisé les mécanismes sous-jacents de l'induction d'effets stressants dans des cultures confluentes de fibroblastes normaux humains exposés à de faibles fluences d'ions fer de 1000 MeV/u (transfert d'énergie linéique (TEL) ~151 keV/μm), d'ions silicium de 600 MeV/u (TEL ~50 keV/μm) ou d'ions carbone de 290 MeV/u (TEL ~13 keV/μm). Nous avons comparé ces résultats avec ceux obtenus dans des cultures cellulaires exposées, en parallèle, à de faibles fluences de particules α de 0,92 MeV/u (TEL ~109 keV/μm).

L'induction de dommages à l'ADN, les changements dans l'expression des gènes, la carbonylation des protéines et la peroxydation lipidique durant les 24 h suivant l'exposition de cultures confluentes à de faibles doses (0,2 cGy et plus) d'ions fer ou d'ions silicium ont très largement contribué à la propagation d'effets stressants des cellules irradiées aux cellules bystander non-irradiées. Pour une dose moyenne de 0,2 cGy, seules ~1 et 3 % des cellules seraient irradiées dans le noyau par un ion, respectivement, fer ou silicium. Les immunoblots ont révélés des augmentations significatives des niveaux de phospho-TP53 (sérine 15), p21$^{\text{Waf1}}$ (CDKN1A), HDM2, phospho-ERK1/2, de carbonylation des protéines et de peroxydation lipidique dans les 24 h suivant l'exposition. L'ampleur de ces réponses suggère la participation de cellules non ciblées dans les effets observés. De plus, lorsque les populations cellulaires irradiées ont été ré-ensemencées dans un milieu de culture frais peu après l'irradiation, les niveaux de ces marqueurs ont aussi augmentés durant 24 h. Ensemble, ces résultats montrent un effet rapidement propagé et persistant. Des analyses *in situ* réalisées

dans des cultures cellulaires confluentes ont montré que la formation de foyers de la protéine 53BP1, marqueur de dommages à l'ADN, touchait un nombre de cellules plus important que celui auguré par la fraction de cellules traversées dans le noyau par un ion fer ou silicium. Cet effet est exprimé dès 15 min suivant l'exposition, atteint son maximum 1 h après l'exposition puis diminue jusqu'à 24 h. Une tendance similaire s'est produite après exposition à une dose moyenne absorbée de 0,2 cGy de particules α de 3,7 MeV, mais non après 0,2 cGy d'ions carbone de 290 MeV/u.

Des analyses utilisant des puits de cultures intégrant une fine épaisseur de CR-39, détecteur solide de traces nucléaires, et permettant ainsi l'identification des cellules irradiées aux ions fer ou silicium, confirment la participation de cellules *bystander* dans la réponse au stress. Des études mécanistiques ont, de plus, indiqué que les jonctions gap permettant la communication intercellulaire, certaines voies de la réparation de l'ADN, ainsi que le métabolisme oxydatif participent à la propagation des effets non ciblés induit par des radiations de haut TEL. Nous avons également examiné la contribution possible des particules secondaires produites le long des traces d'ions primaires dans les réponses biologiques. Les simulations réalisées avec le code de transport de particules FLUKA ont révélé que la dose due aux produits de fragmentation, autres que les électrons, est inférieure à 1 % de la dose absorbée dans les cultures cellulaires exposées à des ions lourds. De plus, la dose radiale des ions lourds secondaires est limitée à ~10-20 μm autour de l'ion primaire. Ainsi, ces derniers sont peu susceptibles de contribuer de manière significative à la réponse biologique observée dans des cellules non ciblées par des ions lourds primaires.

Mots clefs : ions lourds, particules α, faible dose/faible fluence, effet de proximité ou *bystander*, radiations secondaires, FLUKA, CR-39, voie de signalisation de ATM/p53, carbonylation des protéines/peroxydation lipidique, jonction gap, réparation de l'ADN, pression partielle en oxygène

# ABBREVIATIONS

$\gamma$-H2AX = Serine 139-phosphorylated histone H2AX

53BP1 = p53-binding protein 1

AGA = 18-$\alpha$-glycyrrhetinic acid

ATM = Ataxia telangiectasia mutated

ATR = Ataxia telangiectasia mutated and Rad3 related

BSO = Buthionine sulfoximine

CDC = Cell division cycle

CHO = Chinese hamster ovary

c-JNK = c-Jun $NH_2$-terminal kinase

COX-2 = Cyclooxygenase-2

c-PTIO = 2-(4-carboxyphenyl)-4, 4, 5, 5- tetramethylimidazoline-1-oxyl-3-oxide

Cx = Connexin

DDT = 1, 1′bis (pchlorophenyl)-2, 2, 2-trichloroethane

DMSO = Dimethyl sulfoxide

DNA-PK = DNA-dependent protein kinase

DPI = Diphenyleneiodonium

DSBs = DNA double strand breaks

ERK = Extracellular related kinase

GCR = Galactic cosmic rays

GJIC = Gap junction intercellular communication

HDM2 = human homologue of murine double minute 2 (MDM2)

HLF1 = Human lung fibroblasts

Hsp72 = Heat shock protein 72

IL-8 = Interleukin-8

HZE = High charge (Z) and high energy (E)

LET = Linear energy transfer

MAPK = Mitogen-activated protein kinase

MDM2 = Murine double minute 2

MN = Micronucleus

NAD(P)H = Nicotinamide adenine dinucleotide phosphate

NFκB = Nuclear factor κB

NHEJ = Non-homologous end-joining

NO = Nitric oxide

PARP = Poly (ADP-ribose) polymerase

PET = Polyethylene terephthalate

PMA = 4_, 9_ , 12_, 13_, 20-pentahydro-xytiglia-1,6-dien-3-one 12_ -myristate 13-acetate

RNS = Reactive nitrogen species

ROS = Reactive oxygen species

SCE = Sister chromatid exchange

SOD = Superoxide dismutase

SSB = DNA single strand break

TGF-ß1 = Transforming growth factor ß1

TNF- α = Tumor necrosis factor-α

TRAIL = TNF-related apoptosis-inducing ligand

# TABLE OF CONTENTS

# LIST OF FIGURES

# LIST OF TABLES

# Chapter 1    Introduction

## *1.1 Ionizing radiation*

### 1.1.1 Definitions

*Radiation* is the transport of energy through space. The absorption of energy from radiation in biological material may lead to excitation or to ionization. An *ionizing radiation* is a radiation that has sufficient energy to penetrate matter causing localized release of large amounts of energy. The released energy can in turn eject one or more orbital electrons from an atom or molecule of the absorbing material. The loss (or gain) of an electron is called ionization and an ion is a charged atom or molecule.

Ionizing radiation is classified as either electromagnetic or particulate. Whereas X and γ rays belong to electromagnetic radiation, energetic electrons, protons, neutrons, α particles and heavy charged particles are different forms of particulate radiation (Hall and Giaccia 2012).

### 1.1.2 Electromagnetic radiations

X and γ rays are the two major types of electromagnetic ionizing radiation. They consist of a spectrum of waves, like other electromagnetic radiations that are non-ionizing such as radio waves, microwaves, infrared, visible light, and ultraviolet light. However, X and γ rays are distinctly characterized by their short wavelengths, high frequency, and high energy (Figure 1-1). Both types have no charge or mass and can travel long distances through matter.

# THE ELECTROMAGNETIC SPECTRUM

| Penetrates Earth Atmosphere? | Y | | N | | Y | N | |
|---|---|---|---|---|---|---|---|

| Wavelength (meters) | Radio | Microwave | Infrared | Visible | Ultraviolet | X-ray | Gamma Ray |
|---|---|---|---|---|---|---|---|
| | $10^3$ | $10^{-2}$ | $10^{-5}$ | $.5 \times 10^{-6}$ | $10^{-8}$ | $10^{-10}$ | $10^{-12}$ |

About the size of...

| Buildings | Humans | Honey Bee | Pinpoint | Protozoans | Molecules | Atoms | Atomic Nuclei |
|---|---|---|---|---|---|---|---|

| Frequency (Hz) | $10^4$ | $10^8$ | $10^{12}$ | $10^{15}$ | $10^{16}$ | $10^{18}$ | $10^{20}$ |
|---|---|---|---|---|---|---|---|

| Temperature of bodies emitting the wavelength (K) | 1 K | 100 K | 10,000 K | 10 Million K |
|---|---|---|---|---|

**Figure 1-1: Electromagnetic spectrum. Range of electromagnetic radiations, including radio waves, X rays, visible light, ultraviolet light, infrared radiation, γ rays, and other forms of radiation (http://mynasadata.larc.nasa.gov/science-processes/electromagnetic-diagram/)**

X rays and γ rays do not differ in nature or in properties but the designation reflects the way they are produced. X rays are produced extranuclearly, and γ rays are produced intranuclearly (Hall and Giaccia 2012). In practical terms, X rays are produced by electrical devices that accelerate electrons to high energy and then stop them in a target material, usually made of tungsten or gold; part of the kinetic energy of the electrons is converted into X rays. On the other hand, γ rays are emitted by radioactive isotopes; they represent the excess energy that is given off as the unstable nucleus breaks up and decays in its effort to reach a stable form (Hall and Giaccia 2012).

### 1.1.3 Particulate radiations

Particulate radiations consist of atomic or subatomic particles which carry energy in the form of kinetic energy or mass in motion. They include the following:

**Electrons** are small negatively charged particles. They can be accelerated to high energies and are widely used for cancer therapy and industrial applications.

**Protons** are positively charged particles with a mass 1836 times greater than that of electrons; they are found in the nucleus of an atom. Hydrogen atoms that are stripped of their single electron are known as "protons". Protons can also be accelerated to high energy in specialized equipment such as cyclotrons and accelerators. Due to their dose distribution, they are increasingly being used for cancer treatment.

**Neutrons** have a mass similar to that of protons and are also found in the nucleus of an atom. Because they carry no charge, they cannot be accelerated in an electrical device. They are produced when charged particles (e.g. deuteron) impinge on suitable target material (e.g. beryllium). They are also emitted when heavy nuclei (e.g. uranium, plutonium) undergo fission. They are an important component of space radiation. They are also used in cancer therapy in a procedure whereby they are captured by boron that is injected into patients (Boron Neutron Capture Therapy).

**α particles** are nuclei of helium atoms. They consist of two protons and two neutrons and have a net positive charge; therefore, they can be accelerated in electrical devices similar to those of protons and electrons. An environmental source of α particles is radon gas. Radon ($^{222}$Rn) emits α particles of 5.5 MeV, with a half-life of 3.8 days (BEIR VI 1998). An α particle has a mass ~8000 times greater than an electron; as a result, it can only travel a few millimeters in air. Its range is further reduced when the density of the absorbing medium increases. Alpha particles cannot penetrate human skin, but can be inhaled and thereby damage lung tissue. They are used in immune-radiotherapy.

**Heavy charged particles** are generally classified as particles with atomic number (Z) greater than two (i.e. greater than that of α particles) and with higher energy (E). High charge and high energy (HZE) particles are encountered by astronauts during prolonged deep space travel (e.g. iron) and are used in cancer therapy (e.g. carbon). For experiments and therapeutic use, their electrons are stripped, which allows their acceleration to high energies (e.g. 300-1000 MeV/u) in particle accelerators. In this project, HZE particles generated at the NASA Space Radiation Laboratory (NSRL) located at Brookhaven National Laboratory (Upton, NY, USA) were used. HZE particles have been used for biomedical purposes since 1975 (Jermann 2010). Heavy ions can be accelerated to high energies (e.g. thousands of millions of volts) either by acceleration of the particles of interest, or by a nuclear interaction between an accelerated particle and a target material from which the desired particles can be obtained.

In addition to the above, other types of particulate radiations are being used in physics experiments or considered for radiotherapy (e.g. negatively charged pi-mesons or pions ($\pi^-$), antiprotons). This thesis project is focused on biological effect of particulate radiation, namely α particles and iron, silicon and carbon ions. The results are pertinent to terrestrial environmental exposures, radiation protection of astronauts during space travel and to radiotherapy.

## 1.2  Interaction with matter

The biological effects of ionizing radiation depend on the amount of energy absorbed by living matter and by the spatial distribution of the absorbed energy. To comprehend the physics of tissue irradiation, the mechanisms of energy transfer must be understood (Cember 1996).

### 1.2.1 Linear energy transfer

The Linear Energy Transfer (LET) is defined as the amount of energy lost per unit length along the path traveled by the radiation. It is expressed in keV $\mu m^{-1}$. LET is an average quantity: the energy deposition events in tissues have a particular distribution that varies as a function of tissue depth. In contrast to electromagnetic radiation (e.g. X rays, $^{137}Cs$ and $^{60}Co$ $\gamma$ rays), whose energy deposition decreases exponentially as a function of penetration-depth in target material, charged particles (e.g. HZE particles) have a well-defined range in matter. Specifically, energy deposition by HZE particles is characterized by a low entrance dose in the target material and a pronounced sharp maximum near the end of their range (the Bragg peak) (Katz and Cucinotta 1999). Beyond the Bragg peak, the energy may be close to zero (Figure 1-2). Extremely high-LET-values in tissue can be reached at the Bragg peak (Tobias, Blakely et al. 1982; Nelson 2003), and this characteristic energy deposition profile of charged particles is exploited in cancer radiotherapy. By positioning the patient so that the location of the tumor coincides with the Bragg peak of the impacting particles, most of the energy is deposited in the tumor, while the surrounding tissue is exposed to a significantly reduced amount of energy (Figure 1-2). Thus, cell killing is enhanced in the tumor region but not in the normal tissue surrounding the tumor (Durante and Loeffler 2010).
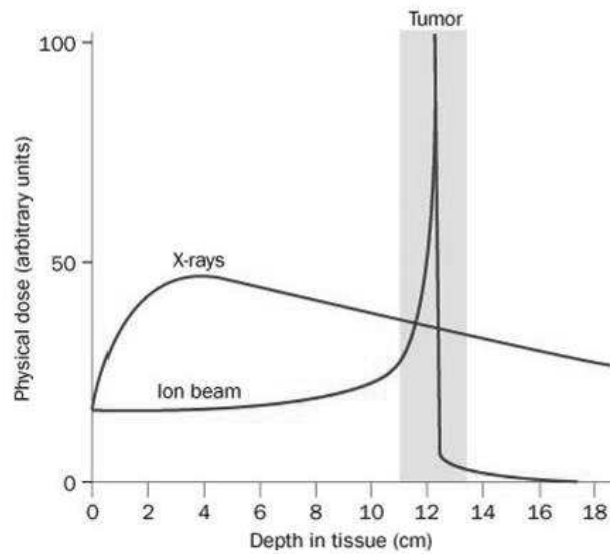
**Figure 1-2: Typical energy loss profiles for X rays and heavy ions as a function of travel in tissue (Adapted from Durante and Loeffler 2010)**

It is well-established that the complexity of radiation damage increases with the LET (Rossi 1959; Tobias, Blakely et al. 1982; Ward 1994). The LET effects, known also as track structure effects, determine the relative potency of different types of radiation in causing biological changes (Goodhead, Thacker et al. 1993; Goodhead 1994; Ottolenghi, Merzagora et al. 1997; LaVerne 2000). High energy X rays, $^{137}$Cs and $^{60}$Co γ rays, electrons and high energy protons are typical low-LET radiations; α and HZE particles are on the other hand typical high-LET radiations. The demarcation value between low- and high-LET radiations is ~10 keV/μm (Podgorsak 2005; Hall and Giaccia 2006).

Track structure depends greatly on LET (LaVerne 2000), and this project focuses on the biological effects of low fluences of high LET radiation. To this end, understanding the yield and precise location of the radiation-induced bursts of reactive oxygen species is critical to our understanding of the events involved in the cellular responses to stress induced by low fluences of energetic particles.

The energy track trajectory of a high-LET particle can be thought of as consisting of a cylindrical "core" dense in radiolityc species and surrounded by a concentric region known as

"penumbra" formed by secondary electrons (low LET δ rays) (Figure 1-3). Therefore, certain high-LET radiations will have combined high- and low-LET radiation components to their tracks (Cucinotta, Katz et al. 1998; Muroya, Plante et al. 2006), which may greatly affect the biological response. Signaling events induced by the low-LET component may modulate biochemical and molecular events induced by the high-LET component of the radiation and vice-versa.
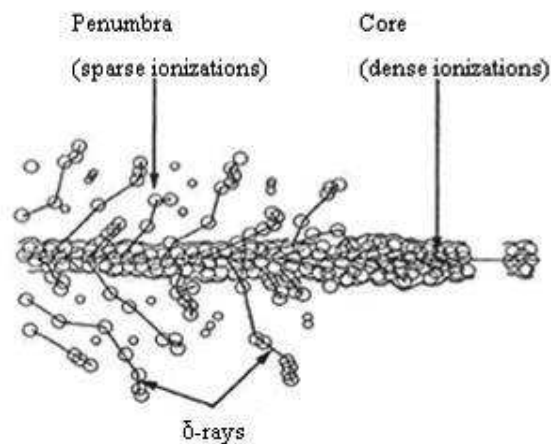


**Figure 1-3: Energy deposition of high-LET heavy ion (from Ferradini 1979)**

## 1.2.2 Physical interactions between radiation and matter

The physical interactions between radiation and matter are of 3 main types.

**Ionization of atoms**: when the energy of the impacting radiation exceeds the binding energy of electrons in target atoms, the electron may be ejected from its orbital resulting in ionization of the atom. If the ejected electron has sufficient energy, it can in turn create secondary ionizations.

**Excitation of atoms**: the process of raising an electron to a higher energy level without causing its ejection is known as excitation. An excited atom returns to normal state by emission of specific secondary electromagnetic radiation.

**Heat transfer**: depending on the type and energy of the radiation, target atoms or molecules may be neither excited nor ionized. However, the radiation may increase the kinetic energy of translation, rotation and vibration of the atom, the so-called heat transfer effect.

Absorption of ionizing radiation energy by biological materials causes all the three above types of interactions.

### 1.2.3 Track structure and LET

Understanding the radiation track structure is of crucial importance in specifying the spatial distribution of the radiolytic species and free radical intermediates created by the passage of the impacting ion (Meesungnoen and Jay-Gerin 2011). Characterizing the distribution of the radiolytic products would aid in understanding the mechanisms implicated in modulation of signaling effects and induction of subsequent damage in cell cultures exposed to radiations of different LET. The induced molecular changes are likely to be dependent on the biochemical status and physical organization of the cellular organelle(s) traversed by the irradiating particle. In chapter 3 and 5 of this thesis, the role of the cellular redox environment in the response of normal human fibroblasts to low fluences of 3.7 MeV α particles is investigated and discussed.

Predicting the effects of radiation type and energy in radiolysis not only requires a description of the early physical aspects of the radiation track structure, but also a modeling of the temporal dependence of the spatial distributions of the radiation-induced reactive species in the tracks (Muroya, Plante et al. 2006). For example, simulation studies for high-LET radiations with the same LET show that ionizations along the track may differ, which could lead to different spectrum of damage (Muroya, Plante et al. 2006).

The projections in Figure 1-4 illustrate track simulation in liquid water at 25 °C of different energetic ions, namely $^1H^+$ (0.15 MeV), $^4He^{2+}$ (1.75 MeV/u), $^{12}C^{6+}$ (25.5 MeV/u), $^{20}Ne^{10+}$ (97.5 MeV/u) with an identical LET of ~70 keV/μm. They show that the spatial extent of the distributions of all radiolytic species increases with increasing energy of the incident ion. This is readily explained by the greater penetration range of the ejected secondary electrons due to traversal of the higher velocity ion. Thus, more energetic incident ions transfer more energy to secondary electrons (δ rays) generated along the ion track. It is the δ rays that determine the penumbra extension in the tracks (Magee and Chatterjee 1980; Muroya, Plante et al. 2006; Plante and Cucinotta 2008). Predicting the range and energy of these electrons is significant to understanding the nature and magnitude of biological responses triggered in cells that are not directly traversed by a primary HZE particle. In chapter 4 of this thesis, the dose imparted by δ rays and the radial range of the electrons and other fragmentation products is calculated following exposure of confluent human cell cultures maintained on soda-lime glass surface to 1000 MeV/u $^{56}Fe$ or 600 MeV/u $^{28}Si$ ions.
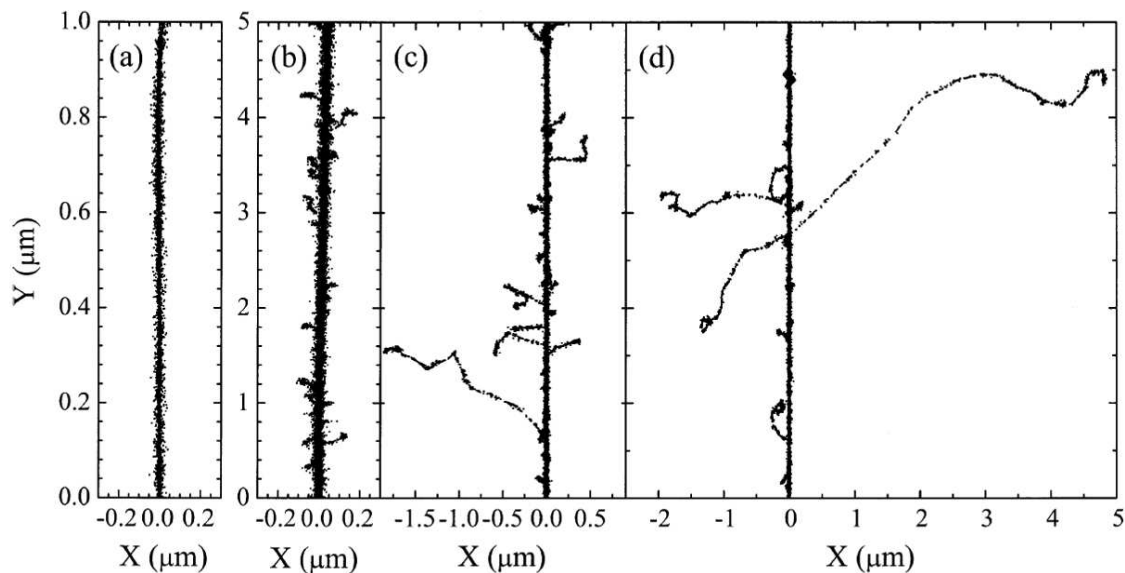


**Figure 1-4: Projections over the XY-plane of simulated tracks segments (calculated at ~10$^{-13}$ s) for the following impact ions: $^1H^+$ (0.15 MeV) (panel a), $^4He^{2+}$ (1.75 MeV/u) (panel b), $^{12}C^{6+}$ (25.5 MeV/u) (panel c) and $^{20}Ne^{10+}$ (97.5 MeV/u) (panel d). Dots represent the energy deposited at points where an interaction occurred and an ionization was created. Ions are generated at the origin along the Y-axis in liquid water at 25 °C under identical LET conditions (~70 keV/μm) (Muroya, Plante et al. 2006).**

The central region of the tracks is made up of the reactive species that are generated not only by the heavy ion itself, but also by the numerous low-energy secondary electrons that are ejected from the ion trajectory. The core of tracks is then initially comprised of "spurs"[a] (<100 eV) and "blobs"[b] (~100-500 eV) (Mozumder and Magee 1966) with sizes reaching a few tens of nanometers (Meesungnoen, Jay-Gerin et al. 2002). As we can see from Figure 1-4, these secondary electrons are so dense that this central region appears continuous. The second, peripheral region extends above ~20-50 nm from the incident ion path. It is much larger and less dense in radiolytic species. Figure 1-4 shows that this region is negligible for the proton track while its importance increases with the energy of the irradiating ion, from helium to carbon to neon ions. It corresponds to the region where energetic secondary electrons ($\delta$ rays), ejected from the core in knock-on collisions, can go. As seen in Figure 1-4, the production of these $\delta$ rays is sporadic and their tracks are generally well separated from each other, giving a highly non-uniform geometric distribution of absorbed energy.

### 1.2.4 Direct and indirect effects of ionizing radiation

When cells are exposed to ionizing radiation, the induced biological effects result mainly from two processes: direct action and indirect action. Due to their unique inherent physical properties and energy deposition patterns, high-LET radiations cause biological changes mainly by *directly* damaging critical targets in the cells like DNA. Alternately, low-LET electromagnetic radiations (X and $\gamma$ rays) interact with other atoms or molecules in the cell, especially water to produce free radicals (*e.g.* hydroxyl, superoxide radicals) and other reactive species that go on to damage critical targets in the vicinity; therefore, they cause

---

[a] Spur: concentration of ~3 ion pairs in a volume ~4 nm in diameter
[b] Blob: concentration of ~12 ions pairs in a region ~7 nm in diameter

cellular damage largely by an *indirect* manner (Lehnert 2008). Ultimately, these direct and indirect effects of ionizing radiation produce biological and physiological alterations in the cell or organism that manifest in seconds to even decades after irradiation. This thesis further explores the mechanisms underlying the early responses of human cells to high-LET particulate radiations.

### 1.2.5  Absorption of photons

There are three principal mechanisms by which X and γ rays interact with living tissue: photoelectric effect, Compton scattering and pair production.

In the *photoelectric process*, the photon interacts with a bound electron of an atom of the absorbing material. It gives up all of its energy to the electron; some is used to overcome the binding energy of the electron and release it from its orbit; the remainder is given to the electron as kinetic energy of motion. The vacancy left in the atomic shell as the result of ejection of the electron is filled by another electron falling in from an outer shell of the same atom or by conduction electron from outside the atom. Photoelectron absorption is the dominant process for X ray absorption up to energies of about 500 keV. The mass absorption coefficient for photoelectric absorption varies rapidly with the atomic number; as a result, photons used in diagnostic radiology have an energy range in which photoelectric absorption dominates (Hall and Giaccia 2012).

At high energies (characteristic of $^{60}$Co γ rays), the *Compton process* dominates. The photon interacts with a "free" electron, an electron whose binding energy is negligibly small compared with the photon energy. Part of the energy (from 0 to 80 %) of the photon is given to the electron as kinetic energy, whereas the photon, with whatever energy remains, continues on its way, being deflected from its original path.

Pair production occurs when an electron and positron are created with the annihilation of the photon. Positrons are very short lived and disappear (positron annihilation) with the formation of two photons of 0.51 MeV energy. Pair production is of particular importance when high-energy photons pass through materials of a high atomic number; it occurs when the photon energy is greater than 1.02 MeV, but only becomes significant at energies around 10 MeV.

## 1.2.6 Physical and Physicochemical Effects of Ionizing Radiation: Water radiolysis and generation of reactive chemical species

Liquid water is the major constituent of cells, comprising ~80 % of their matter. A thorough knowledge of water radiolysis is therefore critical for understanding radiobiological effects. The excitations and ionizations resulting from the absorption of energetic radiations by water lead to production of free radicals that in turn can attack other critical molecules (indirect effect) (Figure 1-5).
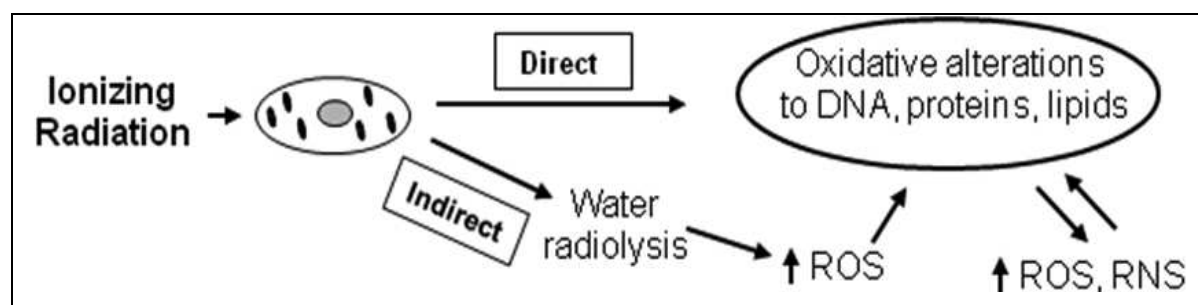


**Figure 1-5: Direct and indirect actions of radiation (Azzam, Jay-Gerin et al. 2011)**

For brevity, the complex events that accompany the absorption of high-energy photons or the passage of fast charged particles can be divided into four, more or less clearly demarcated, consecutive, temporal stages (Platzman 1958). During the first or "physical"

stage, the energy deposition is caused as discussed earlier (section 1.2.3) by the incident radiation and the secondary electrons generated. The chemical species resulting from these interactions are extremely unstable and undergo fast reorganization in the second or "physicochemical" stage. These processes produce radical and molecular products of radiolysis that are distributed in the highly non-homogeneous track structure described earlier (section 1.2.3). Secondary electrons slow down to sub-excitation energies and following thermalization, they become trapped and hydrated ($e^-$ aq). The initial ($\sim 10^{-12}$ s) spatial distribution of reactants is then directly used as the starting point for the so-called stage of "non-homogeneous chemistry". During this third stage, the various chemically reactive species diffuse and react with one another or with the environment, until all intra-track reactions are complete ($\sim 10^{-6}$ s). Finally, in a physiologic system, there follows a "biological" step in which the cells respond to the damage resulting from the products formed in the preceding levels. During this stage ($\sim 10^{-3}$ s or longer, depending very much upon the medium), the biological responses affecting the long-term consequences of radiation exposure are induced. In addition to ROS produced as a result of radiolysis of cellular water or activation of oxidases, reactive nitrogen species are also generated due to activation of nitric oxide synthases (Figure 1-5) (Azzam, Jay-Gerin et al. 2011).

In summary, the radiolysis of water is a major source of ROS in irradiated cells under ambient oxygen. Interestingly, the yield of these species is strongly modulated by different types of radiation. With increasing LET of the irradiating particles, an increase in the yield of molecular products (such as $H_2O_2$) is accompanied by a corresponding decrease in the yield of radicals (such as $^\bullet OH$, hydroxyl radical). In contrast, $O_2^{\bullet-}$ (superoxide radical) is the most abundant radical species produced by radiations with high-LET character (LaVerne 2004; Meesungnoen and Jay-Gerin 2011). Evidently, the yield of these products and their concentrations along the tracks of irradiating particles has important consequences to the

extent and nature of induced DNA damages (Goodhead 1989; Campa, Ballarini et al. 2005; O'Neill and Wardman 2009). Radiation-induced ROS are similar in nature to those produced by normal respiratory chain in mitochondria; however, they are distinguished by their cellular distribution. Unlike free radicals formed by endogenous production (respiratory chain), those formed after irradiation are concentrated along the radiation track. They are not produced uniformly in large numbers but in a relatively small volume, in "clusters" of ionizations of nanometer size. In an aerobic cellular environment at physiological pH, the major reactive species at homogeneity ($\sim 10^{-6}$ s) include superoxide radical ($O_2^{\bullet -}$), hydroxyl radicals ($^\bullet OH$) and hydrogen peroxide ($H_2O_2$).

Radiation-induced reactive chemical species result in short-term immediate cellular alterations as well as long term changes that occur hours, days or months after irradiation due to disruption of oxidative metabolism (Petkau 1987; Spitz, Azzam et al. 2004). Persistent generation of ROS/RNS may cause continuous covalent changes to nucleic acids, proteins and lipids.

Whereas ~60 ROS per nanogram of tissue were estimated to be generated from a hit caused by $^{137}$Cs γ rays (Meesungnoen, Benrahmoune et al. 2001), it has been estimated that 2000 ROS are generated from an α particle traversal, corresponding to a concentration of ~19 nM in the nucleus of a typical human fibroblast (Autsavapromporn, de Toledo et al. 2011). Such concentration can obviously cause extensive oxidative damage and alter normal homeostasis.

## *1.3 Units of Dose*

The most common description of radiation exposure uses the concept of dose.

### 1.3.1 Definitions

The **Roentgen** is the unit of exposure to ionizing radiation named after Wilhelm Röentgen, the German scientist who discovered X rays in 1895. It is the amount of γ or X rays required to produce ions carrying one electrostatic unit of electrical charge (either positive or negative) in 1 cm$^3$ of dry air under standard conditions.

The **absorbed dose** relates to the amount of energy deposited by any type of radiation. It is defined by the International Commission on Radiological Units and Measurements (ICRU) as the energy absorbed, at a specific point, per unit mass (inert or living). The unit is the Gray (Gy) in tribute to the British physicist Harold Gray. One gray is equivalent to one joule of radiation energy absorbed per kilogram of tissue. This is not to be confused with the equivalent dose.

The concept of **dose equivalent** was introduced for radiation protection purposes. It rests on the notion that at equal absorbed dose, the induced damaging effects observed vary with the nature of radiation, with high-LET radiations being more capable of causing damage per unit absorbed dose than low-LET radiations. According to ICRU Report 51, the dose equivalent is defined as the amount of absorbed dose multiplied by a quality factor or weighting factor ($W_R$) of the type of radiation in question (Table 1-1). It is calculated in Sievert (Sv) as a tribute to Rolf Sievert, a Swedish radiobiologist.

| Type of radiation | | $W_R$ |
|---|---|---|
| Photons | | 1 |
| Electrons | | 1 |
| Neutrons | E < 10 keV | 5 |
| | 10 keV < E < 100 keV | 10 |
| | 100 keV < E < 2 MeV | 20 |
| | 2 MeV < E < 20 MeV | 10 |
| | > 20 MeV | 5 |
| Protons | | 5 |
| α particles, heavy charged particles | | 20 |

**Table 1-1: Weighting factors for various radiations (ICRP 1991)**

Table 1-1 shows that the weighting factors for α particles, HZE particles and low energy neutrons can be 20 times greater than for photons and high energy electrons.

The **effective dose** is a quantity that has been introduced to assess detriments in terms of effects in the whole body. Calculated from the equivalent dose for each body part, the effective dose takes into account the different sensitivities of tissues that result in weighting factors for organs ($W_T$). The unit is also the Sievert.

As will be discussed in this thesis, considering the biological effects of ionizing radiation, absorbed dose is not always sufficient to quantify the induced damage. Absorbed dose only gives a macroscopic view of energy deposition; it does not reflect the heterogeneity of energy deposition nor does it account for non-targeted biological effects of radiation.

### 1.3.2 Complexity of the concept of dose

Whereas doses of low-LET radiations produce a uniform pattern of ionization throughout a target (cell, tissue, animal), this is not the case for charged particles (Figure 1-6). Indeed, for charged particles, ionization is concentrated along the track. In the center of

a track, the local dose may be thousands of Gray but, a few microns away, the dose may be close to zero (Cucinotta, Nikjoo et al. 2000). Therefore, it is extremely important to understand the pattern of energy deposition specific to the radiation type.
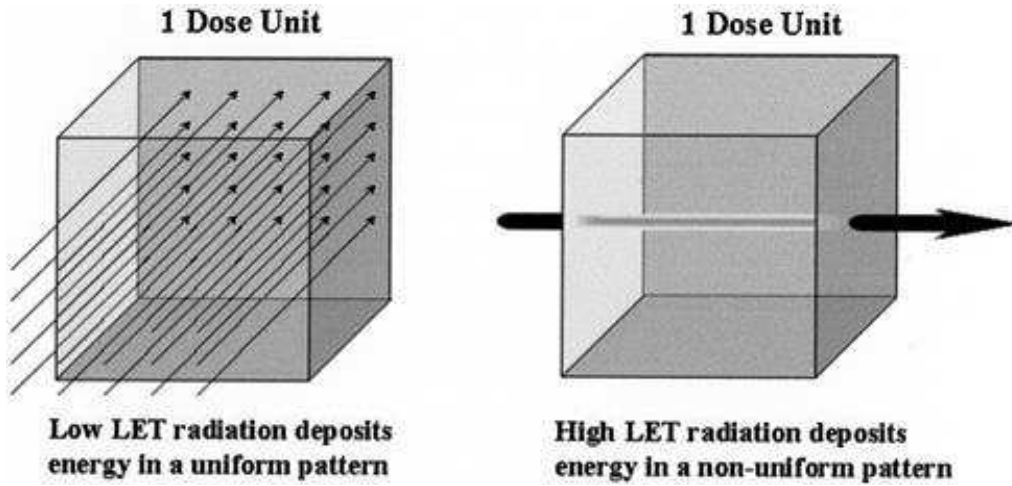


**Figure 1-6: Different pattern of energy deposition of low-LET and high-LET radiations (Nelson 2003)**

To overcome the inadequacies of the traditional concept of dose, a model based on the number of particle (i.e. fluence) may be more appropriate in the context of effects of low level particulate radiations. Fluence is defined as the number of particles that traverse a unit area; it is expressed as particles/cm$^2$. Equation 1-1 links the notion of fluence, dose and LET:

$$\textbf{Equation 1-1: } D = 1.602.10^{-9} \frac{\text{TEL}}{\rho} \times \phi$$

where D represents the dose in $Gy$ ($J\,kg^{-1}$), LET is in $keV\,\mu m^{-1}$, the fluence $\varphi$ is in $particles/cm^2$, and $\rho$ is the density of the medium considered (here, $\rho=1\ g\ cm^{-3}$).

This method ignores the effects of track width due to the lateral extension of high energy secondary particles ($\delta$ rays) that may extend for many micrometers, or even millimeters, such that several adjacent cells will be hit in the passage of a single ion (Cucinotta, Nikjoo et al. 1998).

In the case of low fluence exposure, it is important to know the number of particle traversals through a target cell or cell nucleus. The number of traversals through a target is dependent on the fluence and the area of the target (i.e. geometric cross section). The Poisson distribution (Equation 1-2) gives the probability that cells or cell nuclei are hit by exactly n particles:

$$\textbf{Equation 1-2: } P(n) = \frac{e^{-\lambda} \lambda^n}{n!}$$

where $\lambda$ is the average number of particles per target area; it is the product of the fluence and the target area (nucleus or whole cell).

For confluent AG1522 cell cultures used in our experiments, the nuclear surface is estimated to be between 140 μm² (Azzam, de Toledo et al. 1998) and $165 \pm 7$ μm² (Shao, Furusawa et al. 2006), while the total area of the cell is estimated to be 800 μm² (Gaillard, Pusset et al. 2009) or $1370 \pm 50$ μm² (Shao, Furusawa et al. 2006) for AG01522 cells at confluence. In this project, the values of 140 μm² and 800 μm² for the surface area of the nucleus or the entire cell were used as cells destined for irradiation were maintained in confluence for 4 days with a feeding at 2 days prior to exposure. Under these conditions, at a mean absorbed dose of 0.2 cGy of α particles, ~1 % of cell nuclei are hit by a particle track.

### 1.3.3 Which dose is considered as low dose?

There is a need to clarify what is meant by "low dose". It has been generally understood that a low dose is a dose below which there is no significant difference in incidence of cancers between the exposed and control unexposed groups. On this scientific foundation, the United Nations Scientific Committee on the Effects of Atomic Radiation (UNSCEAR 2000) and the National Academy of Sciences in the United States (BEIR VII 2006) have concluded that the field of "low" dose radiation corresponds to doses below

100 mSv received in a short time. This dose represents 10 cGy when X or γ rays are considered and 0.5 cGy if α particles or energetic heavy ions are considered. For the studies in this thesis project, confluent cell cultures were irradiated with very low mean doses of particulate radiations so that, in a given field, only one cell is irradiated through the nucleus by a primary particle track.

## 1.4 Health Risks of low doses of radiation

### 1.4.1 Exposure to low doses of ionizing radiations

Ionizing radiation is ubiquitous in nature; it is present in terrestrial rocks, in the atmosphere, in agricultural products and within humans and animal biota. Furthermore, with the evolution of society, the use of radiation has become essential to numerous industrial and medical applications.

Radiation therapy, by itself or coupled with other modalities, is the main method of cancer treatment. It generally uses high doses of ionizing radiation. With the exception of this particular case, the human population is increasingly being exposed to low doses of radiation. In addition to natural background radiation representing 2.4 mSv per year per person on average (UNSCEAR 2000), humans are exposed to radiation from industrial activities, energy generation, and especially from an increase of diagnostic radiology examinations. About 70 million are performed in France each year delivering an average of 1 mSv per year per person (Aurengo, Averbeck et al. 2005), a dose equivalent to 10 chest X ray procedures. The worldwide annual effective dose per person for diagnostic medical examinations is 0.4 mSv (UNSCEAR 2000). The majority of the latter exposures consist of low-LET radiations.

Low level exposures to high-LET radiations are mainly from high-altitude airline flights (Bottollier-Depois, Chau et al. 2000) and low concentrations of internal emitters such as inhaled radon progeny (UNSCEAR 2000). With regard to natural exposure, radon (α particle emitter) and its progeny play a major role in contributing to over 50 % of the annual exposure dose (UNSCEAR 2000). Although α particles are non-penetrating and are stopped by the outer layer of skin, they can be nevertheless inhaled and lodge in the lung alveoli. It is assumed that exposure to radon is responsible for 13 % of deaths from lung cancer (about 3350 deaths each year) in France, and 9 % in Europe (Catelinois, Rogel et al. 2006).

Recently, global efforts for space exploration have intensified. The National Aeronautics and Space Administration (NASA) in the U.S. plans a return to the moon by 2020 in anticipation of a trip to Mars around 2035. However, the health risks associated with different types of radiation that astronauts may encounter in deep space limit those efforts. Indeed, astronauts are likely to be exposed to low fluences and low fluences rates (Figure 1-7) of a complex mixture of radiations, such that particle traversals through cells in an astronaut's body are well separated in tissue location and time (Held 2009). In particular, the magnitude of the biological effects of protons and heavy ions, the main constituents of galactic cosmic rays (GCR) is very uncertain (Cucinotta and Durante 2006). It has been estimated that on the Russian Space Station Mir, lymphocytes in an astronaut are traversed by one proton every 12 days, one helium ion in 4 months, one oxygen ion in 24 years and one iron ion in 400 years (Blakely and Kronenberg 1998). Therefore, during long-duration missions, such as a voyage to Mars, astronauts may be exposed to significant cumulative doses.
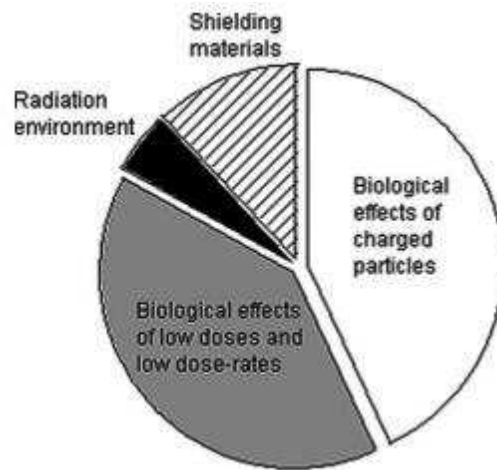
**Figure 1-7: Contributions to space radiation risk uncertainty of the main biological and physical endpoints (NASA 1998; Durante and Kronenberg 2005)**

The exponential growth of low dose X ray diagnostic examinations has recently aroused public and scientific concern. In response, the health risks from exposure to ionizing radiation have been the subject of comprehensive reports of the National Research Council of the National Academy of Sciences in the US (BEIR VII 2006) and of the Académie des Sciences (Aurengo, Averbeck et al. 2005). Moreover, all space agencies around the world are also interested to expand knowledge of the impact of low doses/low fluences of space radiation on astronauts.

## 1.4.2 The validity of the linear no-threshold (LNT) model

The biological effects and health risks of high doses of radiation have been well characterized through extensive experimental studies and epidemiological surveys of survivors of radiation accidents and, in particular, of the A-bombs dropped at Hiroshima and Nagasaki (BEIR VII 2006). These studies have demonstrated that exposure to acute high doses causes deleterious consequences in human and non-human biota, including, but not exclusively, cancer induction (Brenner, Doll et al. 2003).

To estimate health risks at low doses, the International Commission on Radiation Protection (ICRP) has recommended consideration of a linear relationship between dose and cancer risk. In this linear no-threshold (LNT) model, it is assumed that exposure to any dose of radiation, however small, increases the risk of detrimental health effects. Furthermore, the effects of sequential doses are assumed to be additive. In these suppositions, to estimate the risk at low doses of ionizing radiation (below 100 mSv), extrapolations from data obtained at high dose radiation were made.

However, the validity of using this dose-response model is controversial and has been the subject of intense debate. According to the French Academy of Sciences, epidemiological studies did not reveal a significant increase in cancer incidence in humans for doses below 100 mSv (Tubiana and Aurengo 2005): *"In conclusion, this report doubts the validity of using the LNT in the evaluation of the carcinogenesis risk of low doses (< 10,000 mrem) (= 10 cSv) and even more for very low doses (<1000 mrem) (= 1 cSv)"*. Rather, the members involved in examining low dose effects concluded that there is a threshold below which harmful effects are unlikely to arise (curve ***d*** in Figure 1-8). On the other hand, the BEIR VII report of the US Academy of Science (BEIR VII 2006) and analyses by other scientists (*e.g.* (Preston 2003)) support the LNT model (curve ***a*** in Figure 1-8) as the best representation to estimate cancer risk at low doses. However, members of the committee that wrote the BEIR VII report also agreed that at doses below 100 mSv, statistical limitations make it difficult to evaluate cancer risk in humans.

Indeed, epidemiological studies evaluating the effects of low dose radiation require the follow-up of large populations for extended periods of time to determine with confidence the risks of health hazards. As a result, such epidemiological studies are difficult to generate and may be biased by modulating factors in the intervening years between exposure and manifestation of adverse health effects (*e.g.* diet, smoking, exposure to diagnostic radiology,

stress *etc.*). Due to these difficulties, mechanistic *in vitro* cellular studies and *in vivo* studies with model animal systems were suggested as a source of knowledge that would help formulate adequate radiation protection guidelines.
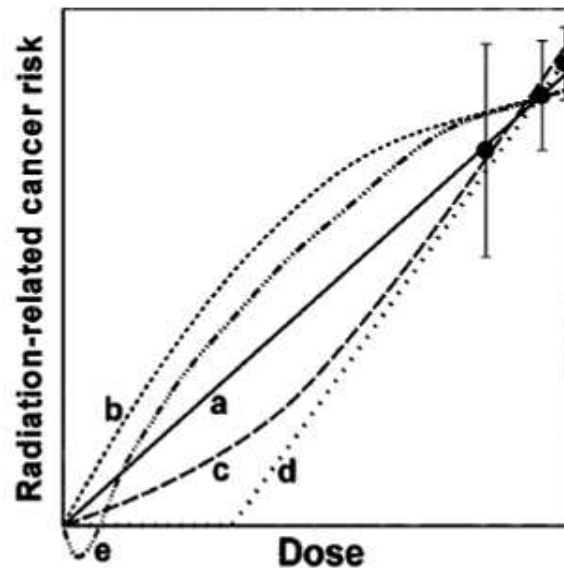


**Figure 1-8: Different possible extrapolations of cancer related radiation risk (Brenner, Doll et al. 2003)**

Growing evidence has emerged for a number of biological phenomena that may be important in modulating the cellular responses to low doses of ionizing radiation supporting the non-linear biological responses at low doses/fluences of radiation (Nagasawa and Little 1992; Azzam, de Toledo et al. 1996; Redpath, Liang et al. 2001).

Based on data providing evidence for these phenomena and the uncertainty of estimating health risks at low doses of ionizing radiation, different models have been proposed to represent risk at low doses. Whereas curve *b* in Figure 1-8 postulates that the LNT model underestimates risk, curve c in the same figure assumes that LNT model over-estimates risk. A J-shaped curved (curve *e* in Figure 1-8) has also been advocated. According to the latter curve, exposure to very low dose radiation may be beneficial (hormesis). The extrapolation curves *c*, *d* and *e* (Figure 1-8) challenge the LNT model. These extrapolations

are based on the propagation of stressful effects from low dose/low fluence targeted cells to non-irradiated bystander cells (curve *b*), endogenous defense mechanisms (curve *d*) and stimulatory pro-survival responses (curve *e*).

## 1.5  Non-targeted effect

### 1.5.1  The paradigm

It has been traditionally accepted that the biological effects of radiation exposure were only the consequence of DNA damage in cells whose nuclei were targeted by radiation. According to this paradigm, DNA damage occurs during or shortly after irradiation of cell nuclei (Zirkle and Bloom 1953; Little 2006). However, over the last three decades, significant data have emerged challenging this classical "target theory" that the important biological consequences of irradiation result from targeted DNA damage (reviewed in Matsumoto, Hamada et al. 2007). Cells in the vicinity of directly irradiated cells present also molecular, biochemical and genetic abnormalities. Importantly, stressful effects also manifest in the progeny of the irradiated and bystander cells. Those effects have been coined "non-targeted effects" and include radiation-induced bystander effects, and genomic instability. In contrast to the latter effects, substantial evidence has also been described whereby pre-exposure to a small dose of low LET radiation induces signaling effects that attenuate the damages induced by a subsequent challenge dose of radiation. Moreover, such protective effects may be propagated from low dose/low LET irradiated cells to neighboring bystander cells (reviewed in de Toledo, Buonanno et al. 2011).

## 1.5.2 Experimental approaches to study non-targeted effects

**Tissue culture system**

Different tissue culture systems to study bystander effects can be used; they are divided in two groups (reviewed in Hamada, Maeda et al. 2011). In the first, irradiated and bystander cells are in physical contact at the time of irradiation permitting direct physical interactions between cells (direct intercellular communication). This includes confluent cell monolayers (Figure 1-9 a) (Nagasawa and Little 1992) and, three-dimensional clusters of cultured cells (Bishayee, Rao et al. 1999; Bishayee, Hill et al. 2001) or cultured cells maintained in a matrix (artificial tissue) (Belyakov, Mitchell et al. 2005) exposed to low fluences of particulate radiations that target only a small fraction of the cells in the exposed population. Partially-shielded tissues harvested from rodents where also exposed to electromagnetic radiations (Khan, Hill et al. 1998). More recently, non-targeted effects studies with electromagnetic (Mothersill, Smith et al. 2007; Koturbash, Kutanzi et al. 2008) and particulate (Jain, Li et al. 2011) radiations were performed *in vivo* using fish, mice and rats. The latter studies are reminiscent of abscopal effects observed clinically decades prior to the emergence of non-targeted effect studies using tissue culture systems (Parsons, Watkins et al. 1954; reviewed in Mothersill and Seymour 2004).

In the second group, there is no direct contact between cells at the time of irradiation, but stressful bystander effects can be transmitted through diffusible factors. This involves sparsely seeded cells where irradiated cells and bystander cells coexist at the time of exposure to low fluences of particulate radiations (Figure 1-9 b) and system where irradiated cells are co-cultured with bystander cells after irradiation. Strategies involving the transfer of conditioned medium (Figure 1-9 c) donated from irradiated cells to non-irradiated cells grown in separate dishes (Mothersill and Seymour 1997) or the use of inserts where, after exposure, the irradiated cells interact with bystander cells by sharing medium (Figure 1-9 d)

(Fournier, Becker et al. 2007; Yang, Anzenberg et al. 2007; Yang, Anzenberg et al. 2007) or by physical contact (Figure 1-9 e) (Buonanno, de Toledo et al. 2011) have been used. In the context of studies with HZE particles, in the insert or medium transfer strategies, bystander cells, which are co-cultured with irradiated cells after exposure, are not subject to traversal by δ rays or secondary fragmentation products.
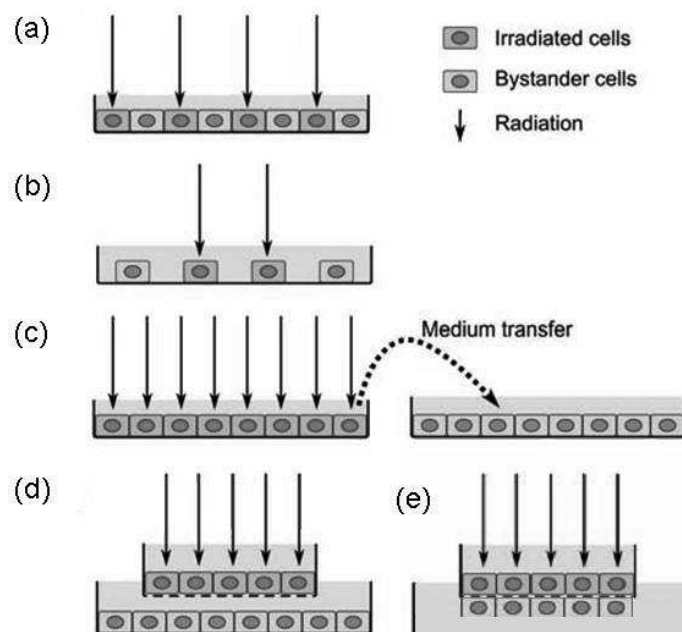


**Figure 1-9: Tissue culture systems used for non-targeted effects studies. (a) Confluent monolayer culture. (b) Sparsely populated monolayer culture. (c) Medium transfer from irradiated culture to non-irradiated one. (d) Two-compartments co-culture dish in contact by sharing medium. (e) Two-compartments co-culture dish in contact by physical contact. (Adapted from Hamada, Maeda et al. 2011)**

## Irradiation systems

There are two types of external irradiation system for non-targeted effect studies. On one hand, precise microbeams of α particles, helium ions, X rays, electrons or protons (Figure 1-10 a) can deliver a preset dose or exact number of particles to a single cell or the sub-structures of a cell (e.g. nucleus (Zhou, Randers-Pehrson et al. 2000) or cytoplasm (Wu, Randers-Pehrson et al. 1999)) with micron precision. On the other hand, broadbeams that emit very low fluences (Figure 1-10 b) of α particles estimated following Poisson distribution

have been effectively used to study bystander effects under non-perturbing conditions (as explained in the paragraph 1.3.2) (Azzam, de Toledo et al. 2001). Broadbeam irradiators are also used in high dose/fluence experiments involving medium transfer, co-culture of irradiated and bystander cells (Figure 1-10 c) (Yang, Anzenberg et al. 2007) and exposure of partially-shielded cell cultures (Figure 1-10 d). In our laboratory, broadbeam irradiation has also been used to examine the propagation of stressful effects among irradiated cells (Autsavapromporn, de Toledo et al. 2011).

In the experiments used in this project confluent cell cultures maintained on plastic or glass surfaces were exposed to α particles or heavy ions, respectively, from broadbeams. In case of heavy ions, the irradiated and non-irradiated cells were subject to δ rays and secondary fragmentation products that may modulate signaling events elicited by the primary impacting particles.
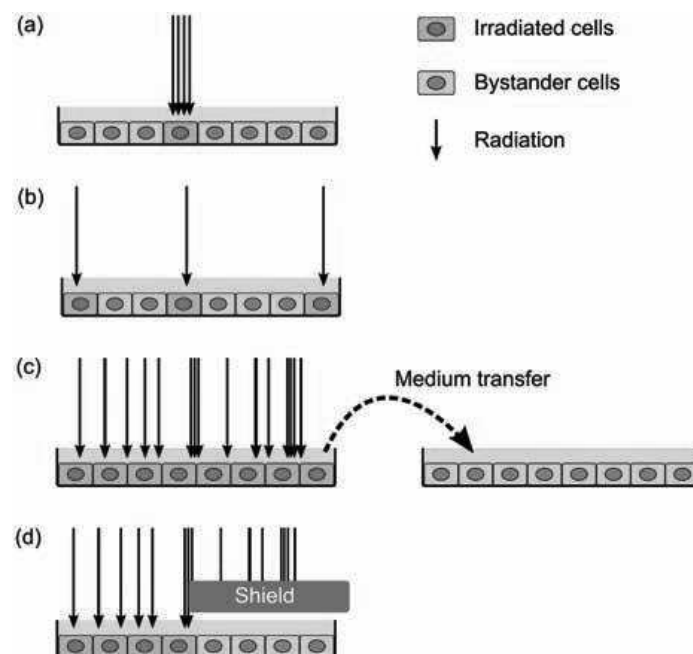


**Figure 1-10: Irradiation systems used for non-targeted effects studies. (a) Precision microbeam. (b) Low-fluence broadbeam. (c) High-Fluence broad beam and medium transfer. (d) Broadbeam with partial shielding. (Adapted from Hamada, Maeda et al. 2011)**

### 1.5.3  The bystander effect

The term bystander effect was borrowed from the gene therapy field where it usually refers to the death of tumor cells as a result of targeting a single cell type within a mixed population.

The bystander effect is a biological/biochemical change expressed by a cell that is not directly targeted by ionizing radiation, but happens to be in proximity to a targeted cell. It is mainly an effect of intercellular signaling by which cells damaged by ionizing radiation transmit signals to neighboring cells leading to important biological change.
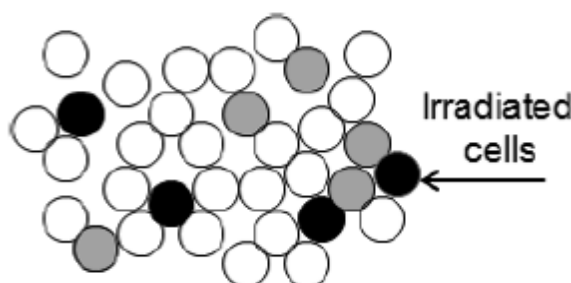


**Figure 1-11: Radiation-induced bystander effect. In an exposed cell culture where only few cells (in black) are directly irradiated, biological effects are observed in neighboring non-irradiated cells (gray cells).**

The pioneering radiation-induced bystander effect in monolayer cell cultures exposed to α particles from a broadbeam irradiator was reported in 1992 by Nagasawa and Little (Nagasawa and Little 1992). A rate of 30 to 45 % of Chinese hamster ovary (CHO) cells displayed an increase in sister chromatid exchanges (SCE) (a type of genetic damage) (Figure 1-9 a) when less than 1 % of nuclei had been traversed by a particles track. Subsequently, the α-particle-induced bystander effect was confirmed by several biological indicators, including sister chromatid exchange (Nagasawa and Little 1992; Deshpande, Goodwin et al. 1996), micronuclei formation (Azzam, de Toledo et al. 2001; Belyakov, Malcolmson et al. 2001; Azzam, De Toledo et al. 2002; Shao, Furusawa et al. 2003; Kashino, Suzuki et al. 2007; Shao, Prise et al. 2008), cell differentiation (Belyakov, Folkard et al. 2006), nuclear DNA

mutation (Nagasawa and Little 1999; Zhou, Randers-Pehrson et al. 2000), modulation of stress-responsive genes (e.g. TP53, CDC2, rad51, NFκB, P38$^{MAPK}$) (Azzam, de Toledo et al. 1998; Azzam, de Toledo et al. 2001) or increase of intracellular reactive oxygen species (ROS) (Narayanan, Goodwin et al. 1997; Azzam, De Toledo et al. 2002) in a proportion of cells greater than those initially traversed by α particles.

On the other hand, the characterization of bystander effects in cell populations exposed to very low fluences of high charge (Z) and high energy (E) (HZE) particles, another type of high-LET radiation, are only emerging, and conflicting data, using different *in vitro* cell culture systems, have been reported. In initial experiments with microbeams (Figure 1-10 a) which allow selected cells to be individually hit with precise numbered particles, stressful effects were shown to be transmitted from HZE-particle-irradiated cells to contiguous bystander cells (Shao, Furusawa et al. 2003; Hamada, Ni et al. 2008; Harada, Nonaka et al. 2009). Even when only a single cell within the confluent culture was hit by one particle of $^{40}$Ar (~1260 keV/μm) or $^{20}$Ne (~380 keV/μm), a 1.4-fold increase of micronucleated cells was detected demonstrating a bystander response. The increase in micronuclei was approximately 2-fold higher than control levels when 49 cells in the culture were individually hit by 1 to 4 particles, but it was independent of the number and LET of the particles (Shao, Furusawa et al. 2003).

In subsequent experiments whereby HZE-particle-irradiated cells were co-cultured with bystander cells in a manner in which they only shared growth medium (Figure 1-9 d), stressful responses were also induced in the bystander cells and were similar in nature to those induced in the targeted cells (Fournier, Becker et al. 2007; Yang, Anzenberg et al. 2007; Yang, Anzenberg et al. 2007). Furthermore, oxidative stress and DNA damage persisted in distant progeny of bystander cells that had been in contiguous co-culture with HZE-particle-irradiated cells (Figure 1-9 e) (Buonanno, de Toledo et al. 2011).

However, other experiments involving the transfer of growth medium from irradiated cultures to recipient bystander cells present in a separate dish (Figure 1-9 c) (Groesser, Cooper et al. 2008; Sowa, Goetz et al. 2010), or the targeting of an exact number of cells in a population with energetic heavy ions from microbeam (Fournier, Barberet et al. 2009) did not detect an effect with a variety of endpoints and cell types. Several factors may underlie the absence of observable effects, in this case, including timing of endpoint measurement, dilution of the inducing factor and the metabolic state/redox environment of the recipient cells.

**Possible mechanisms underlying the bystander effect**

A series of experiments in different laboratories suggested various mechanisms by which signals can be transmitted from irradiated to non-irradiated cells. Gap-junction intercellular communication (GJIC) and secreted diffusible factors have been shown to mediate bystander effects. The ROS seem to be also involved in mediating the intercellular communication. Among the different mechanisms direct evidence for involvement of GJIC in bystander effects was generated (Azzam, de Toledo et al. 2001).

***Gap-junction intercellular communication***

Homeostatic functions of multicellular organisms are based on a complex system of communication, allowing cells to interact with each other in a coordinated manner and with the environment. This organization is based, among other *modes of interactions,* on a method of direct and economic communication through gap junctions.

*Gap junction*

Gap junctions are defined as cell–cell channels where two plasma membranes from contacting cells appose each other with an apparent hydrophilic separation gap of 2–3 nm (Naus and Laird). The gap is bridged by hemichannels or connexons formed from a family of 21 human proteins called connexins (Figure 1-12).
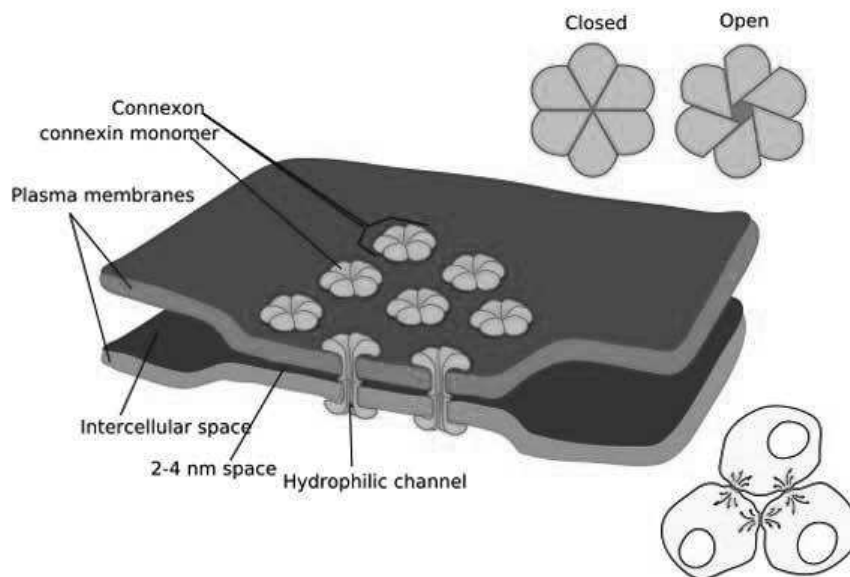


**Figure 1-12: Simple Cartoon Structure of Gap Junction**
**(http://php.med.unsw.edu.au/cellbiology/index.php?title=2011_Group_2_Project).**

Connexons can be homomeric or heteromeric as they are composed by the same or different types of connexins resulting in homotypic or heterotypic channels (Figure 1-13).
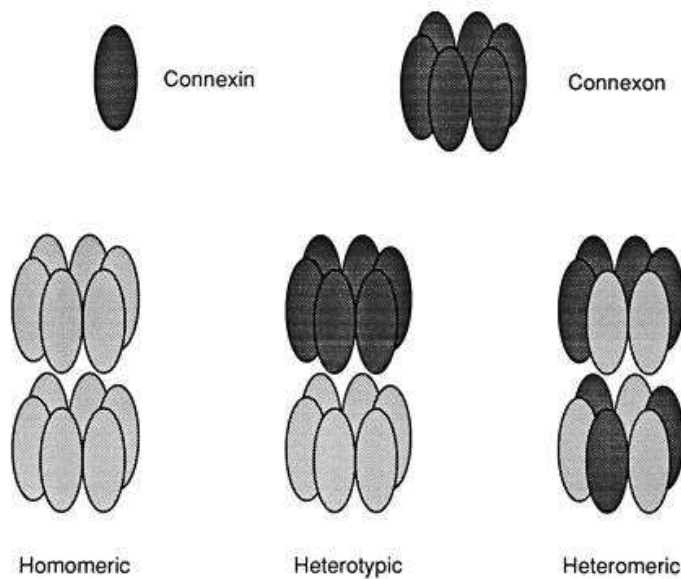
**Figure 1-13: Schematic drawing of possible assembly patterns of connexins into complete gap junction channels (http://php.med.unsw.edu.au/cellbiology/index.php?title=2011_Group_2_Project).**

Gap junction channels exchange small molecules typically ranging in ~2000 Daltons in size (Harris 2007), such as soluble second messengers, amino acids, nucleotides, calcium ions, glucose and electrical signals, through a process called gap junctional intercellular communication (GJIC) (Goodenough and Paul 2009). Recent reports indicate that molecules of 6000 Daltons, such as micro-RNA can also diffuse through gap junctions (Wolvetang, Pera et al. 2007). Junctional communication can be visualized by intracellular microinjection of fluorescent tracers such as Lucifer yellow (Stewart 1978) whose spread into neighboring cells can be monitored microscopically (el-Fouly, Trosko et al. 1987). Junctional channels can be established between all cells belonging to the same tissue. GJIC plays essential roles in a multitude of cellular processes including cell migration, proliferation, differentiation, and apoptosis (Wolvetang, Pera et al. 2007).

Connexin channels have been shown to be highly selective among molecular permeants. The selectivity among cytoplasmic permeants is not simply on the basis of size or charge. Although connexin channels are permeable to second messengers (Harris 2001), different connexins form channels with different selectivities for second messengers

(Niessen, Harz et al. 2000; Goldberg, Moreno et al. 2002; Bedner, Niessen et al. 2006). For example, ATP, ADP, AMP, glutamate and glutathione are significantly more permeable through junctional connexin43 than connexin32 channels. On the other hand, adenosine and inositol triphosphate (IP3) are more permeable through connexin32 than through connexin43 channels.

*Mechanisms*

The role of gap junction communication in the propagation of bystander stressful effects following exposure to low fluence of α particles has been initially studied by Azzam et al. (Azzam, de Toledo et al. 1998) in confluent cell cultures. In early experiments, relative to control, western blot analyses of cell lysates from exposed cultures revealed 3-4 fold increase in level of p53 and p21$^{Wafl}$ when only 5 % of nuclei were traversed by α particles. These increases were reduced when the cultures were irradiated in presence of lindane[c], a gap-junction inhibitor. Subsequent experiments generated direct evidence for the involvement of functional gap junctions in propagation of α particle-induced stressful bystander effects (Azzam, de Toledo et al. 2001). When cultures of an isogenic pair of rat epithelial cells that differ in their ability to perform GJIC were exposed to low fluence α particle, bystander induction of p21$^{Wafl}$, as detected by *in-situ* immunoblotting, was observed in the GJIC proficient cultures only. The induced p21$^{Wafl}$ occurred in characteristic aggregates of neighboring cells, further supporting the view that damage signals were communicated from irradiated to bystander cells in a GJIC-dependent manner. In contrast, in GJIC-deficient cultures exposed to low fluences of α particle, only single isolated and presumably irradiated cells invariably exhibited up-regulation of p21$^{Wafl}$. The magnitude of the contribution of bystander cells to the overall response of irradiated cultures was notably reflected in western blot analyses. While up-

---

[c] Lindane: γ-hexachlorocyclohexane isomer

regulation of p21$^{Wafl}$ was observed in GJIC proficient/connexin43 wild-type mouse embryo fibroblast cultures exposed to mean doses as low as 0.6 cGy; a dose of 10 cGy was required to detect an effect in GJIC-deficient/connexin43 knockout cultures (Azzam, de Toledo et al. 2001).

The participation of gap junctions in bystander effects was further confirmed in cell survival (Bishayee, Rao et al. 1999) and DNA mutation studies (Zhou, Randers-Pehrson et al. 2000). The cytotoxic effect observed in bystander cells when they were grown with tritiated thymidine labeled cells was significantly attenuated by lindane (Bishayee, Rao et al. 1999; Bishayee, Hill et al. 2001). In related experiments, chemical inhibition of GJIC prevented the growth disadvantage effect that occurs within mouse aggregation chimeras comprised of γ-irradiated and non-irradiated cleavage-stage embryos (Vance and Wiley 1999). Furthermore, a pre-treatment of cells with gap junction inhibitors eliminated the 3-fold increase in mutation frequency observed following targeting only 20 % of cells with 20 α particles each using microbeam irradiation. Similarly, propagation of stressful effects from α-particle-irradiated cells leading to DNA mutation in bystander cells was eliminated when cells carrying a dominant negative connexin 43 vector abrogating GJIC were used in experiments (Zhou, Suzuki et al. 2001). Whereas, these studies provide strong evidence for involvement of gap junction intercellular communication, these studies do not exclude other pathways for the propagation of radiation effects to bystander cells. Although many studies with normal cells display evidence that gap-junction intercellular communication is essential, others studies with tumor cells show bystander effects in absence of GJIC.

Participation of GJIC in stress-induced bystander effects is not unique to ionizing radiation; it has also been described in high density cells exposed to chemotherapeutic agents. Toxicity of these compounds was enhanced by functional GJIC in target cells (Freeman, Abboud et al. 1993; Fick, Barker et al. 1995; Kuriyama, Nakatani et al. 1995; Mesnil, Piccoli

et al. 1996; van Dillen, Mulder et al. 2002; Kalvelyte, Imbrasaite et al. 2003; Jensen and Glazer 2004). Thus, many systems show that GJIC enhances the effects of toxic agents on targeted and untargeted cells. Junctional communication may also lead to induction of protective effects that attenuate damage in targeted cells (Wygoda, Wilson et al. 1997). The determinants and mechanism(s) of these effects, however, remain largely undefined.

## Diffusible factors and Involvement of oxidative metabolism

### Diffusible factors

In addition to junctional communication, a large number of studies have shown that bystander responses occur when bystander cells are incubated with culture medium harvested from irradiated cells (Mothersill and Seymour 1997; Mothersill and Seymour 1998; Iyer and Lehnert 2000; Iyer, Lehnert et al. 2000; Barcellos-Hoff and Brooks 2001; Yang, Asaad et al. 2005). The observation of bystander effects under such conditions suggested that cell-to-cell contact via GJIC was not necessarily needed and implied that GJIC was not the only pathway mediating bystander effects. These two pathways, however, are not necessarily exclusive of each other. Moreover, not all cell types can produce bystander signals, and not all cell types would respond to these signals. The mechanisms underlying bystander effects are likely to depend on cell/tissue types, their phenotype (metabolic state, age, pre-exposure to other stresses) and their micro-environment.

The released factor causing the ionizing radiation-induced bystander effect has yet to be elucidated. The factors leading to such effects appeared to be released by irradiated cells within the first few hours after exposure. It was suggested that the released factor may be a protein, as it was labile when heated but stable when frozen. Cytokines or other factors that

act to increase intracellular levels of ROS/RNS in bystander cells have been considered as candidates (Mothersill and Seymour 1997; Iyer and Lehnert 2000; Iyer, Lehnert et al. 2000).

Pro-inflammatory diffusible factors (e.g. IL-8) were reported as initiator of bystander response in primary normal lung fibroblast exposed to α particles (Narayanan, LaRue et al. 1999; Facoetti, Ballarini et al. 2006). Transforming growth factor (TGF)-ß1 has also been shown to play a role in radiation-induced bystander signaling (Barcellos-Hoff and Brooks 2001; Shao, Folkard et al. 2008). Using double-Mylar dishes whereby cells are plated on one or both sides of the dish, a bystander effect was detected when cells on one side were targeted by a high dose of α particles. It was suggested that TGF-β1 secreted by irradiated cells in the medium may have a role in mediating the bystander response (Zhou, Suzuki et al. 2002).

Increased levels of Tumor Necrosis Factor (TNF-α) in A549 cells or TNF-related apoptosis-inducing ligand (TRAIL) in H640 cells were observed after exposure to ionizing radiation under bystander conditions (Shareef, Cui et al. 2007). Importantly, apoptosis has been reported to be a significant pathway of cell death induced by exposure to bystander factors (Belyakov, Malcolmson et al. 2001; Lyng, Seymour et al. 2001). Calcium is an important signaling molecule as changes in intracellular calcium modulate cell functions and can lead to apoptosis (Clapham 1995). Increase in calcium concentration has been shown to cause mitochondrial ROS formation and loss in mitochondrial membrane potential in bystander cells recipient of medium from irradiated cells (Lyng, Seymour et al. 2002).

More recent experiments examined the effect of dilution of the irradiated cell conditioned medium (ICCM) on the bystander effect. Results indicated that the effect of ICCM from different cell lines reached a plateau at different dilutions, which correlated with inherent radiosensitivity of the cells investigated. These finding suggested a role for chemical-mediated activation of a signaling molecules and implicated ROS/RNS in the response (Ryan, Smith et al. 2008).

In earlier studies, it was shown that α-particle irradiation of culture medium devoid of cells caused the generation of SCE-inducing factors; such factors, however, were short-lived (Lehnert, Goodwin et al. 1997). Supernatant from irradiated cells or irradiated medium caused the induction of SCE in non-irradiated cells to the same extent observed following exposure of cell cultures to low fluences of α particles (Lehnert, Goodwin et al. 1997). Interestingly, both medium and cell-derived SCE-inducing effects were inhibited by SOD, suggesting that ROS are involved in these responses.

*Oxidative metabolism*

Cellular exposure to high levels of reactive oxygen species (ROS) produced by endogenous enzymatic reactions or induced by external agents can contribute to numerous human diseases and disorders (Droge 2002). Intracellular accumulation of oxidants results in modification of proteins, DNA and lipids (Halliwell 1996). Persistence of such damages and their transmission to daughter cells may contribute to the development of cancer, atherosclerosis, accelerated aging and other degenerative diseases (Finkel and Holbrook 2000). On one hand, excessive ROS production alters several redox-regulated physiological processes (Droge 2002). On the other hand, low levels of ROS participate in signaling pathways that control essential cellular functions including proliferation (Torres 2003). Together, these studies suggest that ROS maintain normal cellular functions by regulating the expression of specific genes (Price and Calderwood 1992; Allen and Tresini 2000; Herrlich and Bohmer 2000; Meplan, Richard et al. 2000), modulating ion channel activities (Lopez-Barneo, Lopez-Lopez et al. 1988), and mimicking or affecting intermediates (e.g. second messengers) in signal transduction (Schulze-Osthoff, Baur et al. 1997).

Oxidative metabolism has been implicated in radiation-induced bystander effects at the onset of interest in these studies (reviewed in Azzam, de Toledo et al. 2003). Importantly,

oxidative metabolism is a regulator of gap-junction communication (Trosko and Chang 2001; Bertram 2004) that mediate bystander effects (Azzam, de Toledo et al. 1998)

In 1992, Nagasawa and Little postulated the participation of ROS in the mechanism of radiation-induced bystander effects (Nagasawa and Little 1992). This has been confirmed by extensive studies showing the involvement of the superoxide anion ($O_2^{\cdot-}$). A disproportionate increase in the fraction of cells with DNA damage (SCE, micronuclei) in cultures exposed to 1 or 2 cGy of α particles was significantly reduced when the exposed cultures were pre-incubated with SOD or catalase (Narayanan, Goodwin et al. 1997; Azzam, De Toledo et al. 2002). Importantly, incubation of cells with active, but not boiled SOD, attenuated micronucleus formation in bystander cells (Azzam, De Toledo et al. 2002).

Narayanan et al. showed that activation of plasma membrane-bound nicotinamide adenine dinucleotide phosphate (NAD(P)H) oxidase in normal human lung fibroblasts is responsible for the increase of ROS, including intracellular superoxide anion and concomitant increases in hydrogen peroxide ($H_2O_2$) in bystander cells. In their experiments, bystander cells were incubated with serum-containing culture medium exposed to α particles or incubated with supernatants from α-irradiated cells (Narayanan, Goodwin et al. 1997). Subsequent experiments by Azzam et al. generated further support for the role of NAD(P)H-oxidase in the α-particle-induced bystander effect (Azzam, De Toledo et al. 2002). Incubation of normal human skin fibroblast cultures with diphenyleneiodonium (DPI), an inhibitor of flavoproteins oxidases such as NAD(P)H oxidase, reduced the excessive formation of micronuclei and inhibited the up-regulation of p21[Waf1] in bystander cells in confluent cultures exposed to a mean absorbed dose of 0.3 cGy (a dose at which ~1 % of nuclei is traversed by an α particle track).

The role of oxidative stress in the genetic changes induced in bystander cells was also supported by microbeam studies (Wu, Randers-Pehrson et al. 1999) where only the

cytoplasm was traversed by α particles. In presence of dimethyl sulfoxide (DMSO), a scavenger of free radicals (primarily hydroxyl radical), the frequency of mutation at the CD59 locus was suppressed by 4- to 5-fold to near background levels. Incubation of cells with buthationine sulfoximine (BSO), that depletes cells of the antioxidant glutathione, promoted excess ROS levels, and resulted in mutation frequency that was 4- to 5-fold higher than background. Wu et al. suggested that free radicals generated by cytoplasm irradiation have a lifetime long enough to migrate to the nucleus and induce oxidative nuclear DNA damage (Wu, Randers-Pehrson et al. 1999). Similar to bystander effect studies, these results show that DNA damage is not necessarily the result of direct DNA traversal by an irradiating particle. Subsequent studies by Tartier et al (Tartier, Gilchrist et al. 2007) have shown that cytoplasmic irradiation also propagates stressful effects leading to DNA damage in bystander cells.

ROS participate in the regulation of expression and activity of p53 (followed by downstream effectors p21$^{Wafl}$, MDM2, p34cdc2), mitogen-activated protein kinases (MAPK), extracellular related kinase (ERK1/2), and several redox-modulated transcription factors (e.g. c-Jun N-terminal kinase (c-JNK), AP-1, etc...) in bystander cells (Azzam, De Toledo et al. 2002). Incubation of low fluence α-particle-irradiated cultures with antioxidants attenuated the bystander induction of the latter proteins.

Interestingly, although micronuclei induction in low fluence α-particle-irradiated cell cultures was partly reduced by treatment with DMSO, a scavenger of reactive oxygen species (ROS), maximal protection of the bystander cells was observed when the cultures were irradiated in presence of mixture of DMSO and PMA[d], an inhibitor of GJIC (Shao, Furusawa et al. 2003). Accordingly, both ROS and GJIC contribute to bystander responses, and GJIC

---

[d] PMA: 4_ , 9_ , 12_, 13_, 20-pentahydro-xytiglia-1,6-dien-3-one 12_ -myristate 13-acetate

may play an essential role by mediating the release of soluble biochemical factors from targeted cells.

Besides reactive oxygen species, nitric oxide (NO) and other reactive nitrogen species (RNS) were also proposed as mediators of radiation-induced bystander effect (Shao, Stewart et al. 2003). The lifetime of nitric oxide (with duration of seconds) is extensively longer than that of certain ROS (e.g. superoxide) that last only nano- to micro-second). Although $NO^{\bullet}$ is chemically inert toward most cellular constituents (except for heme), it reacts with $O_2^{\bullet-}$ to form the peroxynitrite anion ($ONOO^-$) with a rate constant that is larger than that for the superoxide dismutase (SOD)-catalyzed dismutation of $O_2^{\bullet-}$ (Jay-Gerin and Ferradini 2000). Like hydroxyl radicals, $ONOO^-$ is also highly reactive and capable of attacking a wide range of cellular targets, including lipids, thiols, proteins and DNA bases. This high reactivity of $ONOO^-$ implies low selectivity, confined reactivity with molecules in immediate vicinity, and inability to act as a cellular messenger. By contrast, the much lower reactivity of $O_2^{\bullet-}$ and $H_2O_2$ allows them to rapidly diffuse a longer distance away from the originating site.

In presence of a NO-specific scavenger (c-PTIO[e]), DNA damage induction, revealed by micronuclei, was significantly attenuated in human glioblastoma T98G bystander cells from cultures irradiated with α particles from a microbeam (Shao, Stewart et al. 2003). Nitric oxide mediate also the accumulation of TP53 and heat shock protein 72 (hsp72) levels in wild-type TP53 gliobastoma cells co-cultured with, or recipient of conditioned medium from X-ray-irradiated mutant TP53 gliobastoma cells (Matsumoto, Hayashi et al. 2001). The accumulation of those proteins was abolished by the addition c-PTIO to the medium (Matsumoto, Hayashi et al. 2001). Collectively, these findings indicate the potential importance of an intercellular signal transduction pathway initiated by nitric oxide in the cellular response to ionizing radiation.

---

[e] Nitric oxide scavenger: 2-(4-carboxyphenyl)-4,4,5,5- tetramethylimidazoline-1-oxyl-3-oxide (c-PTIO)

Using a broad beam α particle irradiator and special dishes where the cells to be targeted were grown on a 6 μm polyethylene terephthalate (PET, also known as Mylar), and the bystander cells grown on 38 μm striped PET insert, Zhou *et al.*, showed that the expression of cyclooxygenase-2 (COX-2, also known as prostaglandin endoperoxide synthase-2) signaling cascade play a role in the bystander effect. When COX-2 was inhibited, the bystander effect decreased (Zhou, Ivanov et al. 2005). Moreover, MAPK pathways (ERK1/2, c-JNK, p38) that are essential to activation of COX-2 may play an important role in this process; when MAPKs were suppressed, the bystander effect was inhibited. These results provide evidence that the COX-2-related pathway, an essential mediator of the cellular inflammatory response, is a critical signaling link for the bystander phenomenon.

Hence our understanding of mechanisms has greatly advanced since the bystander effect was first characterized in cell cultures exposed to low fluence α particles.

## 1.5.4 Genomic instability

The genome in mammalian cells is constantly challenged by destabilizing factors including normal DNA replication and cell division, spontaneous DNA damage and oxidative stress from normal oxidative metabolism. In addition, cells may be exposed to stress from extracellular environmental agents, including genotoxic chemicals and exposure to environmental (e.g. radon), diagnostic and occupational radiation (Little 2003). Different mechanisms of DNA repair are activated to maintain genomic integrity. However, failure in those processes can lead to destabilization of the genome. Failure of cells to repair DNA damage correctly may contribute to mutagenesis and/or genome instability that can lead to carcinogenesis, aging, inherited disease, and cell death (Little 2000; Sutherland, Bennett et al. 2000). In the context of high-LET radiation, Kadhim et al. have shown, that cells surviving an α particle exposure harbor genetic lesions that are different in nature from those that

occurred in the irradiated parental cells (Kadhim, Macdonald et al. 1992). Therefore, it has been postulated that exposure to ionizing radiation induces genomic instability that promotes a mutator phenotype that ultimately leads to cancer (Loeb and Loeb 1999; Loeb 2001; Little 2003).

Genomic instability is characterized by genetic changes including chromosomal rearrangements, chromosomal aberrations (Kadhim, Macdonald et al. 1992), micronuclei formation (Belyakov, Prise et al. 1999), gene amplifications, gene mutations and cellular neoplastic transformation (Chang and Little 1991). Reduced plating efficiency (lethal mutations or delayed reproductive death) in cells derived and clonally expanded from an irradiated cell were also observed (Seymour, Mothersill et al. 1986; reviewed in Morgan 2003) (Figure 1-14).
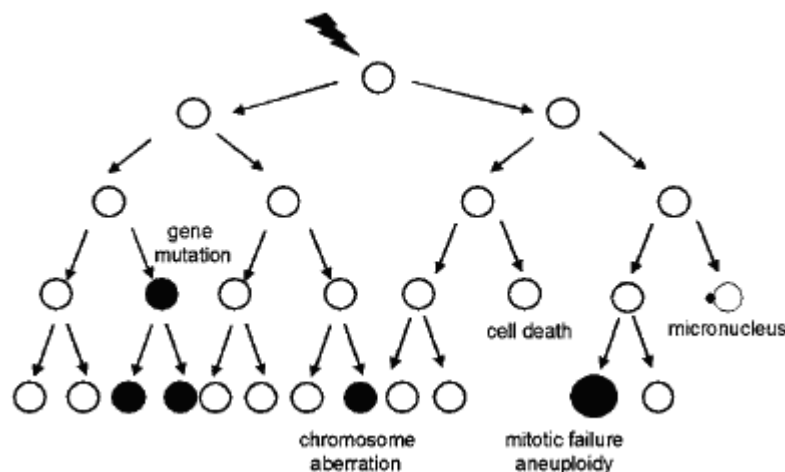


**Figure 1-14: Radiation-induced genomic instability. Progeny of irradiated cells may exhibit genetic alteration including gene mutation and chromosomal aberration many generations of cell divisions after irradiation (Adapted from Lorimore, Coates et al. 2003).**

Genomic instability occurs not only in the progeny of irradiated cells, but also in the progeny of bystander cells. Studies in our laboratory by Manuela Buonanno have shown that stress in bystander cells, which were co-cultured with cells irradiated with iron ions

(1000 MeV/u), persist over several generations in the daughter cells and can lead to neoplastic transformation in these cells (Buonanno, de Toledo et al. 2011).

Similar to its role in the propagation of stressful effects from irradiated to non-irradiated cells in an exposed population, oxidative stress due to perturbations in oxidative metabolism have been implicated in the induction of genomic instability and its propagation to progeny cells (Lorimore, Coates et al. 2003; Morgan 2003). In progeny of bystander cells that were co-cultured with HZE-particle-irradiated cells, an increase in protein carbonylation and lipid peroxidation was observed (Buonanno, de Toledo et al. 2011). Other mechanisms, including dysfunctional DNA repair, epigenetic events and perturbation in gene expression have been implicated in the expression of genomic instability following exposure to ionizing radiation (Kronenberg and Little 1989; Okayasu, Suetomi et al. 2000).

### 1.5.5 Adaptive response

The radiation-induced adaptive response is a protective response whereby exposure to a small priming dose of ionizing radiation protects cells from stress induced by endogenous metabolic processes or a subsequent challenge from ionizing radiation or other environmental agents. Adaptive responses have been mainly observed following *in vitro* or *in vivo* exposures to low doses of LET radiation (typically γ or X rays) delivered at low dose-rate. They are observed, in general, following priming doses between 1 and 100 mGy (Shadley, Afzal et al. 1987). However, they have been also observed following higher γ rays doses delivered at very low dose-rate (Azzam, de Toledo et al. 1992).

Adaptive or hormetic responses were observed as early as the turn of the 20th century by Russian biologists. Renewed interest in their study was stimulated by the landmark study of Olivieri et al. (Olivieri, Bodycote et al. 1984). In that study, the culture of human

lymphocytes with low level of tritiated thymidine protected them from damaging effects leading to chromatid type aberrations induced by a subsequent challenge dose of X rays.

Adaptive responses to ionizing radiation have been found to be dependent on the adapting dose, dose-rate, expression time (Shadley, Afzal et al. 1987; Shadley and Wolff 1987; Shadley and Wiencke 1989), culture conditions (Wolff 1998), pH (Bosi, Micheli et al. 1991) and stage of the cell cycle (Shadley 1994). An adaptive response that protects against DNA damage was shown to be expressed by a reduction in chromosomal aberrations (Khandogina, Mutovin et al. 1991), sister chromatid exchanges (Olivieri, Bodycote et al. 1984), micronucleus formation (Ikushima 1987; Azzam, Raaphorst et al. 1994) and gene mutation (Sanderson and Morley 1986; Kelsey, Memisoglu et al. 1991; Rigaud, Papadopoulo et al. 1993). These observations in cultured mammalian cells mirror the evidence for the existence of radiation-induced protective mechanisms in prokaryotes and lower eukaryotes (Samson and Cairns 1977). Evidence for an adaptive response to ionizing radiation has also been observed *in vivo* (Cai and Liu 1990; Mitchel, Jackson et al. 1999). With direct relevance to cancer risk, exposure to low dose/low dose-rate γ rays was shown to protect against neoplastic transformation in model mouse embryo fibroblasts (Azzam, Raaphorst et al. 1994; Azzam, de Toledo et al. 1996).

Several biological processes may be modulated by low dose/low dose-rate irradiation. Cellular irradiation under such conditions may up-regulate DNA repair mechanisms, affect the overall redox-state of the cell and its anti-oxidation potential. It can also alter chromatin conformation and hence affect the accessibility of DNA lesions to DNA repair machinery. Apoptosis that eliminates heavily damaged cells from the irradiated population may be also involved. Modulation of cell to cell interactions by the low dose priming exposure may also alter the cellular response to the challenge radiation dose (reviewed in de Toledo, Asaad et al. 2006; de Toledo and Azzam 2006; Azzam, de Toledo et al. 2007).

## 1.6  Perspective of the study

In radiation protection, international organizations recommend that the relationship between dose and the risk of developing cancer be considered as linear (BEIR VII 2006). The expression of *bystander effects* induced by energetic particles of high-LET character challenges the traditional dogma that the induction of biological stress is only the product of direct action of radiation on nuclear DNA. The induction of stressful *bystander effects* following low dose radiation exposures suggests that the health risk is underestimated by current radiation protection guidelines (Brenner, Doll et al. 2003).

In case of exposure to environmental radon or galactic cosmic rays encountered during missions in space, only a small fraction of cells in exposed tissues is traversed by an energetic particle (BEIR VII 2006; Cucinotta and Durante 2006; NCRP 2011); the expression of radiation-induced bystander effects, and the observation of genomic instability at extended times after exposure, suggest that a greater fraction of cells may be at risk. In fact, the lack of clear knowledge about non-targeted responses has been singled out by the US National Academies (2008) as one of the important factors limiting accurate prediction of radiation health risks associated with space exploration.

Human epidemiological studies would be ideal to predict the health risks of exposure to low fluences of space particulate radiations; however, given the relatively insignificant number of humans exposed to such radiations, mechanistic studies in tissue culture systems and in animals have been considered essential to estimate corresponding risks to human.

Using molecular, biochemical, physical and computational approaches, this thesis project provides evidence for the propagation of HZE- and α-particle-induced stressful effects from irradiated to neighboring bystander cells. In evaluating biological responses, the structure of HZE-particle-tracks was considered (Goodhead 1989; Ponomarev and Cucinotta 2006). The microscopic structure of the primary HZE-particle-track is characterized by a high

frequency of interactions with the target, which results in highly localized energy depositions (Goodhead 1989; Ponomarev and Cucinotta 2006). Secondary radiations arise from interactions with atomic electrons in target atoms and from fragmentation of the target atoms. These secondaries are produced along the primary particle track and include energetic electrons (δ rays), photons, and α particles and other ions, with different LET. The range of these particles can extend up to several cell diameters (Metting, Rossi et al. 1988; Cucinotta, Nikjoo et al. 1998), thereby potentially irradiating and contributing to biological changes observed in cells that neighbor those targeted by the primary track. In particular, protective mechanisms induced by low-LET secondary radiations (e.g. δ rays, photons) may mitigate stressful effects propagated from cells traversed by the primary particle (Elmore, Lao et al. 2009). To investigate whether secondary particles contribute to bystander effects induced by HZE particles, their contribution to the absorbed dose in relevant targets was calculated using the multi-particle transport code FLUKA (Aiginger, Andersen et al. 2005; Ferrari, Sala et al. 2005; Battistoni, Muraro et al. 2007).

To further understand the mechanisms underlying the biological effects of low fluence particulate radiation, the role of gap junction communication, oxygen tension and DNA repair was investigated in normal human fibroblast cultures exposed to mean absorbed doses as low as 0.2 cGy.

The knowledge gained from these studies may contribute not only to understanding the health risks associated with space exploration but also to radiotherapy. Proton and heavy ion beam therapy as well as immunotherapy with antibodies conjugated to α-emitting particles are being increasingly used worldwide to treat cancer. The propagation of death inducing effects from irradiated to non-irradiated tumor cells may enhance the potency of these treatments. However, the propagation of signaling events that lead to induction of oxidative

stress and DNA damage in neighboring non-irradiated normal cells and their progeny may contribute to long-term health effects, including the emergence of second cancers.

## 1.7  Project hypothesis and Aims

### 1.7.1  General hypothesis

The hypothesis underlying this thesis project is that exposure of normal human diploid fibroblasts to low fluences of particulate radiations with high linear energy transfer (LET) character results in molecular and biochemical events not only in irradiated cells but also in neighbored non-irradiated bystander cells. Further, the magnitude of induced biological responses, in bystander cells, increases with the LET. The effects are modulated by gap junction intercellular communication and by oxidative metabolism; they involve events modulated by the *ATAXIA TELANGIECTASIA MUTATED* (*ATM*) gene and DNA repair activity, and depend on the partial oxygen tension of the medium in which cells are cultured.

### 1.7.2  Aims

**Specific Aim 1**

*To characterize the evolution of biological changes in bystander cells in normal human fibroblast cultures exposed to low fluence of particulate radiations that differ in their LET*

- ✓ Investigate markers of oxidative stress and DNA damage in confluent AG1522 normal human fibroblast populations exposed to mean absorbed doses as low as 0.2 cGy from high charge and high energy (HZE) particles (1000 MeV/u $^{56}Fe^{26+}$ with LET ~151 keV/μm, 600 MeV/u $^{28}Si^{14+}$ with LET~50 keV/μm,

and 290 MeV/u $^{12}C^{6+}$ with LET ~13 keV/μm). Compare the results with those obtained in parallel with 0.92 MeV/u α particles with LET ~109 keV/μm.

✓ Develop a tissue culture system that integrates CR-39 nuclear track detector to distinguish irradiated from non-irradiated cells in cultures exposed to a low fluences of heavy ions.

**Specific Aim 2**

*To calculate, using the multi-particle transport code FLUKA, the doses imparted to AG1522 confluent cells grown on soda-lime glass surface by fragmentation products following exposure to 1000 MeV/u iron ions, 600 MeV/u silicon ions or 290 MeV/u carbon ions.*

**Specific Aim 3**

*To examine mechanisms involved in the propagation of bystander effect in confluent normal human diploid cell cultures exposed to low fluence of HZE particles*

✓ Investigate the involvement of gap junction intercellular communication

✓ Investigate the involvement DNA repair

✓ Investigate the effect of culturing cells at *in vivo*-like oxygen tension

# Chapter 2    Materials and Methods

## *2.1  Cell culture*

AG1522 normal human diploid skin fibroblasts were obtained from the Genetic Cell Repository at the Coriell Institute for Medical Research (Camden, NJ). When actively growing, these cells have a doubling time of 26 h. Cells at passage 10-12 were grown in Eagles' Minimum Essential Medium (MEM) (CellGro, Cat. No. 15010-CV) containing 12.5 % heat inactivated (30 min at 56 ºC) fetal bovine serum (FBS) (Sigma, Cat. No. F6178), supplemented with 4 m$M$ L-alanyl-L-glutamine (CellGro, Cat. No. 25-015-CI), 100 U/mL penicillin and 100 µg/mL streptomycin (CellGro, Cat. No. 30-002-CI). They were maintained in 37 ºC humidified incubators in an atmosphere of 5 % $CO_2$ (vol/vol) in air. For experiments with confluent cultures, cells were seeded at numbers that allowed them to reach the density-inhibited state within 5 days. They were then fed twice on alternate days, and experiments were initiated 48 h after the last feeding. Under these conditions, 95-98 % of cells were in $G_0/G_1$ phase of the cell cycle, as assessed by flow cytometry or tritiated thymidine uptake (Venkatachalam, de Toledo et al. 2008). The synchronization of cells in $G_0/G_1$ phase, by density-inhibition of growth, eliminates complications in interpretation of results that arise from changes in the cellular response to ionizing radiation at different phases of the cell cycle (Terasima and Tolmach 1961).

For experiments with sparse cultures, density-inhibited cells were trypsinized and seeded, 8 h before irradiation, at densities that result in ~50 % confluence. According to this protocol, the cells were in $G_1$ phase of the cell cycle (Venkatachalam, de Toledo et al. 2008).

For HZE-particle-irradiation, the cells were either grown in 25 $cm^2$ polystyrene flasks (Greiner, Cat. No. 690160) for Western blot analyses, or in glass-bottomed flaskettes (Thermo Scientific Nunc, Cat. No. 177453) for *in situ* detection of 53BP1 foci. Cells destined

for α-particle irradiation were seeded in custom-made stainless steel dishes (36 mm internal diameter) with 1.5 μm-thick replaceable polyethylene terephthalate (PET) bottom (known by the brand name "Mylar"). To facilitate cell attachment, the PET surface was precoated with FNC coating mix comprised of fibronectin and collagen (AthenaES™, Cat. No. 0407), overlaid with 2 mL of MEM and incubated at 37 ºC. After 30 min, the medium was aspirated and the cells suspended in growth medium were seeded immediately thereafter.

## 2.2 Irradiation and dosimetry

Confluent density-inhibited cultures of AG1522 fibroblasts were exposed to high-LET radiations. The radiation sources and doses used for experiments, and the distances travelled by the various irradiating particles in water are described in Table 2-1.

**Table 2-1: Characteristics of the radiations and dose delivered to the confluent cell cultures.**

| Radiation source | Symbol $^uX^p$ | Energy MeV/u | LET keV/μm | Range in water Cm | Dose cGy |
|---|---|---|---|---|---|
| **Iron ions** | $^{56}Fe^{26+}$ | 1000 | 151 | 27 | 0.2-10 |
| **Silicon ions** | $^{28}Si^{14+}$ | 600 | 50 | 22 | 0.2-10 |
| **Carbon ions** | $^{12}C^{6+}$ | 290 | 13 | 16 | 0.2-10 |
| **Americium 241 α particles** | $^4He^{2+}$ | 0.92 | 109 | 0.002 | 0.2-10 |

Nucleons (u) = numbers of protons (p) and neutrons. Note that the primary ions are stripped of electrons. Elsewhere in the thesis, the charge is implied but not stated in the text.

For a certain radiation and a specific dose, to calculate the fluence ϕ and fraction of AG1522 cells (800 μm² (Gaillard, Pusset et al. 2009)) or AG1522 cell nuclei (140 μm² (Azzam, de Toledo et al. 1998)), in confluent cultures, traversed by a primary particle, the method of Charlton and Sephton (Charlton and Sephton 1991) was used. The method is outlined in section 1.3.2. The fluences and fractions of cells traversed by an irradiating

particle in confluent cultures exposed to mean absorbed doses ranging from 0.2 to 10 cGy of different particles are reported in Table 2-2. For exposures of 0.2 or 1 cGy, the fluences were confirmed after etching of CR-39 nuclear track detector fused to the bottom of cell culture dishes where the cells grow.

**Table 2-2: Estimates[f] of particle traversals when confluent AG1522 cells (mean nuclear thickness of 1.2 μm (Cornforth, Schillaci et al. 1989), mean nuclear area of 140 μm² (Azzam, de Toledo et al. 1998), and mean cell area of 800 μm² (Gaillard, Pusset et al. 2009)) are exposed to different radiations. P(i) denotes the fraction of cells receiving *i* traversals.**

| Source (Ion) | Dose *cGy* | Fluence *particles/cm²* | Fraction of cells and cell nuclei traversed in average or by specifically 0, 1 or more than 2 particle(s) | | | | |
| --- | --- | --- | --- | --- | --- | --- | --- |
| | | | Whole cell | Nucleus | | | |
| | | | Avg. | Avg. | P(0) | P(1) | P(≥2) |
| **1000 MeV/u iron ions** | 0.2 | $8.3 \times 10^3$ | 0.066 | 0.012 | 0.988 | 0.011 | 0.001 |
| | 1 | $4.1 \times 10^4$ | 0.331 | 0.058 | 0.943 | 0.055 | 0.002 |
| | 5 | $2.1 \times 10^5$ | 1.654 | 0.289 | 0.749 | 0.217 | 0.034 |
| | 10 | $4.1 \times 10^5$ | 3.307 | 0.579 | 0.561 | 0.324 | 0.095 |
| **600 MeV/u silicon ions** | 0.2 | $2.5 \times 10^4$ | 0.200 | 0.035 | 0.965 | 0.034 | 0.001 |
| | 1 | $1.2 \times 10^5$ | 0.999 | 0.175 | 0.840 | 0.147 | 0.013 |
| | 5 | $6.2 \times 10^5$ | 4.994 | 0.874 | 0.417 | 0.365 | 0.218 |
| | 10 | $1.2 \times 10^6$ | 9.988 | 1.748 | 0.174 | 0.304 | 0.522 |
| **290 MeV/u carbon ions** | 0.2 | $9.6 \times 10^4$ | 0.768 | 0.134 | 0.874 | 0.118 | 0.008 |
| | 1 | $4.8 \times 10^5$ | 3.841 | 0.672 | 0.511 | 0.343 | 0.146 |
| | 5 | $2.4 \times 10^6$ | 19.207 | 3.361 | 0.035 | 0.116 | 0.849 |
| | 10 | $4.8 \times 10^6$ | 38.414 | 6.722 | 0.001 | 0.008 | 0.991 |
| **3.7 MeV α particles** | 0.2 | $1.2 \times 10^4$ | 0.092 | 0.016 | 0.984 | 0.016 | 0 |
| | 1 | $5.7 \times 10^4$ | 0.458 | 0.080 | 0.923 | 0.074 | 0.003 |
| | 5 | $2.9 \times 10^5$ | 2.291 | 0.401 | 0.670 | 0.268 | 0.062 |
| | 10 | $5.7 \times 10^5$ | 4.581 | 0.802 | 0.449 | 0.360 | 0.191 |

[f] These estimates do not take into account secondary radiations.

**HZE-particle-irradiations at the NASA Space Radiation Laboratory (NSRL)**

Irradiation with iron ions (1000 MeV/u $^{56}Fe^{26+}$, 'entrance' LET ~151 keV/µm), silicon ions (600 MeV/u $^{28}Si^{14}$+, 'entrance' LET ~50 keV/µm) or carbon ions (290 MeV/u $^{12}C^{6+}$, 'entrance' LET ~13 keV/µm) were performed at the NASA Space Radiation Laboratory (NSRL) at Brookhaven National Laboratory during 2008-2011. Description of the facility and detailed information on the radiation beam can be found at http://www.bnl.gov/medical/nasa/LTSF.asp. Energetic ions are generated in a Tandem Van de Graaff electrostatic accelerator. Ion beams are then transported to the Alternating Gradient Synchrotron (AGS) Booster, where they are pushed to higher energies (Tsoupas, Ahrens et al. 2007) (Figure 2-1). Then, they are extracted slowly into the NSRL beam transport line that generates a uniform beam distribution at the target (Figure 2-2). The energetic ions are usually stripped of their electrons by a 0.051 mm thick copper foil located at the entrance of the NSRL line.
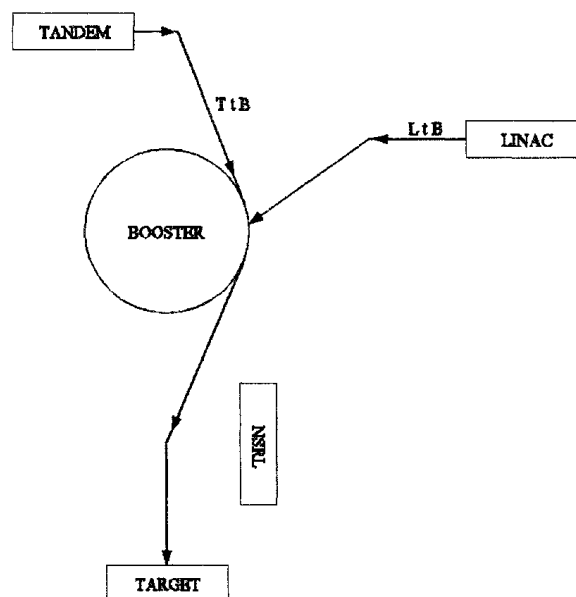


**Figure 2-1: Schematic diagram of the NSRL line in relation to the Booster synchrotron, which accelerates the ions provided by the Tandem accelerator, or the protons produced at LINAC (Tsoupas, Ahrens et al. 2007).**

A set of magnets placed along the transport beam line is used to generate a uniform beam at the target (typical beam uniformities of ± 2 % were achieved over a rectangular area of 20 x 20 cm). Figure 2-2 represents 4 T75 tissue culture flasks with a small amount of medium in the bottom of each flask. The false color image displays relative beam intensity, with black/blue being low intensity and yellow/white being highest. The uniformity of color within the central region of the 20 x 20 cm area shows the uniformity of the beam profile. Hot spots at the periphery are a by-product of octupole focusing magnets.
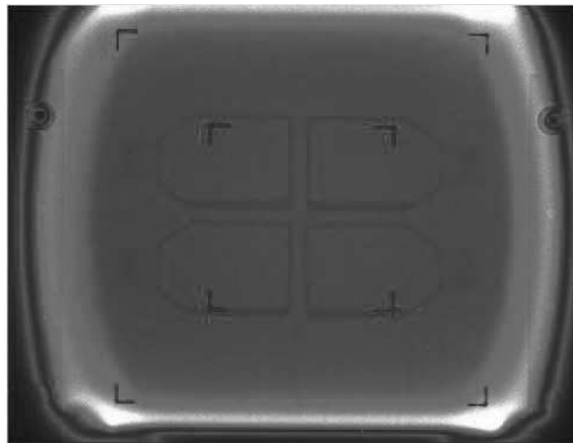


**Figure 2-2: Beam Profile observed using the Digital Beam Imager. Four T75 flasks with a small amount of medium in the bottom of each flask were irradiated. False color indicates the beam intensity is uniform across the 20 x 20 cm exposure area (http://www.bnl.gov/medical/NASA/CAD/Beam_Uniformity_and_Profile.asp).**

The relative LET is measured using the secondary ion chambers as greater and greater thicknesses of high density polyethylene are inserted into the path of the beam. When a critical thickness is reached, the beam particles slow down enough in the polyethylene to stop in the ion chamber, resulting in a peak in LET (i.e. Bragg peak). Typical Bragg curves for 1000 MeV/u iron ions, 600 MeV/u silicon ions and 290 MeV/u carbon ions are shown in Figure 2-3.
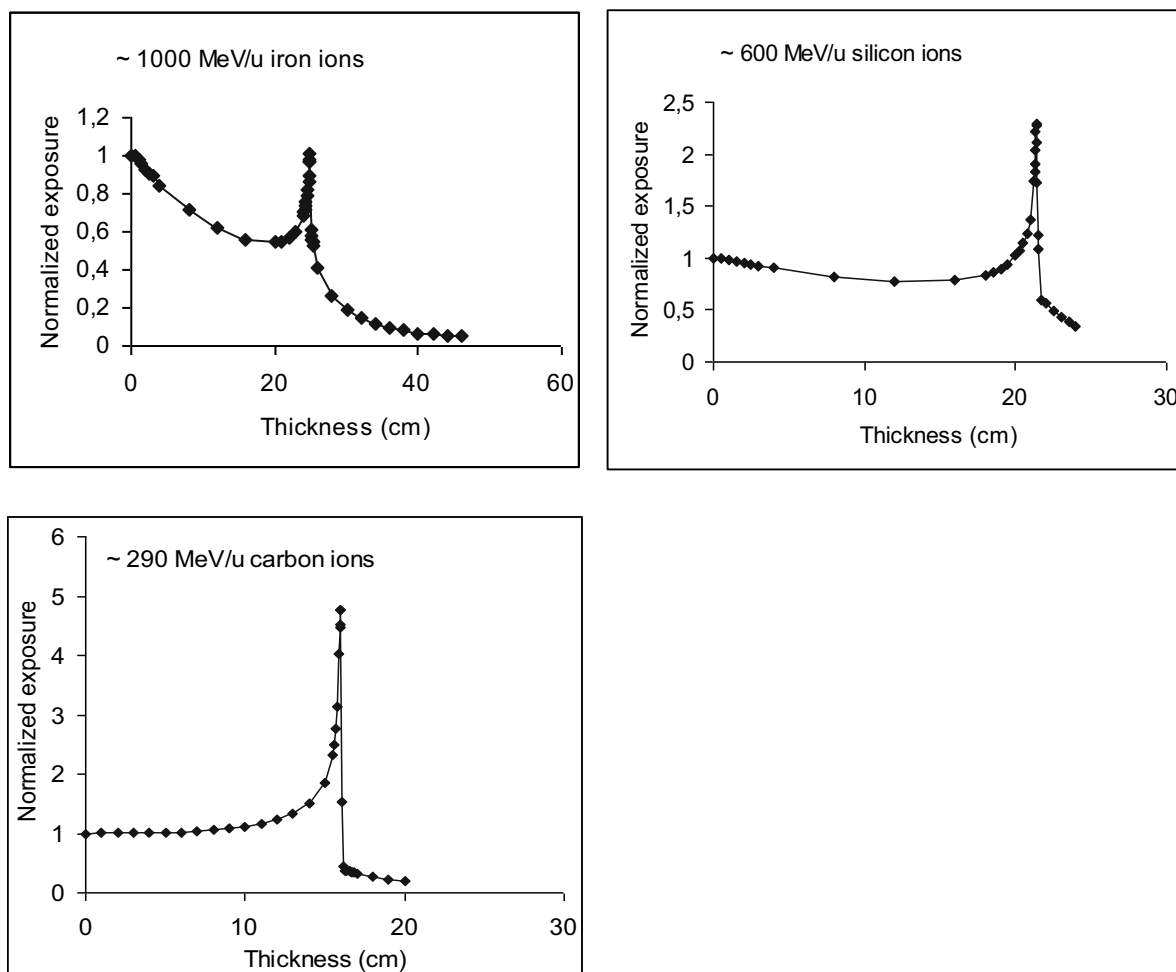
**Figure 2-3: Typical Bragg curves for (A) 1000 MeV/u iron ions, (B) 600 MeV/u silicon ions, (C) 290 MeV/u carbon ions in high density polyethylene ($\rho = 0.97$ g/cm3) with the peak position of, respectively, ~25 cm, ~21 cm, ~16 cm Note that the scales are not the same.**
**(http://www.bnl.gov/medical/NASA/CAD/Bragg/Bragg.asp)**

The cell monolayers were positioned perpendicularly to the beam such as the incident beam first impacted the side of the flask on which the cells were growing and then the growth medium. They were located in the plateau region of the Bragg curve, but were not stacked. The flasks were filled to capacity 3 h prior to irradiation, with pH and temperature-equilibrated growth medium containing 20 % (vol/vol) conditioned medium that was harvested from confluent cultures grown for 48 h. This ensured that during the irradiation, deviation from 37 °C was attenuated and the cells were immersed in this conditioned medium, which alleviates changes in osmolarity and partial oxygen tension. The latter

parameters greatly affect the cellular response to radiation (Gray, Conger et al. 1953 ; Rueckert and Mueller 1960). The incident beam first impacted the side of the flask on which the cells were growing and then the growth medium. The foam sample-holder produces minimal scatter or fragmentation of the incoming heavy ion beam. Note that the foam used to hold the flasks in Figure 2-2 is essentially invisible in the image (www.bnl.gov/medical/NASA/CAD/Sample_Holder_Layout.asp).

Exposures to 0.2, 1 or 10 cGy occurred at mean absorbed dose-rates of 0.2, 1 or 5 cGy/min respectively. Using PMT/Scintillator-based dosimetry measuring the total amount of ionization in a gas sample that is proportional to the square of the beam particle charge, and approximately inversely proportional to the square of the particle velocity, the dose of 0.2 cGy was delivered in 3 or 4 spills at a minimum. Uniformity of the beam across the irradiated flasks was between 1 % and 5 %. The dose just out of the beam (i.e. the beam-related background) is proportional to the beam dose and is on the order of 0.01 % of the dose in the beam. The background radiation due to activation depended on the preceding irradiation; in case our experiment was preceded by a 1 h exposure to the maximum rate of protons delivered at the NSRL, the $\gamma$ ray dose that cells would receive would be at the rate of $\sim 10^{-5}$ cGy/min. Control cells were sham-treated and handled in parallel with the test cultures.

**α-particle-irradiation**

Alpha particle-irradiations were conducted with a 0.2 mCi (7.4 MBq) $^{241}$Am collimated source (half-life of 432.2 years) housed in a helium-filled Plexiglas box located in a custom-made chamber maintained at 37 ºC and an atmosphere of 5 % $CO_2$ (vol/vol) in air. To optimize uniformity of the beam, the source was mounted on a rotating platform (88 rpm) and the exit window was equipped with a beam delimiter. The uniformity was confirmed by etching polyallyl diglycol carbonate plastic (PADC) exposed to the beam for 4 seconds. Cells

were irradiated at a mean absorbed dose-rate of 2 cGy/min (Neti, de Toledo et al. 2004; Gaillard, Pusset et al. 2009). This source disintegrates in three principal emissions of α particles (5.485 MeV (84.5 %), 5.443 MeV (12.8 %), 5.388 MeV (1.6 %)) and photon emission (59.5 keV of γ rays (35.9 %) (Browne. E and Firestone 1986). Irradiation occurred from below, through the PET base. At the cell layer, the α particles have a measured mean energy of 3.7 MeV (0.92 MeV/u) (LET ~109 keV/μm (Watt 1996)) with Full Width at Half Maximum (FWHM) of 0.5 MeV. The irradiator box was fitted with a photographic shutter to allow accurate delivery of the desired mean absorbed dose (Neti, de Toledo et al. 2004). The maximum range of the δ rays produced by a 3.65 MeV α particle is ~0.1 μm (Hamm, Turner et al. 1985); hence, bystander cells in low fluence irradiated cell cultures are unlikely to be targeted by secondary radiation.

## 2.3 Contribution of secondary particles to the absorbed dose

A large portion of the studies in this thesis were performed with cells grown in flaskettes. The purpose was to examine the induction of DNA damage in bystander cells following exposure of the cell cultures to low mean absorbed doses of HZE particles. In these experiments, HZE particles traversed first through the soda-lime glass bottom of the flaskettes before reaching the cells and growth medium (Figure 2-4).
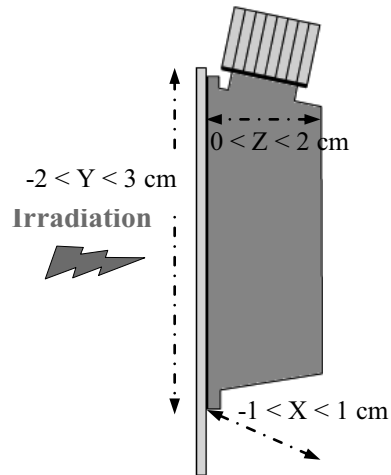
**Figure 2-4: Culture flaskette used in HZE-particle-irradiation of cells**

Some of the HZE interactions with the above target materials may result in fragmentation of the incident (*i.e.* primary) particle and/or of the target material. Fragmentation of the incident HZE particle may produce lower-atomic number (Z) fragments, usually with lower LET. The primary-particle fragments have a high probability to proceed with the same velocity as the primary particle, whereas target fragments generally have lower velocity and can be significantly scattered with respect to the incident-ion-trajectory (Ponomarev and Cucinotta 2006). Furthermore, photons and secondary electrons (δ rays), depending on their energy, can travel significant distances away from the primary particle track (Cucinotta, Katz et al. 1998). Hence, cells that are not directly targeted by the primary ion may be affected by secondary radiation. The effects of these secondary radiations greatly impact the interpretation of results evaluating bystander effects.

To determine whether secondary particles impart a significant absorbed dose to either directly targeted cells, or cells in the vicinity, when a mean absorbed dose of 0.2 cGy is delivered with either 1000 MeV/u $^{56}$Fe ions, 600 MeV/u $^{28}$Si ions or 290 MeV/u $^{12}$C ions, calculations were undertaken, using FLUKA code version 2011.2.15 with the default configuration 'HADROTHErapy'. (Ferrari, Sala et al. 2005; Battistoni, Muraro et al. 2007;

Battistoni, Broggi et al. 2011). FLUKA (FLUktuierende KAskade) is a multi-purpose Monte Carlo particle transport code that considers all particle interactions including electromagnetic interactions, nuclear interactions of the primary or incident particles and the generated secondary particles, energy loss fluctuations and Coulomb scattering.. Several parameters were considered in our simulations with FLUKA. They included transport threshold for particles, delta ray production threshold, and restricted ionization fluctuations. The RQMD model was used, since its interface was developed for the processing of ion-ion interactions from 0.1 GeV/u to 5 GeV/u. The event generators RQMD and DPMJET were linked to ensure ion-ion interactions above 125 MeV/u. The FLUKA evaporation/fission/fragmentation module performed the fragmentation of the primary heavy ions and the de-excitation of the excited fragments. Simulations were undertaken with the transport cut-offs for heavy ions (primary and fragments), photons, protons and α particles set at 1 keV. The transport cut-off for electrons was set at 1 keV when the production threshold for δ rays was 10, 100, and 1000 keV; it was set at 150 eV when the production threshold for δ rays was 1 keV. Production thresholds for δ rays were set at equal value in the cover slip, cell monolayer and medium to ensure that the electronic equilibrium is established (i.e. that the flux of secondary electrons leaving a surface is independent of the surface thickness). This would be a sensitive parameter for a very thin surface like the cell monolayer. Upon reaching the cut-off energy, the particles were assumed to deposit this cut-off energy locally and their tracks were no longer followed.

The contribution of neutrons to the absorbed was calculated but is not shown due to inconsistent results, especially in the cell monolayer. Since the HADROTHErapy option was used, neutrons with energy below 20 MeV cannot be followed with dedicated multi-group library for neutrons with that energy. Benchmarking the FLUKA code with the MCNP code could generate more consistent results for the neutron dose.

Using FLUKA, the radial dose distribution to the AG1522 cell monolayer around the track of a narrow beam of 1000 MeV/u $^{56}$Fe ions was calculated for both the primary particle and its secondaries (HADRONTHErapy configuration with delta rays' production thresholds set at 1, 10, 100, and 1000 keV). Every run was performed with $10^5$ ions, and the absorbed doses to concentric annuli (thickness 1 μm, depth 1 μm) extending to a radius of 100 μm were calculated. The radial distance of 100 μm covers the diameter of an AG1522 cell and extends to adjacent cells.

To re-create experimental conditions, the geometry and the constitutive materials of the flaskettes were specified as input parameters for the code thanks to the graphical user interface named Flair and developed using Python (programming language). The beam at the NSRL is square and has a uniform center of ~20 x 20 cm. Within this area, the flaskette was re-created with a cell growth surface of 10 cm$^2$ and a thickness of 1 μm (Figure 2-4). The cells grew over 1 mm-thick soda-lime glass of 19.152 cm$^2$ in area. The walls of the flaskette consisted of polystyrene. The volumes considered were: soda-lime glass of 1.92 cm$^3$, confluent cell monolayer of 0.001 cm$^3$ and culture medium of 18.8 cm$^3$.

The elemental mole percentage of the soda-lime glass culture surface (ρ ~2.33 g/cm$^3$) was considered to be O (60 %), Si (25 %), Na (10 %), Ca (3 %), Mg (1 %), Al (1 %). The polystyrene (C$_8$H$_8$) walls of the flaskettes have a density of 1.06 g/cm$^3$. For the biological materials, a 1 μm-thick human skin equivalent (W&W type 3 (Woodard and White 1986)) with elemental mass composition of H (10.1 %), C (15.8 %), N (3.7 %), O (69.5 %), S (0.2 %), Cl (0.3 %), Na (0.2 %) and K (0.1 %) and with density of 1.09 ± 0.05 g/cm$^3$ was considered as representative of the cell culture. For simplicity, the growth medium was considered to be water. A water thickness of 1.87 cm represents conditions wherein the flaskette is filled with medium. The absorbed doses calculated by FLUKA were provided in

the output as GeV/g·cm$^3$/primary ion. Radiation absorbed doses in cGy were obtained from the FLUKA output by correcting the values for target volume and the fluence.

The fluence of 8323 of 1000 MeV/u $^{56}$Fe ions/cm$^2$ was experimentally determined at BNL by the scintillator-based dosimetry. This fluence results in 3 329 200 particles over the exposure area of 20 x 20 cm. For 600 MeV/u $^{28}$Si ions, the fluence was 24 480 particles/cm$^2$ resulting in 9 792 000 particles over the 20 x 20 cm exposure area. For 290 MeV/u $^{12}$C ions, the fluence was 96 030 particles/cm$^2$ resulting in 38 412 000 particles over the 20 x 20 cm exposure area. The scintillator-based dosimetry relies on counting the tracks in the beam; when a certain preset number of tracks with high LET characteristic of $^{56}$Fe is reached, the beam is cut-off. This approach was also used in the FLUKA simulations for determining the mean absorbed dose to the various targets from the primary and secondary radiations.

## 2.4 The effect of environmental oxygen concentration on cellular responses to α-particle-irradiation

To examine the effects of environmental oxygen concentration in the cellular responses to low fluence α-particle-irradiation, a custom-made chamber that integrates the latest advances in oxygen monitoring was used. It is equipped with dissolved oxygen sensors that do not consume oxygen, and with controllers for humidity, carbon dioxide and temperature. Oxygen can be controlled at normobaric pressure to within 0.1% of any single set point over the entire 0.1 – 99.9% range. Long-term culturing conditions that permit cells to progressively adapt to various partial oxygen tensions ($Po_2$) thus can be achieved. To reduce stress associated with transfer of cell cultures from ambient $Po_2$ to a more hypoxic

environment, the $Po_2$ can be decreased in a controlled manner at a desired rate (e.g. 1% over 1 h or longer).

For experiments, AG1522 cells were maintained initially in 37 ºC humidified incubators in an atmosphere of 5 % $CO_2$ (vol/vol) in air. After the last feeding, they were transferred to an incubator in the chamber that is maintained at the same atmosphere of 5 % $CO_2$ in ambient air, or in a different incubator within the same chamber where the oxygen concentration was regulated from ambient to a desired concentration below or above 21 % in air over a period of time. For experiments where cells were irradiated at oxygen tension of 0.5 %, the oxygen concentration in air was decreased gradually over 24 h by adding nitrogen gas. Once the desired oxygen level was reached, the cells were further incubated at that atmosphere for additional 24 h. The α particle irradiator used for this project is housed within the chamber; therefore, irradiations were performed at the desired oxygen concentration, 5 % $CO_2$ and 37 ºC.

## 2.5  Chemicals

Different chemicals have been used during experiments.

*Inhibition of DNA repair*

PJ34   or   N-(6-Oxo-5,6-dihydrophenanthridin-2-yl)-N,N-dimethylacetamide,   HCl] (Alexis, Cat. No. 270-289-M005) is an inhibitor of Poly (ADP-ribose) polymerase (PARP), a component of the early response to DNA strand breaks (Huber, Bai et al. 2004). It was dissolved in DMSO. PJ34 was used in the experiments by adding the appropriate volume of stock solution to give a final concentration of 10 μ*M*, 24 h prior to irradiation. The cells were incubated in presence of the drug until they were harvested.

18-α-glycyrrhetinic acid (AGA) (Sigma, Cat. No. G8503), a reversible inhibitor of gap junction communication (Davidson, Baumgarten et al. 1986), was dissolved in DMSO and added to cell cultures at a concentration of 50 $\mu M$ at 30 min prior to irradiation. The cells were incubated in the presence of the drug until they were harvested 3 h later. Under this protocol, AGA did not alter the plating efficiency of unirradiated cells but did inhibit cell coupling. Control cell cultures were incubated with the dissolving vehicle (DMSO).

*t-butyl hydroperoxide treatment*

t-butyl hydroperoxide (Sigma/Aldrich, Cat. No. 458139) was dissolved in growth medium that was conditioned by AG1522 for 48 h and added to cell cultures, 1 h before irradiation, at a concentration of 0.5 $\mu M$. The cells were incubated in the presence of the drug until they were harvested 3 h later.

*ATM Inhibitor*

Ku 55933 or 2-(4-Morpholinyl)-6-(1-thianthrenyl)-4*H*-pyran-4-one (Tocris, Cat. No. 3544), Ataxia-Telangiectasia Mutated Kinase (ATM) inhibitor, was added to cell cultures at a concentration of 10 $\mu M$ at 30 min before irradiation. The cells were incubated in the presence of the drug until they were harvested 3 h later.


## 2.6  Endpoints

### 2.6.1 In situ immune-detection of 53BP1

53BP1 has been proposed as a suitable marker of DNA double-strand breaks (DSB) (Rappold, Iwabuchi et al. 2001). At different times after irradiation, confluent cell cultures were rinsed twice in phosphate buffered saline (PBS), fixed with freshly prepared 3.7 % (vol/vol) paraformaldehyde in PBS for 10 min, and rinsed 5 times with PBS. Subsequently,

the cells were permeabilized with Triton-X buffer (0.25 % Triton-X in water / 0.1 % saponin in Tris-buffered saline (TBS) [25 m$M$ Tris, pH 7.5, 150 m$M$ NaCl, 2 m$M$ KCl in water] for 10 min. The fixed and permeabilized cell monolayers were subsequently blocked for 1 h in blocking buffer [2 % normal goat serum, 2 % BSA, 0.1 % TX-100 (in TBS)] and reacted with rabbit anti-53BP1 antibody (Bethyl, Cat. No. A300-272A) diluted 1:500 (vol/vol) in blocking buffer and incubated for 2 h at room temperature. After incubation with an Alexa Fluor 594 goat anti-rabbit secondary antibody (Invitrogen, Cat. No. A11037), the cells were washed 3 times (5 min/wash) in buffer consisting of 0.2 % normal goat serum, 0.2 % BSA, 0.1 % TX-100 in TBS. SlowFade® Gold antifade reagent with DAPI (Invitrogen, Cat. No. S36938) was used in mounting the samples.

Cells with 53BP1 foci were scored using a UV microscope (Leica DM IL). All the images within the same data set were captured with a ProgRes® camera (Jenoptik) using the same optics and exposure time and were saved for subsequent evaluation. As such, bleaching of the signal was avoided. Identical criteria were followed in defining foci characteristics. Nuclei with atypical size or morphology and those with very high foci counts (presumably appearing in S-phase cells) were not scored (Wilson, Nham et al. 2010). The data described in the thesis represent the excess percent increase of cells with 53BP1 foci in irradiated cultures relative to respective control. They were calculated as follows:

$$\Delta F = 100 \times (F_{irradiated} - F_{control})$$

**Equation 2-1:**

$$\text{where } F = \frac{\text{Number of cells with 53BP1 foci}}{\text{Total number of cells counted}}$$

The data described in Results are representative of at least three independent experiments. For each experiment, 2 irradiated and 2 control dishes were analyzed. For each dish, more than 3000 cells were scored by eye in 40 different fields. Poisson statistics was used to calculate the standard error associated with the percentage of cells with foci over the

total number of cells scored. The Pearson's $\chi^2$ test was used to compare treatment groups versus respective controls. A value of $p \leq 0.05$ between groups was considered significant.

A significant number of cells in control samples harbored foci, which fluctuated between experiments and assay times. When the control samples of all experiments were pooled, the mean $\pm$ SD of the fraction of cells harboring at least one 53BP1 focus was $0.26 \pm 0.12$ with a range of 0.05 to 0.50. The mean $\pm$ SD of spontaneous 53BP1 foci per cell nucleus was $0.35 \pm 0.12$ with a range of 0.06 to 0.68 foci/cell. The mean $\pm$ SD of spontaneous 53BP1 foci per cell nucleus in foci-positive cells was $1.29 \pm 0.11$ foci/cell with a range from 1.04 to 1.35 foci/cell. These results are consistent with those of Ugenskiene et al. who estimated the background level of 53BP1 foci in AG1522 cells to be 1.1 foci/cell (Ugenskiene, Prise et al. 2009). A high background level of nuclear foci indicative of DNA damage was also observed in various cell strains, with inter and intra-individual differences being detected (Wilson, Nham et al. 2010).

## 2.6.2 - Western blot analyses

Following irradiation, the cells were harvested by trypsinization, pelleted, rinsed in PBS, repelleted, and lysed in chilled radio-immune precipitation assay (RIPA) buffer [50 m$M$ Tris-CI (pH 7.5), 150 m$M$ NaCI, 50 m$M$ NaF, 5 m$M$ EDTA, 1 % Nonidet P-40, 0.5 % sodium deoxycholate, 0.1 % SDS] supplemented with sodium orthovanadate (1 m$M$) (Sigma, Cat. No. S3014), protease (1:1000, vol/vol) (Sigma, Cat. No. P8340) and phosphatase (1:1000) (Sigma, Cat. No. 2850) inhibitor cocktails. The mixture of protease inhibitors with broad specificity for the inhibition of serine, cysteine, aspartic proteases and aminopeptidases contains 104 m$M$ 4-(2-aminoethyl)benzenesulfonyl fluoride (AEBSF), 1.5 m$M$ pepstatin A, 1.4 m$M$ E-64, 4 m$M$ bestatin, 2 m$M$ leupeptin, and 80 µ$M$ aprotinin. The mix of phosphatase (e.g. L-isozymes of alkaline phosphatase as well as serine/threonine protein phosphatases

such as PP1 and PP2A) inhibitors contains microcystinLR, cantharidin, and (−)-p-bromotetramisole. The extracted proteins were fractionated by SDS-PAGE and immunoblotted according to standard procedures.

*Protein levels*: The levels of stress responsive proteins were quantified with antibodies against p21$^{Waf1}$ (Millipore, Cat. No. 05-345), p-TP53ser15 (Cell Signaling, Cat. No. 9284S), p-ERK1/2 (Cell Signaling, Cat. No. 9101S), and HDM2 (Sigma, Cat. No. M4308). The anti-connexin 43 (Sigma, Cat. No. c6219) was also used.

*Protein oxidation:* When proteins are oxidized by reactive oxygen species (ROS), some amino acids are modified generating carbonyl groups. These carbonyl groups, specifically of aldehydes or ketones, can react with 2,4-dinitrophenyl hydrazine (DNPH), which in turn can be recognized by anti-2,4 dinitrophenol (DNP) antibodies on immuno-blots (Stadtman 1993). For experiments, the OxyBlot Protein Oxidation Detection Kit (Millipore, Cat. No. S7150) was used. Protein samples were denatured with 6% SDS and derivatized with DNPH (10X 2,4-Dinitrophenylhydrazine Derivatization Solution (100 mM) dissolved in 2 N hydrochloric acid). Negative controls were derivatized with a Derivatization-Control solution (Millipore, Cat. No. S7150). After 15 min incubation at room temperature, neutralization solution (Millipore, Cat. No. S7150) (2 M Tris/30 % glycerol) was added to each tube to stop the reaction and samples were immunoblotted. The DNPH-bound proteins were detected by using rabbit anti-2,4-dinitrophenyl IgG (Millipore, Cat. No. S7150).

*Accumulation of 4-hydroxynonenal protein adducts:* Hydroxyalkenals, such as 4-hydroxynonenal (4-HNE), are among the major products of lipid peroxidation (Voulgaridou, Anestopoulos et al. 2011). Proteins with 4-HNE adducts were identified with goat anti-4-HNE antibody (Millipore, Cat. No. AB5605).

After incubation of the nitrocellulose membranes with a specific secondary antibody conjugated with horseradish peroxidase, protein bands were detected by an enhanced

cheminoluminescence system from GE Healthcare (Amersham, Cat. No. RPN-2209). Luminescence was determined by exposure to X ray film, and densitometry analysis was performed with an EPSON scanner and National Institutes of Health Image J software (NIH Research Services Branch). The secondary antibodies used were anti-mouse (Bio-Rad, Cat. No. 170-6516), anti-rabbit (Bio-Rad, Cat. No. 170-6515 or Santa Cruz, Cat. No. sc 2030) or anti-goat (Santa Cruz Biotechnology, Cat. No. sc-2020).

Staining of the nitrocellulose membranes with Ponceau S Red (Sigma, Cat. No. P7170) (Romero-Calvo, Ocon et al. 2010) or reaction of goat anti-rabbit immunoglobulin G (Santa Cruz, sc 2030,) with a protein of 30 kDa was used to verify equal loading of samples (loading control). Experiments were repeated at least 3 times, and representative data are shown in results. Treated samples were compared with the control of the respective time point.

### 2.6.3 - Micronuclei

Radiation-induced DNA damage was assessed by measuring the frequency of micronucleus formation by the cytokinesis-block technique (Fenech and Morley 1986). Briefly, ~$2 \times 10^4$ cells were seeded in chamber flaskettes (Nalge Nunc International, Cat. No. 154526) in presence of cytochalasin B (Sigma, Cat No. C 6762), an agent that inhibits cytokinesis without preventing nuclear division. Therefore, cells that have divided in the presence of cytochalasin B can be easily identified by the presence of two nuclei. At the concentration of 2 μg/mL, cytochalasin B was not toxic to the cells. After 72 h incubation, the cells were rinsed in saline solution (0.9 % w/w of NaCl dissolved in water), fixed in ethanol, stained with Hoechst 33342 (1 μg/mL in PBS), and viewed with a fluorescence microscope. At least 2500 binucleated cells per treatment in each experiment were examined. The fraction of micronucleated cells and the number of micronuclei per micronucleated cell was evaluated. Each graph is representative of at least three separate experiments, and Poisson

statistics was used to calculate the standard errors associated with the percentage (or fraction) of micronucleated cells in the total number of binucleated cells scored. Comparisons between treatment groups and respective controls were performed using the Pearson's $\chi^2$ test. A value of $p \leq 0.05$ between groups was considered significant.

## 2.7 Cell culture dish with CR-39 and etching

To identify irradiated cells in low fluence HZE-particle-exposed adherent cultures, AG1522 cells were seeded onto glass-bottomed tissue culture dishes (Ibidi®) with 100 μm-thick polyallyl diglycol carbonate (PADC) plastic polymer, commonly known as Columbia Resin #39 or CR-39™ plastic, grafted to the their bottom (Track Analysis Systems Ltd.). Upon cell fixation, the CR-39 was etched in 10 N KOH at 37 ºC for 3.5 h and the pits were visualized using light microscopy. *In situ* analyses of 53BP1 foci formation were performed following etching. Images were obtained by switching from fluorescent to optical imaging and changing the focal plane. Monitoring of confluent cultures during a 3 h period by confocal microscopy using a fixed high magnification field did not reveal any movement of the cells following exposure to mean absorbed doses of 0.1-0.3 cGy of α particles (Gaillard, Pusset et al. 2009).
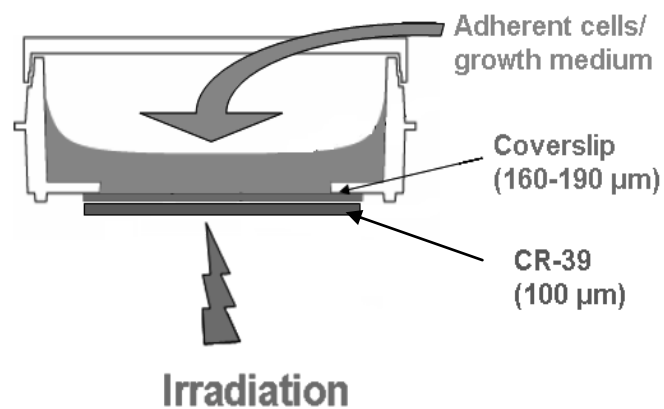
**Figure 2-5: Tissue culture dish with CR-39-bottom for HZE-particle- irradiation. Incorporation of a 100 µm-thick CR-39 film below the glass bottom of the sealable-dish permits visualization of HZE-particle-tracks without interfering with microscopic examination of biological changes. The dishes filled to capacity with pH- and temperature-equilibrated growth medium can be positioned perpendicularly to the incident beam.**

# Chapter 3     <u>Specific Aim 1</u>: To characterize the evolution of biological changes in bystander cells in normal human fibroblast cultures exposed to low fluence of particulate radiations that differ in their LET

## *3.1 Rationale*

As described in section 1.5.3, bystander effects have been extensively observed in cell cultures wherein only a small fraction of the cells is targeted by high linear energy transfer (LET) α particles (LET ranging from ~100 to 120 keV/μm). However, the expression of such effects after exposure to low fluences of HZE particles, another type of high LET radiation but with different physical characteristics, remains unclear. The characterization of bystander effects in cell populations exposed to very low fluences of HZE particles are only emerging, and conflicting data, using different *in vitro* cell culture systems, have been reported. In initial experiments with a microbeam, stressful effects were shown to be transmitted from HZE-particle-irradiated cells to contiguous bystander cells (Shao, Furusawa et al. 2003 ; Hamada, Ni et al. 2008; Harada, Nonaka et al. 2009). In subsequent experiments whereby HZE-particle-irradiated cells were co-cultured with bystander cells in a manner that they only shared growth medium, stressful responses were also induced in the bystander cells and were similar in nature to those induced in the targeted cells (Fournier, Becker et al. 2007; Yang, Anzenberg et al. 2007; Yang, Anzenberg et al. 2007). Furthermore, oxidative stress and DNA damage persisted in distant progeny of bystander cells that had been in contiguous co-culture with HZE-particle-irradiated cells (Buonanno, de Toledo et al. 2011). However, other experiments involving the transfer of growth medium from irradiated cultures to recipient bystander cells present in a separate dish (Groesser, Cooper et al. 2008; Sowa, Goetz et al.

2010), or the targeting of an exact number of cells in a population with energetic heavy ions from a microbeam (Fournier, Barberet et al. 2009) did not detect an effect with a variety of endpoints and cell types. Several factors may underlie the absence of observable effects in these cases, including timing of endpoint measurement, dilution of the inducing factor and the metabolic state/redox environment of the recipient cells.

Providing clear evidence for the expression of HZE-particle-induced bystander effects is pertinent to space exploration during which astronauts are likely to be exposed to low fluences of energetic particles (Cucinotta and Chappell 2010). To gain greater knowledge of HZE-particle-induced bystander effects, we investigated the kinetics of expression of stress markers in confluent density-inhibited normal human fibroblast cultures exposed to low fluences of energetic iron, silicon or carbon ions, and compared the results with those obtained in cultures exposed to low fluences of α particles. Cell cultures were exposed to doses as low as 0.2 cGy wherein only 1-3 % of nuclei are traversed by a particle track. Using endpoints to measure DNA damage (micronucleus formation, *in situ* analyses of 53BP1 foci), expression levels of stress-responsive proteins (p21$^{Waf1}$, p-TP53ser15, HDM2 and p-ERK1/2), protein carbonylation and lipid peroxydation, the work described in this project provides evidence for HZE-particle-induced bystander effects.

In this study, the HZE particles were delivered from a broadbeam irradiator that does not permit identification of the targeted cells. To distinguish irradiated from bystander cells, we developed dishes that incorporate a CR-39 solid state nuclear track detector at their glass bottom where the cells are growing. Following etching of the CR-39, DNA damage in targeted and non-targeted cells was assessed by 53BP1 foci formation, a marker that has been associated with DNA double strand breaks (Schultz, Chehab et al. 2000).

## 3.2  Results

### 3.2.1 Evidence of radiation-induced bystander effect in confluent normal human diploid fibroblast cultures exposed to low mean absorbed doses of α particles or HZE particles

Confluent density-inhibited AG1522 fibroblasts were exposed to low mean absorbed doses of 3.7 MeV α particles (LET ~109 keV/μm), and in parallel to 1000 MeV/u iron ions (LET ~151 keV/μm), 600 MeV/u silicon ions (LET ~51 keV/μm) or 290 MeV/u carbon ions (LET ~13 keV/μm).

Radiation-induced DNA damage is associated with signaling pathways that recognize genetic alterations and cause the recruitment of specific repair proteins at the site of the damage. One of the first proteins recruited to the site of DNA double-strand breaks is the p53 binding protein-1 (53BP1). Mutation of *53BP1* has been shown to be associated with carcinogenesis (Naidu, Har et al. 2011), and the gene is considered a "tumor suppressor" (Huo and Yang 2011). The 53BP1 protein is a key factor in the repair of DNA double strand breaks; it becomes rapidly hyper-phosphorylated and forms discrete foci in nuclei of cells that have sustained DNA damage (Rappold, Iwabuchi et al. 2001). As a result, 53BP1 foci formation has been extensively used as a biomarker to examine DNA damage and repair. In this study, it is used to evaluate DNA damage not only in irradiated cells but also in their neighboring "bystanders". Analyses of the appearance and decay of 53BP1 foci were coupled with evaluation of the formation of micronuclei, a form of DNA damage representing mainly DNA double strand breaks (Fenech 2008). The focus was on effects induced by low mean doses of particulate radiations by which only a fraction of the cells in exposed cultures is traversed through the nucleus by a particle track.

Three hours after exposure to mean absorbed doses of 0.2 to 10 cGy of 3.7 MeV α particles, the fractions of binucleated cells with micronuclei and cells presenting 53BP1 foci increased with dose (Figure 3-1). The augmentations however were not proportional to the mean absorbed doses. At 0.2 cGy, the increases in binucleated cells with micronuclei and cells presenting 53BP1 foci were significant and were much higher than the percentage (1.4 %) of cells that would have been traversed by a particle track through the nucleus. These results suggest the involvement of cells other than those initially irradiated in the response of the exposed cultures to α particles.

A                                                B
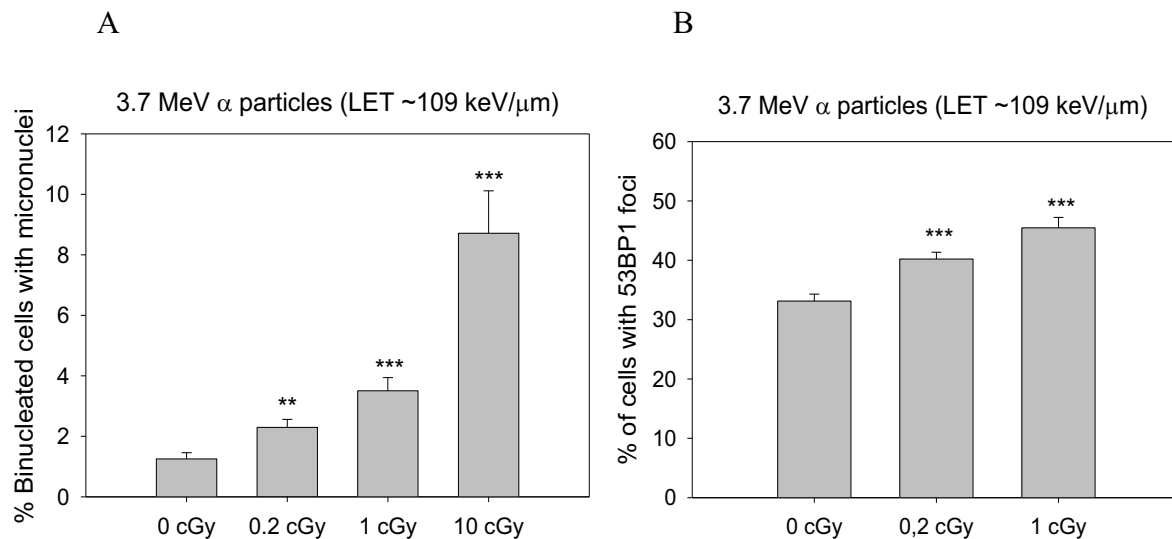


Figure 3-1: The induction of stressful effects in confluent AG1522 fibroblast cultures at 3h after exposure to low doses of 3.7 MeV α particles. (a) Percentage of binucleated cells with micronuclei cells; (b) percentage of cells with 53BP1 foci (number of cells with 53BP1 foci over the total number of cells counted). (*: $p < 0.05$, **: $p < 0.01$ and ***: $p < 0.001$ derived by $\chi^2$ test).

The above results confirm earlier observations from several laboratories that exposure to α particles triggers the propagation of stressful effects from irradiated to bystander cells (Nagasawa and Little 1992; Azzam, de Toledo et al. 1998; Azzam, de Toledo et al. 2001; Belyakov, Malcolmson et al. 2001; Azzam, De Toledo et al. 2002; Shao, Furusawa et al. 2003; Kashino, Suzuki et al. 2007; Shao, Prise et al. 2008; Hanot, Hoarau et al. 2009). Using AG1522 fibroblasts, we expanded these studies to investigate whether low mean absorbed

doses of HZE particles induce similar stressful bystander effects. To this end, confluent cultures were exposed to 0.2 cGy of 1000 MeV/u iron ions (LET ~151 keV/μm), 600 MeV/u silicon ions (LET ~51 keV/μm) or 290 MeV/u carbon ions (LET ~13 keV/μm), where only 1.2%, 3.5%, or 13.4% of the cells, respectively, were irradiated in the nucleus. The kinetic of 53BP1 foci formation were examined *in situ* at 15 min, 1 h, 3 h and 24 h after exposure.

Relative to respective control, the percent of cells with 53BP1 foci was increased at 15 min, 1 h and 3 h by 6.8 % ($p < 0.001$), 15 % ($p < 0.001$) and 10.6 % ($p < 0.001$), respectively for $^{56}$Fe ions (Figure 3-2), and by 1.9 %, 7.7 % ($p < 0.001$), and 5.3 % ($p < 0.001$), respectively, for 3.7 MeV α particles (Figure 3-2). Increases of 8.2 % ($p < 0.001$), 11.4 % ($p < 0.001$) and 2.8 % ($p < 0.05$), at 15 min, 1 h and 3 h, respectively, were also observed after exposure to 0.2 cGy of $^{28}$Si ions (Figure 3-3, Panel A). By 24 h, the percent increase of cells with 53BP1 foci was null for $^{56}$Fe ions, was increased by 3.1 % ($p < 0.01$) for $^{28}$Si ions, and by 2 % for α particles ($p < 0.05$). The significant increase in the percentage of cells with foci (5 – 50 %) over what would be expected based on the percentage of cells irradiated through the nucleus (1.2-3.5 %) strongly supports the participation of non-targeted bystander cells in the response of the overall cell population to irradiation by low fluences of high LET particles.
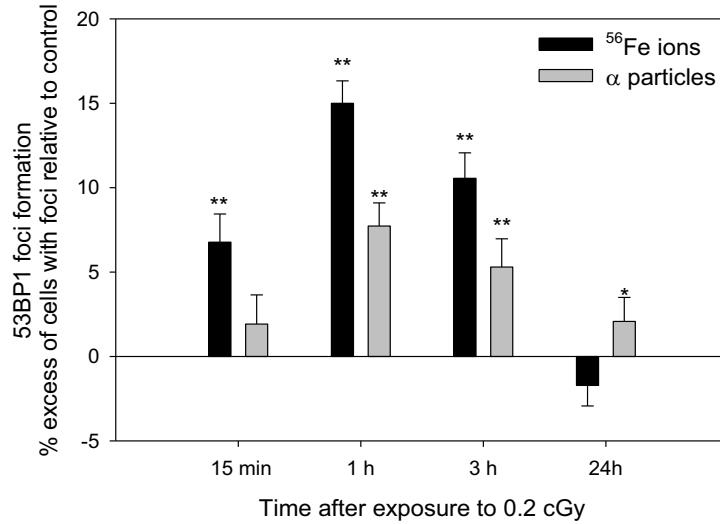
**Figure 3-2: Kinetics of the appearance of 53BP1 foci in confluent AG1522 cell cultures exposed to 0.2 cGy from 1000 MeV/u $^{56}$Fe ions and 3.7 MeV α particles. The data represent the excess percent increase (ΔF) of cells with 53BP1 foci in irradiated populations relative to respective control calculated as ΔF = 100 (F$_{irradiated}$ – F$_{control}$) where F is the ratio of the number of cells with 53BP1 foci over the total number of cells counted. Each graph is representative of 4 experiments. $χ^2$ test was performed on the total number of cells compared with respective control in irradiated populations . \*: $p < 0.05$, \*\*: $p < 0.01$ and \*\*\*: $p < 0.001$).**

The fraction of cells with 53BP1 foci was shown to decrease by 2 h after exposure to DNA damaging agents (low-LET radiations) (Schultz, Chehab et al. 2000). Thus, the increases observed at 1-3 h over those detected at 15 min in cultures exposed to $^{56}$Fe ions or α particles suggest the recruitment of additional cells in the response. Presumably, these are bystander cells wherein signaling molecules propagated from irradiated cells had time to exert effects that result in DNA damage. The attenuation of the percent increase of cells with 53BP1 foci at 24 h may reflect repair of DNA damage in bystander cells. In contrast to $^{56}$Fe ions (LET ~151 keV/μm), $^{28}$Si ions (LET ~50 keV/μm) and α particles (LET ~109 keV/μm), exposure of confluent cultures to 0.2 cGy from 290 MeV/u $^{12}$C ions (LET ~13 keV/um) did not result in significant increase in 53BP1 foci formation (Figure 3-3, Panel B). For a given dose, the number of cells traversed by a particle increases when the LET decreases; however, the energy per particle also decreases. At mean absorbed dose of 0.2 cGy of 290 MeV $^{12}$C

ions, the number of cells traversed is more than 10 times higher than after exposure to 1000 MeV/u $^{56}$Fe ions or 3.7 MeV α particles. This suggests that HZE particles with lower LET may be less efficient at inducing stressful bystander effects under the conditions used in this study. Further it highlights the importance of absorbed radiation dose per cell (in particular the nucleus) in induction of bystander effects.

A                                                                B
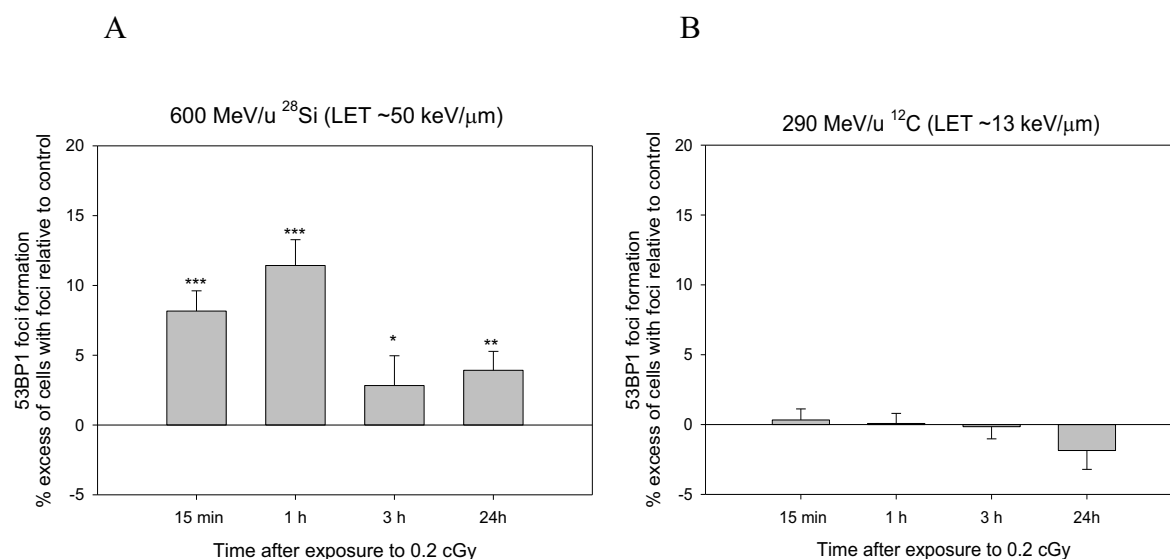


**Figure 3-3: Kinetics of the appearance of 53BP1 foci in confluent AG1522 cell cultures exposed to 0.2 cGy from (A) 600 MeV/u $^{28}$Si ions, (B) 290 MeV/u $^{12}$C ions. The data represent the excess percent increase (ΔF) of cells with 53BP1 foci in irradiated populations relative to respective control calculated as ΔF = 100 (F$_{irradiated}$ − F$_{control}$) where F is the ratio of the number of cells with 53BP1 foci over the total number of cells counted. The data are representative of 2 and 1 experiments for silicon ions and carbon ions respectively. χ$^{2}$ test was performed on the total number of cells compared with respective control in irradiated populations (\*: $p$ <0.05, \*\*: $p$ <0.01 and \*\*\*: $p$ <0.001).**

## 3.2.2 Levels of stress-responsive proteins are rapidly modulated in human cell populations exposed to low fluences of HZE particles

We examined the phosphorylation of serine 15 in TP53 (p-TP53ser15), a marker that accumulates in response to DNA damage (Siliciano, Canman et al. 1997; Canman, Lim et al. 1998), and of the stress-responsive and pro-survival extracellular signal-related kinases,

ERK1 and ERK2 (p-ERK1/2) (Valerie, Yacoub et al. 2007), in confluent AG1522 cell cultures exposed to doses of 0.2 or 1 cGy of energetic iron or silicon ions at different times after exposure, and compared the results with those obtained in AG1522 cell cultures exposed in parallel to α particles.

Relative to control, at 15 min after exposure to 0.2 or 1 cGy from 1000 MeV/u $^{56}$Fe ions (LET ~151 keV/μm) or 600 MeV/u $^{28}$Si (LET ~50 keV/μm), an increase in p-TP53ser15 and p-ERK1/2 levels was consistently observed (Figure 3-4, Panel A).
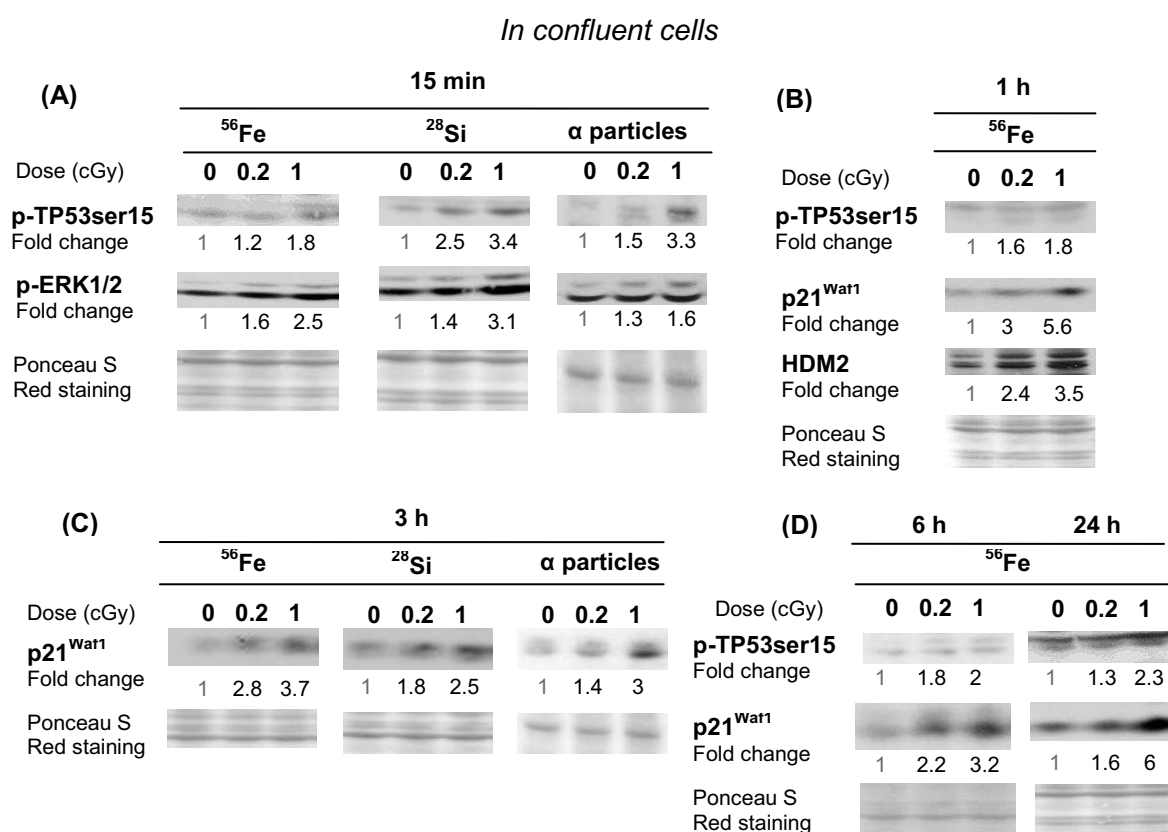


**Figure 3-4: Western blot analyses of the levels of p-TP53ser15, p-ERK1/2, p21$^{Waf1}$ and HDM2 in AG1522 cell populations (A) 15 min, (B) 1 h, (C) 3 h, (D) 6 and 24 h after exposure to a dose of 0, 0.2 or 1 cGy from 1000 MeV/u $^{56}$Fe ions, 600 MeV/u $^{28}$Si ions or 3.7 MeV α particles. Staining with Ponceau S Red was used as loading control. Each immunoblot is representative of 3-4 experiments. Fold change represents relative change compared to the respective control.**

The representative data in figure 3-4 (Panel A) indicate increases of ~1.2- and 2.5-fold in p-TP53ser15 levels and 1.6- and 1.4-fold in p-ERK1/2 levels in cultures exposed to 0.2 cGy of $^{56}$Fe or $^{28}$Si ions, respectively. At this mean absorbed dose, only ~1.2 and 3.5 % of nuclei are traversed by either ion, respectively. Similarly, at 1 cGy, wherein ~6 % of nuclei are traversed by an iron ion and 17.5 % by a silicon ion, respective increases of 1.8- and 3.4-fold in p-TP53ser15 levels and of 2.5- and 3.1-fold in p-ERK1/2 levels were observed. These data indicate that p-ERK1/2 and p-TP53ser15 are sensitive markers that are rapidly modulated after exposure of human cell cultures to very low mean absorbed doses of high-LET HZE radiations. The levels of p-TP53ser15 and p-ERK1/2 were similarly increased at 15 min after exposure of confluent AG1522 cultures to 0.2 or 1 cGy of 3.7 MeV α particles (LET ~109 keV/μm) (Figure 3-4figure 3-4, Panel A). The enhanced stress, implied by the increase in p-TP53ser15 level, correlated with increases ranging from 1.8- to 5.6-fold in levels of HDM2 and p21$^{Wafl}$ at 1 h (Figure 3-4, Panel B) and 3 h (Figure 3-4, Panel C) after exposure, suggesting activation of TP53, a central protein involved in maintenance of genomic integrity. Similar to micronucleus formation and 53BP1 foci formation, the magnitude of these changes implies participation of a greater fraction of cells than the 1.2-3.5 % fraction traversed by a particle track through the nucleus at a mean dose of 0.2 cGy.

The increases in p-TP53ser15 detected at 15 min (Figure 3-4, Panel A).and in p21$^{Wafl}$ and HDM2 at 1-3 h (Figure 3-4, Panels B and C) also occurred at 6 and 24 h after exposure (Figure 3-4, Panel D). The persistence of the effect may be due to sustained stress in the targeted and bystander cells that were affected early after exposure (15 min – 3 h), or to the recruitment of new bystander cells in the stress response. These new bystander cells may be affected by events propagated from irradiated cells or other bystander cells that have sustained stress (DNA damage) earlier.

### 3.2.3 Exposure to low fluences of HZE particles induces significant oxidative stress

The persistence of stress in low fluence exposed cell cultures as evaluated by markers of DNA damage and up-regulation of stress-responsive proteins was further supported by analyses of protein oxidation and lipid peroxidation. The majority of ROS produced in targeted cells at the time of irradiation persist for milliseconds (Muroya, Plante et al. 2006). These ROS can oxidize proteins and increase their susceptibility to proteolytic attack (Berlett and Stadtman 1997). The detection of oxidized proteins long after exposure is likely due to ROS generated from perturbations in oxidative metabolism (Petkau 1987; Spitz, Azzam et al. 2004).

*In confluent cells*
**Oxidative Stress Dose Response to $^{56}$Fe ions**
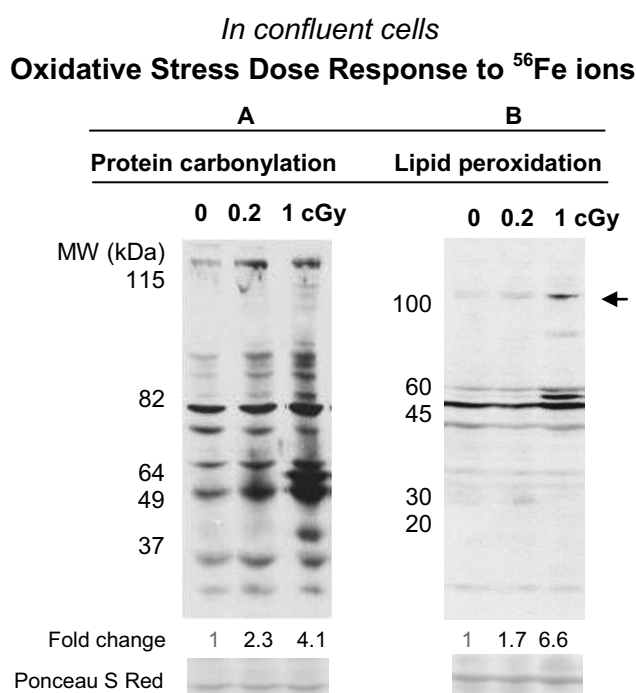


**Figure 3-5: Immunoblots showing oxidative stress in confluent AG1522 cell populations harvested 24 h after exposure to low mean absorbed doses of 1000 MeV/u $^{56}$Fe ion: (A) Protein carbonylation and (B) Lipid peroxidation as measured by 4-HNE protein adduct accumulation. In the case of protein carbonylation, the relative intensity (i.e. fold-change) in oxidation of the overall spectrum of proteins (~30-130 kDa) in irradiated cells was compared to that in control cells. For 4-HNE protein adduct accumulation, the relative intensity refers to the level of the band with arrow relative to control. Staining with Ponceau S Red was used as loading control. Each immunoblot is representative of 3 experiments**

The representative data in figure 3-5 (Panel A) show ~2- to 4-fold increases in overall protein carbonylation in cells from cultures harvested 24 h after exposure to 0.2 and 1 cGy of 1000 MeV/u iron ions, respectively. The accumulation of 4-hydroxynonenal (HNE) adducts in proteins from the same cultures indicates that increased lipid peroxidation was involved (Figure 3-5, Panel B).

The rapid propagation of stressful effects and their persistence was further revealed when confluent cell populations exposed to a mean dose of 1 cGy from 1000 MeV/u $^{56}$Fe ions were subcultured, by 15 min after irradiation, to lower density (1:3) in fresh medium. Similar to results in confluent cultures, relative to respective control, increases in the levels of p-TP53ser15, p21$^{Waf1}$ and HDM2 occurred at 8 and 24 h after subculture (Figure 3-6).
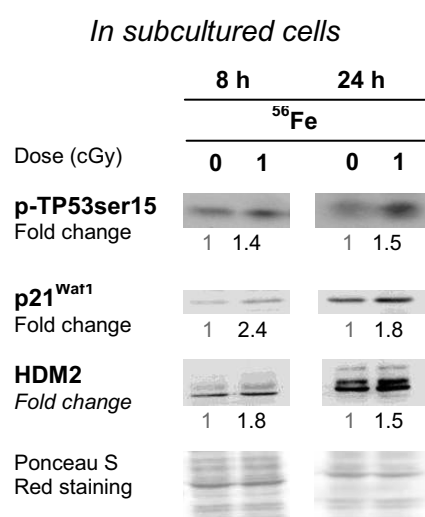


**Figure 3-6: Western blot analyses of the levels of p21$^{Waf1}$, p-TP53ser15 and HDM2 in AG1522 cell populations exposed to 1000 MeV/u $^{56}$Fe ions. Confluent cells were exposed to a mean dose of 1 cGy and subcultured in fresh medium (1:3). Samples were harvested for analyses 8 and 24 h after irradiation. Staining with Ponceau S Red was used as loading control. Each immunoblot is representative of 4 experiments. Fold change represents relative change compared to the respective control.**

### 3.2.4 Identification of cells targeted by primary incident HZE particles: The development of glass-bottomed dishes incorporating CR-39 solid state nuclear track detector

To distinguish irradiated cells from bystander cells, a 100 µm-thick CR-39 solid state nuclear track detector was bonded to the bottom edges of the cell culture surface (Figure 2-5 in Materials and Methods section). After etching of CR-39, cells traversed in the nucleus could be identified, and induced biological effects may be assessed by suitable markers in targeted and bystander cells. The data in Figure 3-7 show 53BP1 foci in a confluent cell culture exposed to 0.2 cGy of 1000 MeV/u $^{56}$Fe ions followed by 15 min incubation.
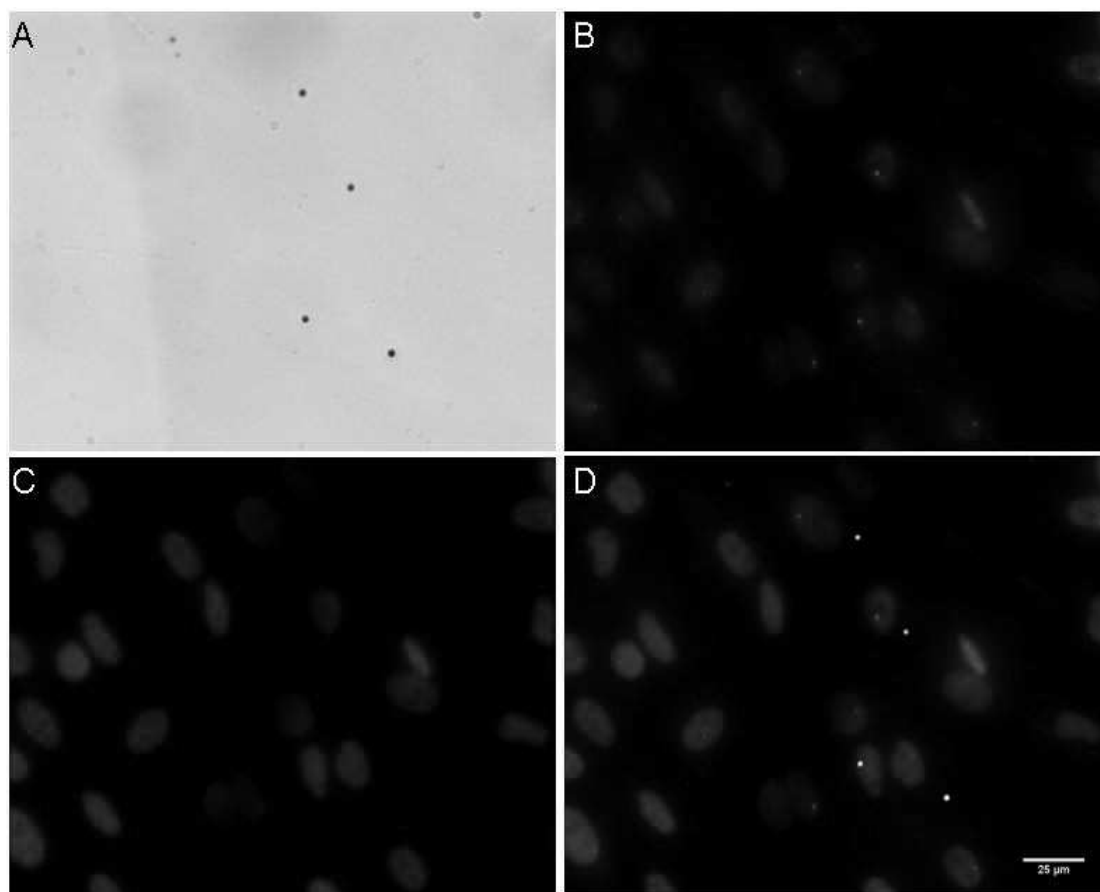


**Figure 3-7: Representative images of etched tracks and 53BP1 foci in AG1522 cell cultures grown on dishes with CR-39-nuclear track detector bottom, at 15 min after exposure to 0.2 cGy of 1000 MeV/u $^{56}$Fe ions: (A) visualization of etched tracks; (B) 53BP1 immuno-detection (red); (C) stained with DAPI; (D) images in A-C are super-imposed with the black dots representing etched tracks in (A) converted to white for better visualization.**

Following etching, the iron ion tracks were visible as black dots (Figure 3-7, Panel A). As expected, exposure to 0.2 cGy resulted in ~1.5 % of cells being superimposed on pits. The formation of 53BP1 foci (Panel B) in nuclei (revealed by DAPI staining, Panel C) that superimpose the black dots (inverted in white for better visualization, Panel D) indicates that these cells sustained DNA damage as would be expected from nuclear traversal by a high LET particle. The two cells with foci adjacent to the traversed cell are likely affected bystander cells (Panel D). They may however be cells subject to secondary radiations. The absence of CR-39-pits below these adjacent cells indicates lack of hot-spots; it suggests that the strategy of incorporating CR-39 solid state nuclear track detector is suitable to investigate the kinetics of biologic responses in situ in targeted and non-targeted cells.

## 3.3 Discussion

The data reported here highlight the manifestation of stressful bystander effects in confluent normal human cell cultures exposed to low absorbed doses of HZE or α particles by several endpoints.

The DNA DSB is a serious threat to the integrity of eukaryotic genomes; it can affect survival and may induce events that lead to neoplastic transformation (Iliakis 1991). Following exposure to DNA damaging agents, a battery of damage sensing and repair proteins localize at the site of DNA breaks. Among these proteins, 53BP1 forms discrete foci within minutes after exposure (Schultz, Chehab et al. 2000) (Rappold, Iwabuchi et al. 2001) (Asaithamby, Uematsu et al. 2008). Using the same microscope optics and exposure time, and scoring by eye, to accurately differentiate 53BP1 foci, as well as using separate controls for each time point, the results from cultures exposed to a dose by which only 1-3 in 100 cells is traversed through the nucleus by an energetic ion, strongly supported the participation of

bystander cells in the response. At 15 min after exposure to a mean absorbed dose of 0.2 cGy from α particles, $^{56}$Fe ions or $^{28}$Si ions, the fraction of cells with 53BP1 foci was higher than predicted based on the percentage of cells directly targeted by radiation, which highlights rapid propagation of bystander effects.

In general, it is thought that 53BP1 foci formation is transient; it peaks at ~20 min after exposure to DNA damaging agents and return to basal level within 1 to 2 h (Schultz, Chehab et al. 2000). In our study, the maximum increase of 53BP1 foci detected at 1 h, and its persistent elevation at 3 h, may be due to the induction of DNA damage in non-targeted cells. Although 53BP1 foci in directly targeted cells would be expected to disappear by 3 h, the results in Figure 3-2 indicated a significant increase in foci formation not only relative to control but also compared to data acquired in cells fixed 15 min after exposure ($p$ <0.001). These results suggest the propagation of signaling events leading to DNA damage in bystander cells. The return to near basal level by 24 h after irradiation may be due to the decay of signaling events leading to recruitment of additional bystander cells suffering DNA damage or to repair of the induced damage. Events that lead to other forms of stress may be however propagated.

In contrast to $^{56}$Fe, $^{28}$Si ions and α particles, no excess 53BP1 foci formation has been detected after exposure of cell cultures to 0.2 cGy from 290 MeV/u carbon ions (LET ~13 keV/μm) at any time between 15 min and 24 h after irradiation. This may be due to less energy deposition per traversed cell, which leads to less complex DNA damage being induced in the targeted cells. These effects likely affect the nature of the propagated signaling events. The lack of increase in 53BP1 foci formation in carbon ion exposed cell cultures also suggests that radiations of lower LET may be less efficient at inducing stressful bystander effects at low doses. Different outcomes may however occur following delivery of multiple

ions that result in a large absorbed dose to the targeted cells. The use of microbeams would greatly facilitate such experiments.

Similar to earlier results describing effects in cell cultures exposed to low fluences of α particles (Azzam, de Toledo et al. 2003), increases in proteins that participate in p53 and ERK1/2 signaling pathways were observed in normal human fibroblast cultures exposed to mean absorbed doses as low as 0.2 cGy of 1000 MeV/u iron ions or 600 MeV/u silicon ions. The increases in stress-responsive proteins were detected as early as 15 min after irradiation and persisted for at least 24 h.

Relative to control, higher levels of p-TP53ser15, a marker of DNA damage, was detected in confluent AG1522 fibroblasts exposed to 0.2 cGy wherein only 1-3 % of cells are traversed, on average, through the nucleus by one ion. This was associated 1-3 h after exposure with increased level of p21$^{Wafl}$, a p53 effector and key component of the DNA damage induced $G_1$ checkpoint. The increases in the levels of these stress markers persisted for at least 24 h after exposure and were associated with an increase in protein carbonylation and in accumulation of 4-HNE protein adducts. The enhanced oxidative stress highlighted by the latter markers may have, in part, contributed to the persistent increases in p-TP53ser15 and p21$^{Wafl}$ levels 24 h after exposure of the cultures to a low dose of HZE particles. These appreciable increases in stress markers in cultures exposed to low fluences of high LET radiations suggested the involvement of non-targeted cells in the overall response.

The induction of stressful bystander effect in $^{56}$Fe ion-irradiated cell cultures was supported through the use of culture dishes that incorporate a nuclear track detector (Gaillard, Pusset et al. 2009). The latter strategy allowed identification, on a cell per cell basis, of irradiated and bystander cells in the population after irradiation by a broadbeam of HZE particles. It expands earlier observations with α particles in our laboratory (Gaillard,

Pusset et al. 2009). The use of these CR-39 bottomed-dishes unequivocally identified the irradiated cells and showed that neighboring non-targeted cells also harbored 53BP1 foci.

The results describing induction of 53BP1 foci at 15 min after irradiation (Figure 3-7) further show that propagation of the signaling events leading to stressful effects in bystander cells is rapid. However, the reaction to the signal(s) is likely to be cell-dependent and may require time to be expressed. It may manifest through certain endpoints but not others, and its occurrence/magnitude/nature is likely to depend greatly on the identity/concentration of the mediating signal and phenotype (e.g. redox environment) of the recipient cell (Autsavapromporn, de Toledo et al. 2011).

*Data pertaining to this aim have been included in a manuscript (Gonon G., Groetz J.-E., de Toledo S.M., Howell R.W., Fromm M., Azzam E.I. Non-Targeted Stressful Effects in Normal Human Fibroblast Cultures Exposed to Low Fluences of High Charge, High Energy (HZE) Particles: Kinetics of Biologic Responses and Significance of Secondary Radiations. (manuscript accepted for publication in Radiation Research)*

# Chapter 4 <u>Specific Aim 2</u>: To calculate, using the multi-particle transport code FLUKA, the doses imparted to AG1522 confluent cells grown on soda-lime glass surface by fragmentation products following exposure to 1000 MeV/u iron ions, 600 MeV/u silicon ions or 290 MeV/u carbon ions.

## 4.1 Rationale

The studies described in Chapter 3 generated clear evidences of HZE-particle-induced bystander effects. However, in contrast to cellular exposure to α particles where the ranges of the generated δ rays are small compared to the nuclear diameter (Neti, de Toledo et al. 2004) (maximum range of the δ rays produced by a 3.65 MeV α particles is about 0.1 μm (Hamm, Turner et al. 1985)), in case of HZE-particle-irradiation, secondary particles such as other heavy ions, electrons, photons, protons and α particles can be produced due to the interaction of the primary HZE particle with the target. The interaction of these secondary particles with cells not targeted by primary ions may have contributed to the observed stressful effects.

Depending on their charge (positive in case of ions), the particles interact with matter following three different processes leading directly or indirectly to ionizations or excitations (as seen in section 1.2.2): on one hand, collisions with target electrons, and on the other hand, nuclear interactions including elastic[g] and inelastic collisions may occur. The first two mechanisms are respectively responsible for the "electronic" energy loss (production of

---

[g] An elastic collision is defined as a collision between two bodies wherein kinetic energy is conserved; the total kinetic energy is redistributed between the colliding bodies Cember, H. (1996). <u>Introduction to health physics</u>. New York, McGraw-Hill, Health Professions Division, ibid.

δ rays and X rays) and deflection of ions in matter, while the latter is responsible for fragmentation. Considering nuclear interactions, elastic collisions play an important role in the spread angle, while inelastic collisions change the nature of projectile and target. It should be noted that elastic nuclear collisions (Rutherford scattering) cross-sections are proportional to the inverse of kinetic energy squared; thus at the energies used in our experiments, the probability for such elastic scattering remains extremely low.

As for inelastic nuclear collisions, even if the probability of a nuclear interaction between projectile and target is small, due to their respective size ($10^{-15}$ m for the nucleus compared to $10^{-10}$ m for the atom), the cumulative effect of these interactions can affect the spatial distribution of the absorbed energy in tissue and may contribute to the observed bystander effect. As fragmentation can generate additional high-LET components into the radiation field, the fragmentation phenomena need to be quantified. To address the possibility that secondary radiations can contribute to the observed bystander effect, Jean-Emmanuel Groetz (Head of the Radiation-Matter Interaction group of the Laboratoire de Chimie Physique et Rayonnements) evaluated the contribution to the absorbed dose of secondary particles by performing a simulation. We chose FLUKA multi-particles transport code where nucleus-nucleus interactions are considered.

## *4.2 Definitions*

### 4.2.1 Monte Carlo simulation

FLUKA multi-particles transport code is based on a Monte Carlo simulations package for the interaction and transport of particles and nuclei in matter. The Monte Carlo method is a numerical solution to a problem that models objects' interaction with other objects or their environment based upon simple object-object of object environment relationship. However,

several types of problems have been solved by Monte-Carlo simulation such as traffic flow, finance, genetics, population growth, radiation sciences, radiation dosimetry (Beilajew 2001). In radiobiology, Monte Carlo simulations permit to follow the path of an individual representative particle and resulting secondaries through matter until they are no longer of interest, to determine dose, fluence and other distribution in cell cultures or patients. The particle is followed from its birth; that is the incident beam to its stopping due to capture by a nucleus, annihilation, or if the particle drops below the cut-off pre-defined energy. Basic physics interaction probabilities composed of different random phase, the distance between two interactions, the type of interaction induced and energetic and kinetic parameters needed to characterize the given interaction are used to determine the fate of the representative particles. Sufficient representative particles are transported to produce statistically acceptable results. In our case, we considered 300 000 primary ions per cycle (300 000 histories) and 10 cycles were repeated for each type of primary ions ($^{56}$Fe, $^{28}$Si or $^{12}$C ions). Increasing the number of particles transported will not affect the results that are normalized per incident particle but will improve statistics by the square root of the number of particles.

## 4.2.2  Fluence, fluence differential in energy, solid angle

Secondary particles can propagate from a radiating source in all possible directions and are emitted over a range of energy. Thus, the magnitude of emitted radiations must be described by its spectral and its directional components. So, we need to define the fluence, the fluence differential in energy, the double differential fluence and the solid angle.

In section 1.3.2, the fluence $\varphi$ was defined as the number of particles traversing a planar area. To be more specific, the **fluence $\varphi$** is defined by $\phi = \dfrac{dN}{da}$ where $dN$ is the number of particles incident on a sphere of cross-section $da$. The use of a sphere expresses the fact that

one considers the area perpendicular to the direction of each particle. The unit is in particle/cm².

The **fluence differential in energy _φ(E)_**, or the distribution of fluence with respect to energy is defined by $\phi(E) = \dfrac{d\phi}{dE}$, where $d\varphi$ is the fluence of particles with energy between _E + dE_. Therefore, the unit is in particle/cm²/GeV; in our case, as the results are normalized per primary ion (incident ion), the unit used here is particle/cm²/GeV/primary. The **particle fluence** (particle/cm²/primary) can be obtained by integrating the differential spectrum over all energy channels. It can be also considered as an infinitesimal volume dV with particles passing through it $\phi = \dfrac{\sum d\ell}{dV}$, where $\sum d\ell$ is the sum of all path lengths of the particles that traverse the volume.

There is an analogous definition for the direction distribution, the **double differential of fluence _φ(E, Ω)_**, that is defined as $\phi(E, \Omega) = \dfrac{d^2\phi}{dEd\Omega}$ where $\Omega$ is the solid angle.

The **solid angle**, $\Omega$, is the two-dimensional angle in three-dimensional space that an object subtends at a point. It is a measure of how large that object appears to an observer looking from that point. A solid angle equals the area of a segment of unit sphere in the same way a planar angle equals the length of an arc of unit circle. The SI units of solid angle are steradian (sr). Although the surface area of a sphere is $4\pi$ steradian, in our case, the calculation were done with a solid angle included between 0 and $2\pi$ steradian corresponding to the hemisphere whose base is the surface separating the coverslip and cell culture. Thus, only particles going in one direction (soda-lime glass › cell culture) are considered.
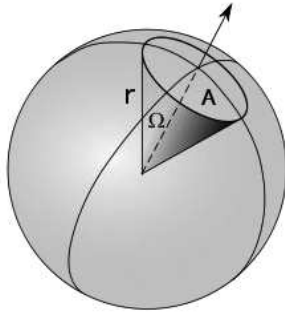
**Figure 4-1: The solid angle Ω corresponds to a cone with angle of Ω included in the projection unit sphere (http://fr.wikipedia.org/wiki/Fichier:Angle_solide_coordonnees.svg)**

The half-angle α at the apex of the cone of revolution representing the solid angle is defined as $\Omega = 2\pi\,(1\text{-cos }\alpha)$. Spectral and angular distributions are calculated from the normal to the surface coverslip/cell culture that is the axis of the incident beam in our case.

The binning was carried out according to seven intervals of solid angles (Figure 4-2), which gives the following correspondences (Table 4-1).

**Table 4-1: Correspondences between the solid angle Ω (sr) and the half-angle of the cone (°) using the relation α = Arcos (1- Ω/(2π))*180/π**

| Solid angle Ω (sr) | Half angle α (°) |
|---|---|
| 0.8976 | 31.0028 |
| 1.7952 | 44.4154 |
| 2.6928 | 55.1502 |
| 3.5904 | 64.6232 |
| 4.4880 | 73.3986 |
| 5.3856 | 81.7870 |
| 6.2832 | 90.0001 |
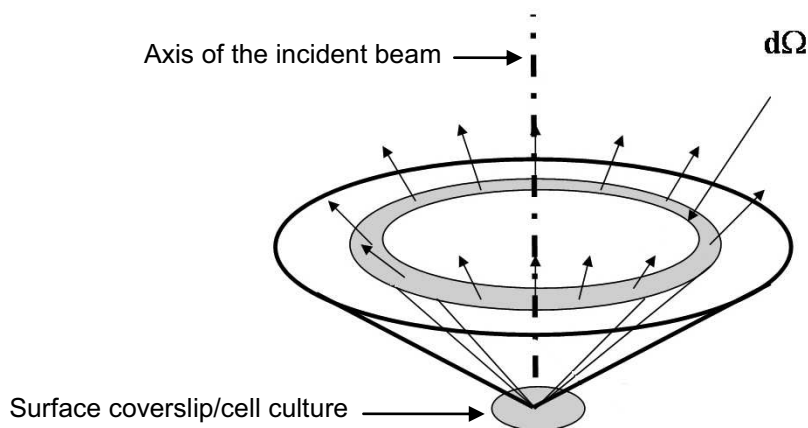


**Figure 4-2: Geometric range of a beam defined by a diaphragm plane and a cone, open, symmetrical around its axis**

**(adapted from http://www.optique-ingenieur.org/fr/cours/OPI_fr_M05_C05/res/Image7_1.jpg)**

- 111 -

## *4.3  Results*

### 4.3.1  Contribution of secondary particles to the total dose

The contribution of heavy ions (primary and fragments), electrons, photons, protons and α particles after exposure of cell cultures maintained on the glass-bottom of flaskettes, filled with medium to capacity, to a dose of 0.2 cGy of 1000 MeV/u $^{56}$Fe, 600 MeV/u $^{28}$Si ions or 290 MeV/u $^{12}$C ions are reported, respectively, in Table 4-2, Table 4-3, Table 4-4.

For the requested mean dose of 0.2 cGy, the scintillator provided the counts of particles from which a total delivered dose was calculated according to the relation between fluence, dose and LET given in Materials and Methods.

**Table 4-2: Contribution of primary and secondary particles to the mean absorbed dose in the glass coverslip, cell culture and medium when 1000 MeV/u $^{56}$Fe ions were used to deliver 0.2 cGy to cell cultures grown on glass-bottomed flaskettes with a nominal fluence of 8323 $^{56}$Fe ions/cm² which results in 3 329 200 particles over the exposure area of 20 x 20 cm. The production thresholds of δ rays were set at [A] 1 keV, [B] 10 keV, [C] 100 keV, [D] 1 MeV. The transport cut-off was set at 1 keV for HZE particles, protons, photons, and α particles. For electrons, it was set at 150 eV (Panel A) or 1 keV (Panels B, C and D).**

**Errors represent standard deviations of the mean. When the standard deviation is < 0.0001 cGy, it is expressed and noted in % as it can represent a high deviation. The term "total heavy ion" refers to the primary 1000 MeV/u $^{56}$Fe ions and the fragments.**

**[A]**

| 1 keV | Glass coverslip (1.91512 cm$^3$) | Cell Culture (0.0010 cm$^3$) | | Medium (water) (18.7990 cm$^3$) |
|---|---|---|---|---|
| **Particles** | **Dose ± standard deviation** *cGy* | **Dose ± standard deviation** *cGy* | **Contribution to total dose** *%* | **Dose ± standard deviation** *cGy* |
| Total heavy ions | 0.1000 ± 0.0007 | 0.1228 ± 0.0022 | 60.22 *0.35* | 0.1185 ± 0.0022 |
| $^{56}$Fe ions | 0.0997 ± 0.0007 | 0.1221 ± 0.0022 | 59.87 | 0.1114 ± 0.0022 |
| Electrons | 0.0623 ± 0.0004 | 0.0807 ± 0.0014 | 39.57 | 0.0756 ± 0.0014 |
| Photons | 3.2609 x 10$^{-6}$ ± 0.69 % | 2.2013 x 10$^{-6}$ ± 82.22 % | 0.00 | 2.3844 x 10$^{-6}$ ± 1.11 % |
| Protons | 1.2438 x 10$^{-4}$ ± 8.72 % | 2.3514 x 10$^{-4}$ ± 21.97 % | 0.12 | 5.1421 x 10$^{-4}$ ± 2.57 % |
| Alpha | 4.3250 x 10$^{-5}$ ± 16.40 % | 5.1070 x 10$^{-5}$ ± 102.92 % | 0.03 | 1.5104 x 10$^{-4}$ ± 3.47 % |
| **Total** | **0.1626 ± 0.0012** | **0.2039 ± 0.0036** | **100** | **0.1950 ± 0.0036** |

**[B]**

| 10 keV | Glass coverslip (1.91512 cm$^3$) | Cell Culture (0.0010 cm$^3$) | | Medium (water) (18.7990 cm$^3$) |
|---|---|---|---|---|
| **Particles** | **Dose ± standard deviation** *cGy* | **Dose ± standard deviation** *cGy* | **Contribution to total dose** *%* | **Dose ± standard deviation** *cGy* |
| Total heavy ions | 0.1206 ± 0.0011 | 0.1452 ± 0.0020 | 71.67 *0.44* | 0.1404 ± 0.0019 |
| $^{56}$Fe ions | 0.1202 ± 0.0011 | 0.1443 ± 0.0020 | 71.23 | 0.1320 ± 0.0018 |
| Electrons | 0.0412 ± 0.0004 | 0.0569 ± 0.0009 | 28.08 | 0.0529 ± 0.0007 |
| Photons | 2.7719 x 10$^{-6}$ ± 0.92 % | 1.9991 x 10$^{-6}$ ± 14.62 % | 0.00 | 2.1064 x 10$^{-6}$ ± 1.35 % |
| Protons | 1.6855 x 10$^{-4}$ ± 7.96 % | 2.8335 x 10$^{-4}$ ± 16.52 % | 0.14 | 6.1175 x 10$^{-4}$ ± 3.49 % |
| Alpha | 5.7126 x 10$^{-5}$ ± 16.36 % | 9.6370 x 10$^{-5}$ ± 57.56 % | 0.05 | 1.7112 x 10$^{-4}$ ± 4.38 % |
| **Total** | **0.1622 ± 0.0015** | **0.2025 ± 0.0029** | **100** | **0.1943 ± 0.0026** |

**[C]**

| 100 keV | Glass coverslip (1.91512 cm³) | Cell Culture (0.0010 cm³) | | Medium (water) (18.7990 cm³) |
|---|---|---|---|---|
| **Particles** | Dose ± standard deviation cGy | Dose ± standard deviation cGy | Contribution to total dose % | Dose ± standard deviation cGy |
| Total heavy ions | 0.1420 ± 0.0008 | 0.1698 ± 0.0018 | 84.94  0.48 | 0.1642 ± 0.0018 |
| $^{56}$Fe ions | 0.1416 ± 0.0008 | 0.1688 ± 0.0018 | 84.46 | 0.1546 ± 0.0016 |
| Electrons | 0.0198 ± 0.0.001 | 0.0294 ± 0.0004 | 14.72 | 0.0301 ± 0.0003 |
| Photons | $1.5099 \times 10^{-6}$ ± 0.79 % | $1.0620 \times 10^{-6}$ ± 74.71 % | 0.00 | $1.3329 \times 10^{-6}$ ± 2.33 % |
| Protons | $1.8447 \times 10^{-4}$ ± 8.36 % | $3.5205 \times 10^{-4}$ ± 12.33 % | 0.18 | $7.0077 \times 10^{-4}$ ± 2.84 % |
| Alpha | $5.6496 \times 10^{-5}$ ± 13.10 % | $1.5287 \times 10^{-4}$ ± 98.28 % | 0.08 | $1.9140 \times 10^{-4}$ ± 4.40 % |
| **Total** | **0.1622 ± 0.0009** | **0.1999 ± 0.0021** | **100** | **0.1954 ± 0.0021** |


**[D]**

| 1 MeV | Glass coverslip (1.91512 cm³) | Cell Culture (0.0010 cm³) | | Medium (water) (18.7990 cm³) |
|---|---|---|---|---|
| **Particles** | Dose ± standard deviation cGy | Dose ± standard deviation cGy | Contribution to total dose % | Dose ± standard deviation cGy |
| Total heavy ions | 0.1633 ± 0.0008 | 0.1922 ± 0.0027 | 97.66  0.61 | 0.1858 ± 0.0016 |
| $^{56}$Fe ions | 0.1628 ± 0.0008 | 0.1910 ± 0.0028 | 97.05 | 0.1751 ± 0.0016 |
| Electrons | 0.0016 ± 0.72 % | 0.0040 ± 0.0001 | 2.03 | 0.0069 ± 0.0001 |
| Photons | $3.0758 \times 10^{-7}$ ± 2.36 % | $4.9817 \times 10^{-8}$ ± 75.16 % | 0.00003 | $1.7904 \times 10^{-7}$ ± 14.80 % |
| Protons | $2.0372 \times 10^{-4}$ ± 7.36 % | $3.4352 \times 10^{-4}$ ± 8.05 % | 0.17 | $7.4120 \times 10^{-4}$ ± 3.54 % |
| Alpha | $6.1595 \times 10^{-5}$ ± 12.03 % | $1.1259 \times 10^{-4}$ ± 78.06 % | 0.05 | $2.0916 \times 10^{-4}$ ± 4.68 % |
| **Total** | **0.1653 ± 0.0008** | **0.1968 ± 0.0029** | **100** | **0.1939 ± 0.0016** |

**Table 4-3: Contribution of primary and secondary particles to the mean absorbed dose in the glass coverslip, cell culture and medium when 600 MeV/u $^{28}$Si ions were used to deliver 0.2 cGy to cell cultures grown on glass-bottomed flaskettes with a nominal fluence of 24 480 $^{28}$Si ions/cm² which results in 9 792 000 particles over the exposure area of 20 x 20 cm. The production thresholds of δ rays were set at [A] 1 keV, [B] 10 keV, [C] 100 keV, [D] 1 MeV. The transport cut-off was set at 1 keV for HZE particles, protons, photons, and α particles. For electrons, it was set at 150 eV (Panel A) or 1 keV (Panels B, C and D).**

**Errors represent standard deviations of the mean. When the standard deviation is < 0.0001 cGy, it is expressed and noted in % as it can represent a high deviation. The term "total heavy ion" refers to the primary 600 MeV/u $^{28}$Si ions and the fragments.**

**[A]**

| 1 keV | Glass coverslip (1.91512 cm$^3$) | Cell Culture (0.0010 cm$^3$) | | Medium (water) (18.7990 cm$^3$) |
|---|---|---|---|---|
| **Particles** | **Dose ± standard deviation** *cGy* | **Dose ± standard deviation** *cGy* | **Contribution to total dose** *%* | **Dose ± standard deviation** *cGy* |
| Total heavy ions | 0.1006 ± 0.0003 | 0.1236 ± 0.0012 | 61.16 *0.20* | 0.1209 ± 0.0004 |
| $^{28}$Si ions | 0.1003 ± 0.0010 | 0.1232 ± 0.0012 | 60.96 | 0.1170 ± 0.0012 |
| Electrons | 0.0611 ± 0.0006 | 0.0777 ± 0.0012 | 38.44 | 0.0720 ± 0.0007 |
| Photons | 3.1033 x 10$^{-6}$ ± 1.40 % | 1.1169 x 10$^{-6}$ ± 82.11 % | 0.00 | 2.1527 x 10$^{-6}$ ± 2.25 % |
| Protons | 2.7759 x 10$^{-4}$ ± 5.06 % | 4.7413 x 10$^{-4}$ ± 26.76 % | 0.23 | 9.7519 x 10$^{-4}$ ± 5.20 % |
| Alpha | 1.0644 x 10$^{-4}$ ± 13.94 % | 1.4144 x 10$^{-4}$ ± 73.98 % | 0.07 | 2.6864 x 10$^{-4}$ ± 5.03 % |
| **Total** | **0.1622 ± 0.0016** | **0.2021 ± 0.0024** | **100** | **0.1945 ± 0.0019** |

**[B]**

| 10 keV | Glass coverslip (1.91512 cm$^3$) | Cell Culture (0.0010 cm$^3$) | | Medium (water) (18.7990 cm$^3$) |
|---|---|---|---|---|
| **Particles** | **Dose ± standard deviation** *cGy* | **Dose ± standard deviation** *cGy* | **Contribution to total dose** *%* | **Dose ± standard deviation** *cGy* |
| Total heavy ions | 0.1218 ± 0.0008 | 0.1467 ± 0.0014 | 73.11 *0.26* | 0.1436 ± 0.0016 |
| $^{28}$Si ions | 0.1215 ± 0.0008 | 0.1462 ± 0.0014 | 72.85 | 0.1389 ± 0.0016 |
| Electrons | 0.0392 ± 0.0003 | 0.0531 ± 0.0009 | 26.44 | 0.0479 ± 0.0005 |
| Photons | 2.5971 x 10$^{-6}$ ± 0.75 % | 1.0276 x 10$^{-6}$ ± 54.41 % | 0.00 | 1.8470 x 10$^{-6}$ ± 2.18 % |
| Protons | 3.4229 x 10$^{-4}$ ± 7.30 % | 5.7103 x 10$^{-4}$ ± 22.19 % | 0.28 | 1.2144 x 10$^{-3}$ ± 3.40 % |
| Alpha | 1.2456 x 10$^{-4}$ ± 8.93 % | 1.0788 x 10$^{-4}$ ± 82.28 % | 0.05 | 3.4464 x 10$^{-4}$ ± 4.14 % |
| **Total** | **0.1617 ± 0.0010** | **0.2007 ± 0.0023** | **100** | **0.1934 ± 0.0021** |

**[C]**

| 100 keV | Glass coverslip (1.91512 cm$^3$) | Cell Culture (0.0010 cm$^3$) | | Medium (water) (18.7990 cm$^3$) |
|---|---|---|---|---|
| **Particles** | Dose ± standard deviation *cGy* | Dose ± standard deviation *cGy* | Contribution to total dose *%* | Dose ± standard deviation *cGy* |
| Total heavy ions | 0.1434 ± 0.0004 | 0.1708 ± 0.0011 | 86.74  *0.31* | 0.1671 ± 0.0014 |
| $^{28}$Si ions | 0.1431 ± 0.0012 | 0.1702 ± 0.0011 | 86.43 | 0.1616 ± 0.0013 |
| Electrons | 0.0175 ± 0.0.001 | 0.0250 ± 0.0003 | 12.70 | 0.0241 ± 0.0002 |
| Photons | 1.3178 x 10$^{-6}$ ± 0.90 % | 6.7873 x 10$^{-7}$ ± 157.79 % | 0.00 | 1.0610 x 10$^{-6}$ ± 2.89 % |
| Protons | 3.9845 x 10$^{-4}$ ± 7.79 % | 7.0894 x 10$^{-4}$ ± 14.22 % | 0.36 | 1.3842 x 10$^{-3}$ ± 1.63 % |
| Alpha | 1.3043 x 10$^{-4}$ ± 12.69 % | 1.8740 x 10$^{-4}$ ± 67.54 % | 0.10 | 3.4464 x 10$^{-4}$ ± 4.14 % |
| **Total** | **0.1616 ± 0.0014** | **0.1969 ± 0.0013** | **100** | **0.1933 ± 0.0016** |


**[D]**

| 1 MeV | Glass coverslip (1.91512 cm$^3$) | Cell Culture (0.0010 cm$^3$) | | Medium (water) (18.7990 cm$^3$) |
|---|---|---|---|---|
| **Particles** | Dose ± standard deviation *cGy* | Dose ± standard deviation *cGy* | Contribution to total dose *%* | Dose ± standard deviation *cGy* |
| Total heavy ions | 0.1633 ± 0.0012 | 0.1938 ± 0.0041 | 98.43  *0.36* | 0.1887 ± 0.0030 |
| $^{28}$Si ions | 0.1630 ± 0.0122 | 0.1931 ± 0.0409 | 98.07 | 0.1827 ± 0.0296 |
| Electrons | 0.0007 ± 0.0000 | 0.0019 ± 0.0001 | 0.96 | 0.0027 ± 0.0000 |
| Photons | 1.4358 x 10$^{-7}$ ± 5.34 % | 1.8106 x 10$^{-8}$ ± 210.82 % | 0.00 | 6.5495 x 10$^{-8}$ ± 20.30 % |
| Protons | 3.7917 x 10$^{-4}$ ± 9.00 % | 6.5103 x 10$^{-4}$ ± 14.40 % | 0.48 | 1.4250 x 10$^{-3}$ ± 3.29 % |
| Alpha | 1.3149 x 10$^{-4}$ ± 11.76 % | 1.1953 x 10$^{-4}$ ± 38.38 % | 0.06 | 3.8005 x 10$^{-4}$ ± 4.26 % |
| **Total** | **0.1647 ± 0.0012** | **0.1969 ± 0.0041** | **100** | **0.1937 ± 0.0031** |

**Table 4-4: Contribution of primary and secondary particles to the mean absorbed dose in the glass coverslip, cell culture and medium when 290 MeV/u $^{12}$C ions were used to deliver 0.2 cGy to cell cultures grown on glass-bottomed flaskettes with a nominal fluence of 96 030 $^{12}$C ions/cm² which results in 38 412 000 particles over the exposure area of 20 x 20 cm. The production thresholds of δ rays were set at [A] 1 keV, [B] 10 keV, [C] 100 keV, [D] 1 MeV. The transport cut-off was set at 1 keV for HZE particles, protons, photons, and α particles. For electrons, it was set at 150 eV (Panel A) or 1 keV (Panels B, C and D).**

**Errors represent standard deviations of the mean. When the standard deviation is < 0.0001 cGy, it is expressed and noted in % as it can represent a high deviation. The term "total heavy ion" refers to the primary 290 MeV/u $^{12}$C ions and the fragments.**

**[A]**

| 1 keV | Glass coverslip (1.91512 cm$^3$) | Cell Culture (0.0010 cm$^3$) | | Medium (water) (18.7990 cm$^3$) |
|---|---|---|---|---|
| Particles | Dose ± standard deviation *cGy* | Dose ± standard deviation *cGy* | Contribution to total dose *%* | Dose ± standard deviation *cGy* |
| Total heavy ions | 0.1024 ± 0.0001 | 0.1270 ± 0.0013 | 62.15 *0.09* | 0.1265 ± 0.0001 |
| $^{12}$C ions | 0.1023 ± 0.0006 | 0.1268 ± 0.0013 | 62.06 | 0.1249 ± 0.0011 |
| Electrons | 0.0613 ± 0.0004 | 0.0755 ± 0.0015 | 36.94 | 0.0710 ± 0.0006 |
| Photons | 3.0082 x 10$^{-6}$ ± 0.93 % | 8.7095 x 10$^{-7}$ ± 138.13 % | 0.00 | 1.9454 x 10$^{-6}$ ± 2.67 % |
| Protons | 6.0239 x 10$^{-4}$ ± 10.79 % | 1.0729 x 10$^{-3}$ ± 34.90 % | 0.53 | 2.2658 x 10$^{-3}$ ± 4.59 % |
| Alpha | 2.6778 x 10$^{-4}$ ± 15.20 % | 3.5004 x 10$^{-4}$ ± 84.32 % | 0.17 | 7.1590 x 10$^{-4}$ ± 4.49 % |
| **Total** | **0.1649 ± 0.0011** | **0.2043 ± 0.0029** | **100** | **0.2011 ± 0.0018** |

**[B]**

| 10 keV | Glass coverslip (1.91512 cm$^3$) | Cell Culture (0.0010 cm$^3$) | | Medium (water) (18.7990 cm$^3$) |
|---|---|---|---|---|
| Particles | Dose ± standard deviation *cGy* | Dose ± standard deviation *cGy* | Contribution to total dose *%* | Dose ± standard deviation *cGy* |
| Total heavy ions | 0.1256 ± 0.0010 | 0.1525 ± 0.0019 | 74.89 *0.21* | 0.1521 ± 0.0019 |
| $^{12}$C ions | 0.1254 ± 0.0010 | 0.1521 ± 0.0020 | 74.68 | 0.1501 ± 0.0019 |
| Electrons | 0.0378 ± 0.0003 | 0.0490 ± 0.0009 | 24.05 | 0.0443 ± 0.0005 |
| Photons | 2.4343 x 10$^{-6}$ ± 1.24 % | 9.3402 x 10$^{-7}$ ± 105.77 % | 0.00 | 1.6359 x 10$^{-6}$ ± 4.67 % |
| Protons | 7.7265 x 10$^{-4}$ ± 14.18 % | 1.3566 x 10$^{-3}$ ± 36.62 % | 0.67 | 2.7321 x 10$^{-3}$ ± 4.26% |
| Alpha | 3.5199 x 10$^{-4}$ ± 13.32 % | 2.3531 x 10$^{-4}$ ± 98.87 % | 0.12 | 7.0770 x 10$^{-4}$ ± 5.66 % |
| **Total** | **0.1648 ± 0.0013** | **0.2037 ± 0.0030** | **100** | **0.2007 ± 0.0024** |

**[C]**

| 100 keV | Glass coverslip (1.91512 cm$^3$) | Cell Culture (0.0010 cm$^3$) | | Medium (water) (18.7990 cm$^3$) |
|---|---|---|---|---|
| **Particles** | Dose ± standard deviation *cGy* | Dose ± standard deviation *cGy* | Contribution to total dose *%* | Dose ± standard deviation *cGy* |
| Total heavy ions | 0.1489 ± 0.0001 | 0.1787 ± 0.0033 | 88.92 *0.20* | 0.1772 ± 0.0015 |
| $^{12}$C ions | 0.1486 ± 0.0012 | 0.1783 ± 0.0032 | 88.72 | 0.1749 ± 0.0016 |
| Electrons | 0.0148 ± 0.001 | 0.0198 ± 0.0006 | 9.86 | 0.0183 ± 0.0002 |
| Photons | $1.1053 \times 10^{-6} \pm 1.82\%$ | $3.7904 \times 10^{-7} \pm 170.03\%$ | 0.00 | $7.8355 \times 10^{-7} \pm 5.69\%$ |
| Protons | $8.5832 \times 10^{-4} \pm 14.21\%$ | $1.5021 \times 10^{-3} \pm 21.36\%$ | 0.75 | $3.0876 \times 10^{-3} \pm 4.44\%$ |
| Alpha | $3.4244 \times 10^{-4} \pm 15.08\%$ | $4.6763 \times 10^{-4} \pm 59.71\%$ | 0.23 | $9.3214 \times 10^{-4} \pm 6.61\%$ |
| **Total** | **0.1653 ± 0.0013** | **0.2009 ± 0.0031** | **100** | **0.2004 ± 0.0018** |


**[D]**

| 1 MeV | Glass coverslip (1.91512 cm$^3$) | Cell Culture (0.0010 cm$^3$) | | Medium (water) (18.7990 cm$^3$) |
|---|---|---|---|---|
| **Particles** | Dose ± standard deviation *cGy* | Dose ± standard deviation *cGy* | Contribution to total dose *%* | Dose ± standard deviation *cGy* |
| Total heavy ions | 0.1654 ± 0.0013 | 0.1971 ± 0.0038 | 98.30 *0.15* | 0.1958 ± 0.0014 |
| $^{12}$C ions | 0.1652 ± 0.0014 | 0.1910 ± 0.0038 | 98.15 | 0.1934 ± 0.0013 |
| Electrons | $5.0037 \times 10^{-7} \pm 73.15\%$ | $7.0334 \times 10^{-7} \pm 83.07\%$ | 0.00 | $1.7944 \times 10^{-6} \pm 26.38\%$ |
| Photons | $3.2179 \times 10^{-7} \pm 101.49\%$ | 0.0000 ± 0.0000 | 0.00 | $1.6590 \times 10^{-11} \pm 78.71\%$ |
| Protons | $7.5727 \times 10^{-5} \pm 11.64\%$ | $1.5147 \times 10^{-4} \pm 26.84\%$ | 0.08 | $2.8089 \times 10^{-4} \pm 3.62\%$ |
| Alpha | $3.4659 \times 10^{-4} \pm 16.25\%$ | $6.5669 \times 10^{-4} \pm 0.0006$ | 0.33 | $9.9823 \times 10^{-4} \pm 7.15\%$ |
| **Total** | **0.1670 ± 0.0014** | **0.2005 ± 0.0037** | **100** | **0.2010 ± 0.0013** |

In cell cultures exposed to 0.2 cGy from any of the primary ions, the majority of the cellular absorbed dose was from their respective primary ions. The remainder was due to electrons, photons, protons, α particles and other heavy ions resulting from fragmentation. In FLUKA terminology, the term heavy ion represents the heavy ions with atomic numbers ranging from Z=3 to the Z of the primary ions (Z=26 for $^{56}$Fe, Z=14 for $^{28}$Si and Z=12 for $^{12}$C); it excludes α particles (Z=2). The difference between the delivered dose from heavy ions and that from the incident primary beam gives the dose due to fragments. The secondary radiations consisting of HZE fragments, photons, protons and α particles, with a production threshold and a transport cut-off set at 1 keV, constituted <1 % of the total absorbed dose (Panels A of Table 4-2, Table 4-3, Table 4-4). In contrast, electrons with a production threshold set at 1 keV and transport cut-off set at 150 eV contributed ~37-40 % of the total dose. The mean absorbed dose deposited in the cell monolayer by HZE fragments was very small (0.0007 cGy, 0.0004 cGy and 0.0005 cGy following exposure to $^{56}$Fe ions, $^{28}$Si ions or $^{12}$C ions, respectively) (Panels A of Table 4-2, Table 4-3, Table 4-4). The dose contributed by photons, protons and α particles was minimal in all cases (Panels A of Table 4-2, Table 4-3, Table 4-4).

Estimates of the mean absorbed doses to the glass cover-slip, cell monolayer and growth medium due to secondary radiations when the production threshold of δ rays was set at 1, 10 100 or 1000 keV and the transport cut off was set at 1 keV are described in Table 4-2, Table 4-3, Table 4-4. As the production threshold of the δ rays increased, the contribution of secondary electrons to the total mean absorbed dose delivered to the *cell monolayers* decreased and that of primary ions increased. Specifically, when the δ rays' production threshold was set at 1000 keV, the contribution of primary ions to the total mean absorbed dose to a *cell monolayer* exposed to 1000 MeV/u $^{56}$Fe ions increased to ~97 % and that of electrons decreased to ~2 % (Table 4-2, Panel D). In case of 600 MeV/u $^{28}$Si ions and

290 MeV/u $^{12}$C ions, the secondary electrons represented, respectively, 0.96 % and almost nil of the total mean absorbed dose to the *cell monolayer* (Panels D of Table 4-3, Table 4-4).

Considering δ rays, the maximal dose is delivered in the center of the flaskette filled to capacity with medium. This can be linked with the LET of the incident ions; for example, $^{56}$Fe ions lose some energy through the coverslip and the cell culture, leading to higher LET. Moreover, for such energies, the major part of the LET comes from electronic losses and is equal to 152.46 keV/μm, while the nuclear component is equal to 0.024 keV/μm. In this case, for iron ions, at 56 GeV, the initial LET used was calculated with SRIM[h] 2010 (Ziegler) and was equal to 152.5 keV/μm instead of the 151 keV/μm, the value of LET measured at NSRL and reported in the other chapters. The dose delivered by photons is very low and negligible relative to the total dose; they are thought to come from Bremsstrahlung[i] of the ions and electrons, and de-excitations (radiative cascades) of the ionized atoms in the coverslip followed by the cell monolayer and the medium. As the matters traversed are not really dense and are composed of low-Z-compounds, the intensity of Bremsstrahlung is weak.

In case of protons and α particles, their spatial distribution is not really homogeneous and is more important in the growth medium (water) and at the exit of the flaskettes; it is due to fragmentation of the ions in the polystyrene side of the flaskette.

The major contribution to the total dose is due to the primary ions, electrons and fragments; however, participation of the heavy ion fragments seems to be negligible compared to the primary beam contribution to the total dose. Nevertheless, their energy and spatial distributions will be determined in order to try to quantify how much they are able to hit neighboring cells.

---

[h] SRIM (Stopping and Range of Ions in Matter) is a group of computer programs which calculate interaction of ions with matter : Ziegler, J. F. "Particle interaction with matter, SRIM (Stopping and Range of Ions in Matter) " http://www.srim.org/.
[i] Bremsstrahlung: X rays resulting from interaction of a charged particle with a target nucleus or electron cloud.

## 4.3.2  Spectral fluence distributions

Spectral fluence distributions after exposure to 0.2 cGy of 1000 MeV/u $^{56}$Fe or 600 MeV/u $^{28}$Si ions (respectively Figure 4-3 and Figure 4-4) are given from differential energy fluence expressed in particles/GeV/cm²/primary ion. To obtain the fluence for a given energy channel, the differential energy fluence need to be multiplied by the width of the channel energy considered.

Each graph of Figure 4-3 and Figure 4-4 represents the fluence of different types of particles versus energy. It should be noticed that the logarithmic scales of the energy and fluence, respectively, in X and Y axes, are not the same for all the graphs. The minimal energy considered was 1 keV (cut-off energy), energy at which particles deposit all their energy locally. The maxima were those of primary ions (i.e. 56 GeV for 1 GeV/u **$^{56}$Fe ions** and 16.8 GeV for 600 MeV/u **$^{28}$Si ions**).

Panels A in Figure 4-3 and Figure 4-4 represent the spectral distribution of the **heavy ions** including primary ions at 56 GeV and 16.8 GeV, respectively for $^{56}$Fe and $^{28}$Si, and other fragments whose energy is lower than the primary ions. Those distributions are bimodal: an energy distribution that ranges from ~3 to 56 GeV for $^{56}$Fe primary ions and another that ranges from several keV to ~100 MeV in the medium (Figure 4-3, Panel A) . For the cell culture, the error bars of the first part of the curve (between ~700 keV to 2 MeV) are too important to give good statistical results (Figure 4-3, Panel A). The results obtained for silicon ion are similar. The maximum of the fluence is ~0.001 ions/GeV/cm²/primary.

The majority of the **electrons** (Figure 4-3 and Figure 4-4, Panels B) have energy less than 1 MeV but nevertheless, some of them can reach ~500 MeV. In cell culture, the fluence of the majority of the electrons is in the region of 0.07 electrons/GeV/cm²/primary, and reaches in the medium more than 1000 electrons/GeV/cm²/primary in case of $^{56}$Fe primary

ions (Figure 4-3, Panel B). For $^{28}$Si primary ions, the fluences are lower (Figure 4-4, Panel B).

For **photons** (Figure 4-3 and Figure 4-4, Panels C), the maximal fluences (~0.05 photons/GeV/cm²/primary in the cell culture and ~1000 photons/GeV/cm²/primary in the medium for $^{56}$Fe primary ions) are reached for an energy of ~20 keV with a majority of the photons having an energy less than 10 MeV.

The fluences of the **protons** (Figure 4-3 and Figure 4-4, Panels D) seem to be rather constant between 1 keV and 1 GeV in the medium as well as in the cell culture.

The spectral distributions of **α particles** (Figure 4-3 and Figure 4-4, Panels E) are also bimodal with a first part between 1 keV and 100 MeV and the other part between 1 GeV and 10 GeV.
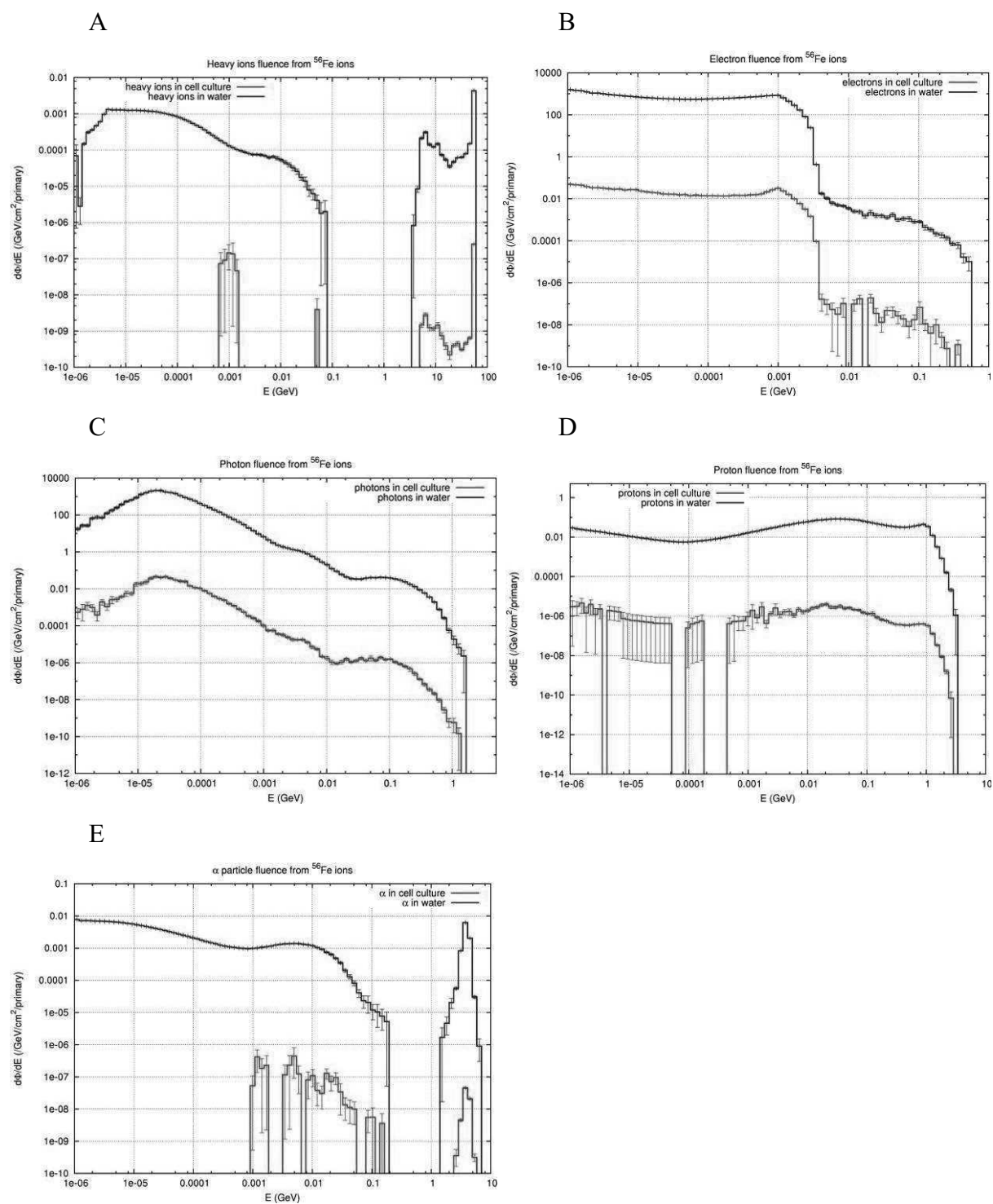
**Figure 4-3: Spectral fluence distribution of (A) heavy ions, (B) electrons, (C) photons, (D) protons, (E) α particles in cell culture and in medium (water) contained in a flaskette exposed to 0.2 cGy of 1000 MeV/u $^{56}$Fe ions.**

A



B



C



D



E
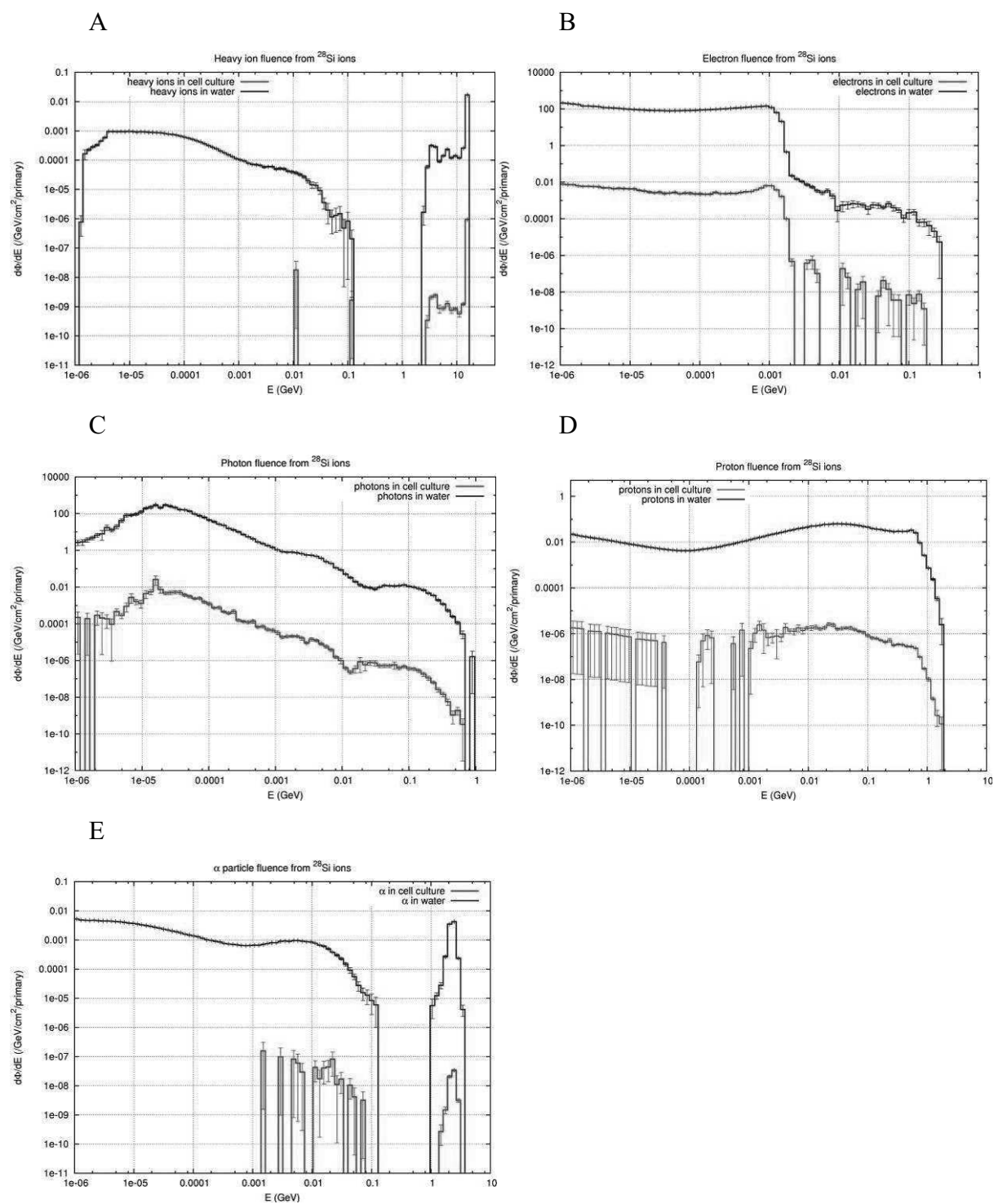


**Figure 4-4: Spectral fluence distribution of (A) heavy ions, (B) electrons, (C) photons, (D) protons, (E) α particles in cell culture and in medium (water) contained in a flaskette exposed to 0.2 cGy of 600 MeV/u $^{28}$Si ions.**

The tendency is similar between exposures to 0.2 cGy from 1 GeV/u $^{56}$Fe ions and from 600 MeV/u $^{28}$Si ions but the fluence is 10 times less along the Y-axis. In case of exposure to 0.2 cGy from 290 MeV/u $^{12}$C ions, the values are typically 100 times less than for iron ions. Concerning electrons and photons, this may be explained by the LET of the particles, the higher is the LET, the higher is the production of those secondary particles. Moreover, the electrons and photons produced in the medium filling the flaskette are less following $^{12}$C ions-irradiation than following exposure to silicon or iron ions. On the other hand, as it is known that the fragmentation cross sections on different atomic targets display different behaviour with increasing energy (Zeitlin, Fukumura et al. 2006; Bao-An, Feng-Shou et al. 2008), it is difficult to explain the observed behaviour in simple words.

Here, the fluence was considered unidirectional; however, the particles can be spread in different direction after being created.

The total fluences in the cell culture and in the medium, separately, are the sum of the products of differential fluence of each channel by the width of the channel and are reported in Table 4-5 for 1 GeV/u $^{56}$Fe ions and Figure 4-6 for 600 MeV/u $^{28}$Si ions. They represent the fluence in volume and can be viewed as track lengths of the particles in the volume considered (cm/cm$^3$). Due to the way by which these quantities are computed, i.e. it is necessary to divide the fluences by the volume. The data give the impression that fluences in the volume of the medium are much lower than those in the cell cultures. In fact, data are here computed in order to be compared within a same given column of the table (Cell Culture or Medium); data on a same line in the table are not to be compared.

**Table 4-5: Fluence in the cell monolayer (1 µm of thickness) and in the medium from different particles after exposure of the flaskettes to 0.2 cGy from 1 GeV/u $^{56}$Fe ions. When the standard deviation is < 0.0001 cGy, as it can represent a high deviation, it is expressed and noted in %.**

| | Cell Culture | | Medium | |
|---|---|---|---|---|
| | Fluence ± standard deviation $particle/cm^2/$ $2.4565 \times 10^{-6}$ primary | Fluence $particle/cm^2/$ primary | Fluence ± standard deviation $particle/cm^2/$ $0.0416$ primary | Fluence $particle/cm^2/$ primary |
| **Total heavy ions** | $2.4927 \times 10^{-6} \pm 0.29\%$ | 1.0147 | $0.0470 \pm 0.0001$ | 1.1284 |
| **$^{56}$Fe** | $2.4565 \times 10^{-6} \pm 0.27\%$ | 1.0000 | $0.0416 \pm 0.0001$ | 1.0000 |
| **Electrons** | $3.8606 \times 10^{-5} \pm 0.50\%$ | 15.7156 | $1.2483 \pm 0.0032$ | 29.9807 |
| **Photons** | $3.6237 \times 10^{-6} \pm 1.81\%$ | 1.4751 | $0.1691 \pm 0.0016$ | 4.0618 |
| **Protons** | $7.2868 \times 10^{-7} \pm 2.56\%$ | 0.2966 | $0.0510 \pm 0.0005$ | 1.2250 |
| **Alpha** | $5.3299 \times 10^{-8} \pm 4.18\%$ | 0.0217 | $0.0064 \pm 0.0001$ | 0.1527 |

**Table 4-6: Fluence in the cell monolayer (1 µm of thickness) and in the medium from different particles after exposure of the flaskettes to 0.2 cGy from 600 MeV/u $^{28}$Si ions. When the standard deviation is < 0.0001 cGy, as it can represent a high deviation, it is expressed and noted in %.**

| | Cell Culture | | Medium | |
|---|---|---|---|---|
| | Fluence ± standard deviation $particle/cm^2/$ $2.4759 \times 10^{-6}$ primary | Fluence $particle/cm^2/$ primary | Fluence ± standard deviation $particle/cm^2/$ $0.0434$ primary | Fluence $particle/cm^2/$ primary |
| **Total heavy ions** | $2.4935 \times 10^{-6} \pm 0.49\%$ | 1.0071 | $0.0463 \pm 0.0002$ | 1.0667 |
| **$^{28}$Si** | $2.4759 \times 10^{-6} \pm 0.48\%$ | 1.0000 | $0.0434 \pm 0.0002$ | 1.0000 |
| **Electrons** | $5.9678 \times 10^{-6} \pm 0.70\%$ | 2.4104 | $0.1589 \pm 0.0008$ | 3.6629 |
| **Photons** | $6.6834 \times 10^{-7} \pm 7.08\%$ | 0.2699 | $0.0246 \pm 0.0003$ | 0.5667 |
| **Protons** | $3.8213 \times 10^{-7} \pm 3.54\%$ | 0.1543 | $0.0253 \pm 0.0002$ | 0.5825 |
| **Alpha** | $2.4334 \times 10^{-8} \pm 6.17\%$ | 0.0098 | $0.0032 \pm 0.0001$ | 0.0734 |

## 4.3.3 Angular distributions

We consider now the fluences determined at the surface separating the different environments (interfaces between soda-lime glass/cell culture). The angular distributions have been computed considering a ring area delimited by the base of two cones with different solid angles as shown in Figure 4-2 at the level of the cell monolayer. It is defined as double

differential fluence with respect to energy and angle and is expressed in particles/GeV/cm²/sr/primary.

Figure 4-5 shows that the angular deflection of heavy ions after exposure to 0.2 cGy from 600 MeV $^{28}$Si ions does not exceed 7° measured with respect to the incident beam passing through the interface between soda-lime glass and cell culture.
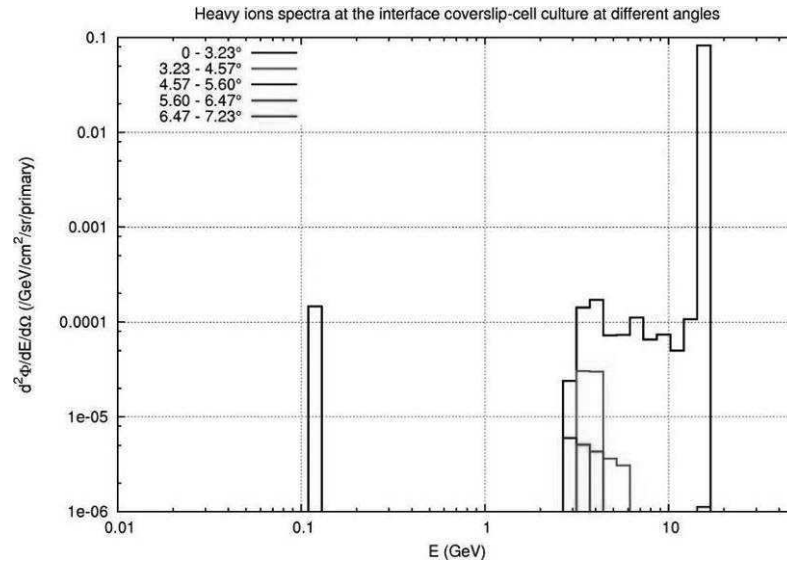


**Figure 4-5: Heavy ions fluence at the soda-lime glass/cell culture interface for different angular sectors after exposure to 0.2 cGy of 600 MeV/u $^{28}$Si ions.**

However, a fragment that is emitted at the entrance of the soda-lime glass would affect a bigger area at the level of the cell culture and greater number of cells.
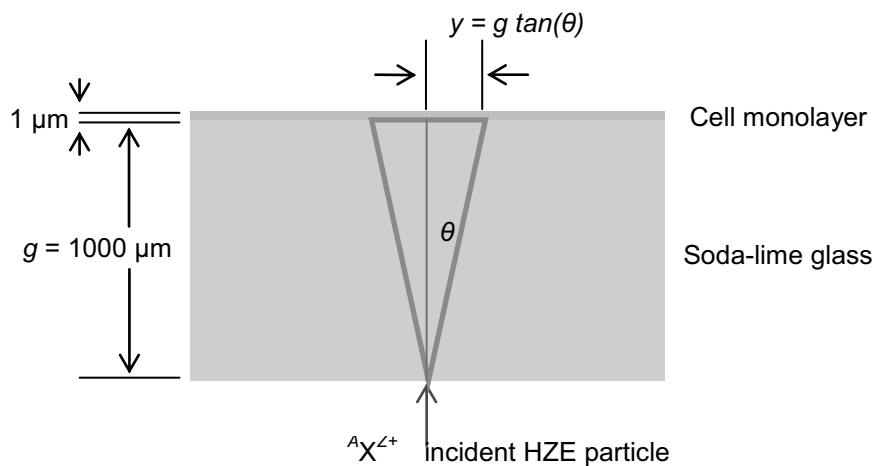


**Figure 4-6: Emission of the secondary particle if the interaction occurs at the entrance of the soda-lime glass.**

Nevertheless, the double differential fluences given by FLUKA at the entrance of the soda-lime glass are so low that they can be neglected. The worst case that can be considered is when a fragment is emitted at the maximum angle of 7° measured with respect to the incident path just after the entrance of the soda-lime glass within our culture conditions. As for fibroblasts, the mean nuclear thickness has been evaluated to be 1.2 μm (Cornforth, Schillaci et al. 1989) (Figure 4-7) and there is considerable heterogeneity among cells in such a monolayer. We therefore consider that the center of a AG1522 nucleus is situated at a 1 μm height in the cell culture layer. In such a case, the heavy-ion-fragments can affect an area of 123 μm in radius (Figure 4-6) that represents an area of ~47000 μm². As the total area of the cell is estimated to be 800 μm² (Gaillard, Pusset et al. 2009), the fragment can affect 1 cell over ~59 cells that cover this area. However, the fluence is very low and as the mean nuclear area is estimated to be 140 μm² (Azzam, de Toledo et al. 1998), it is therefore very unlikely that a heavy fragment will hit the nucleus of neighboring cells.
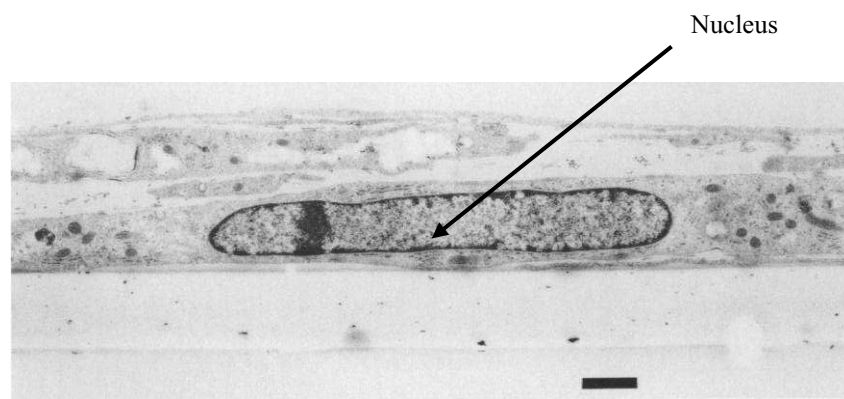


**Figure 4-7: Cross-section of a density-inhibited AG1522cell, shown growing attached to a thin Mylar substrate (1.5 μm). The prominent cell nucleus located close to the Mylar/cell interface. Although the cell depicted here is quite typical, there is considerable heterogeneity among cells in such a monolayer. Bar ~1 μm (Cornforth, Schillaci et al. 1989)**

Electrons have been estimated to have a range up to 270 μm when generated by 1GeV/u $^{56}$Fe ions (Metting, Rossi et al. 1988) spread out in transverse directions as they penetrate matter. Some of them even are scattered perpendicular to the incident beam in case

of exposure to either 1 GeV/u $^{56}$Fe or 600MeV/u $^{28}$Si ions (Figure 4-8 and Figure 4-9). Most of the electrons have energies less than 1 MeV (Figure 4-8 and Figure 4-9). Note that the X-axes of Figure 4-8 and Figure 4-9 are not the same. However, for 290 MeV/u $^{12}$C ions, the electrons spectra are not significant due to the very low values of the double differential fluences and important uncertainties (not shown).
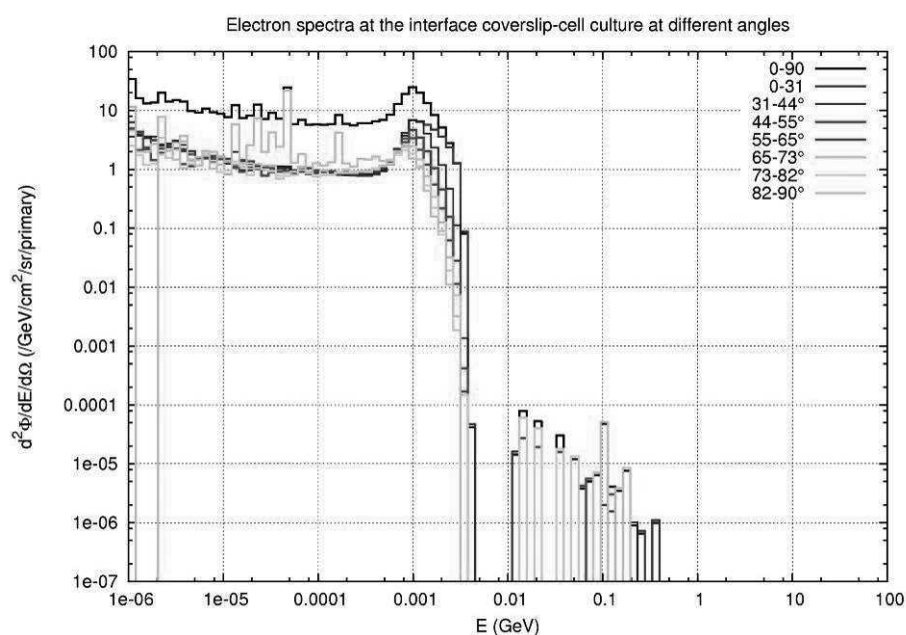


**Figure 4-8: Electrons fluence at the coverslip/cell culture interface for different angle particles after exposure to 0.2 cGy of 1000 MeV/u $^{56}$Fe ions.**
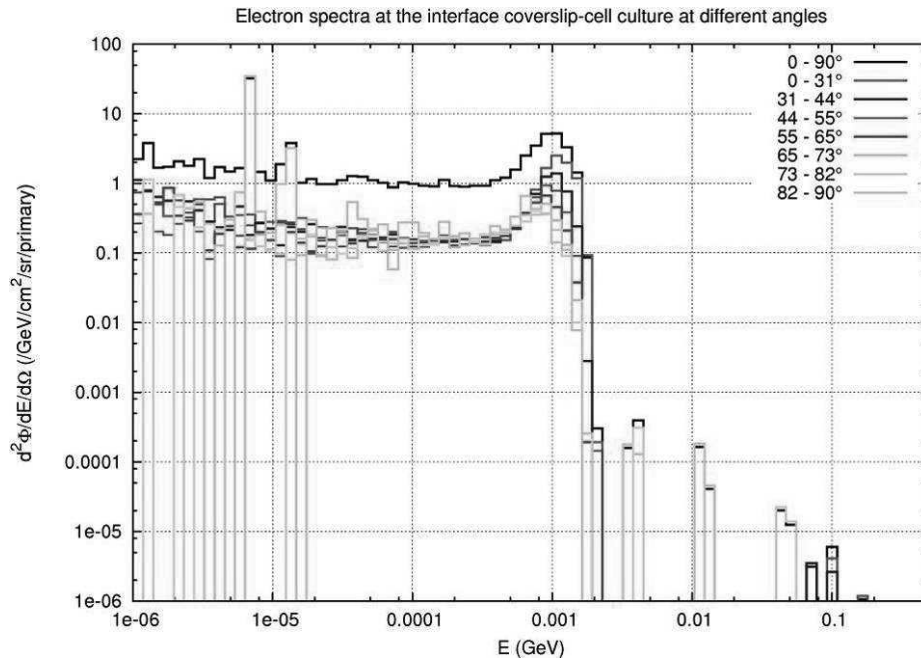
**Figure 4-9: Electrons fluence at the coverslip/cell culture interface for different angle particles after exposure to 0.2 cGy of 600 MeV/u [28]Si ions.**

When all the values of double differential fluence with respect to energy and angle in particles/cm²/GeV/deg/primary are multiplied by their respective energy interval, and then multiplied by the angular binning chosen, we obtained the fluence in particles/cm²/primary. As shown in Figure 4-2, it is thus possible to define concentric rings depending each on an angular interval (Figure 4-10) in which a given fluence in particles/cm²/primary was passing through. Figure 4-10 represents such distributions superimposed on Figure 3-7 (Panel D) for electrons, photons, protons and α particles around the incident track (visualized with CR-39) at 1 µm height in the AG1522 cell culture layer (approximately at the level of cell nuclei) considering the fluence at the interface soda-lime glass/cell culture. Figure 3-7 (Panel D) is a representative image of etched tracks, cell nuclei stained with DAPI (blue) and 53BP1 foci (red) in AG1522 cell cultures grown on dishes with a CR-39-nuclear track detector bottom, at 15 min after exposure to 0.2 cGy of 1 GeV/u [56]Fe ions. The angle relative to each concentric ring and the associated fluence are reported in the table that follows Figure 4-10. The rings corresponding to the angles "81.79° - 90°" are not represented in Figure 4-10 as they would

cover the whole pictures due to the elevated radius of the rings. Nevertheless, the values corresponding to "81.79° - 90°" are presented in the table following Figure 4-10. Such a representation makes it possible to scale to the size of the cell nuclei the area affected by secondary particles. However, the information about energy of the particles is lost (each concentric ring has been obtained by integration over the whole energy interval) and the fluence at the interface of soda-lime glass/cell cultures does not take into account all of the secondary particles appearing due to interactions in the 1 mm soda-lime glass thickness. Except the heavy ion fragments appearing in the 1 mm soda-lime glass thickness that will not be deflected in the sequel, all of the others particles will be subject of other interactions before reaching the interface soda-lime glass/cell culture. Thus, it might not be judicious to determine the double differential fluence at the entrance of the soda-lime glass. Lastly, it should be mentioned that the radial distributions of fragments are not represented due to their very small angular deflection (no more than 7°).
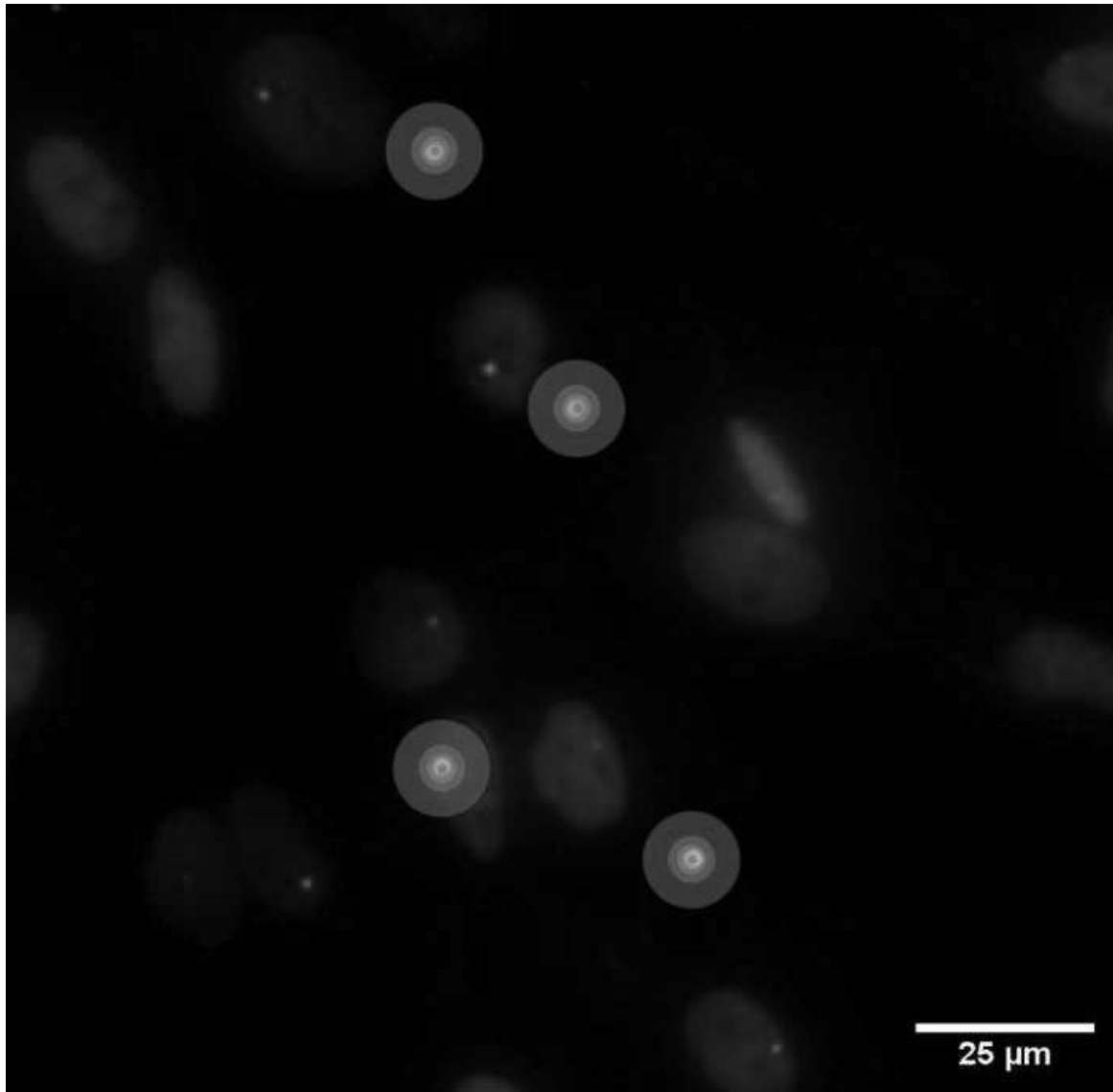
| | | Fluence particles/cm²/primary | | | |
|---|---|---|---|---|---|
| | Angle | **Electrons** | **Photons** | **Protons** | **α particles** |
| | 0° - 31.00° | 4.1834 | 0.1069 | 0.1570 | 0.0205 |
| | 31.00° - 44.41° | 2.6852 | 0.0754 | 0.0248 | 0.0002 |
| | 44.41° - 55.15° | 1.7104 | 0.0620 | 0.0166 | 0.0001 |
| | 55.15° - 64.62° | 1.2504 | 0.0575 | 0.0130 | 0.0001 |
| | 64.62° - 73.40° | 0.9914 | 0.0658 | 0.0122 | 0.0003 |
| | 73.40° - 81.79° | 0.8328 | 0.0784 | 0.0145 | 0.0002 |
| | 81.79° - 90° | 1.0603 | 0.1496 | 0.0232 | 0.0000 |
| | Total | 12.7139 | 0.5956 | 0.2613 | 0.0215 |

**Figure 4-10: Visualization of radial distribution around the incident track at 1 μm height in the AG1522 cell culture layer (approximately at the level of cell nuclei) of electrons, protons, protons and α particles considering the fluence at the interface soda-lime glass/cell culture when the flaskettes is exposed to 0.2 cGy from 1 GeV/u $^{56}$Fe ions**

When the double differential fluences of each type of particles are integrated over $2\pi$ steradian (hemispherical solid angle), they become differential fluence per energy interval ($\phi(E) = \dfrac{d\phi}{dE}$). Figure 4-11 represents the fluence of secondary particles versus energy for 1 GeV/u $^{56}$Fe. Table 4-7 and Table 4-8 report the fluence integrated over energy at the interface between coverslip and cell culture for 1 GeV/u $^{56}$Fe and 600 MeV/u $^{28}$Si ions respectively.
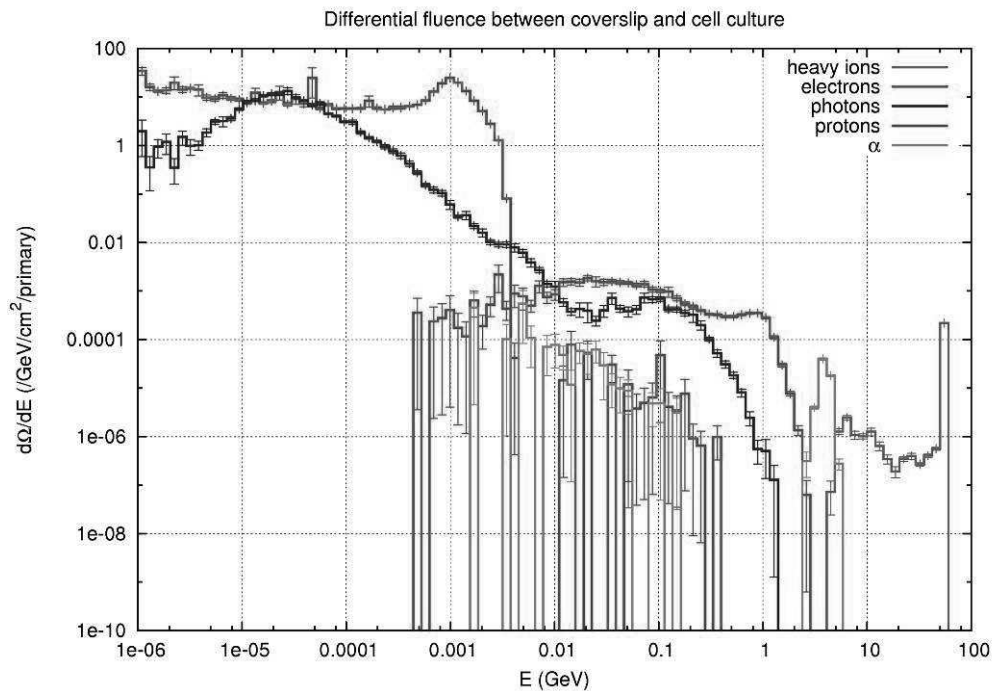


**Figure 4-11: Fluences of secondary particles versus energy at the coverslip/cell culture interface integrated over on $2\pi$ steradian after exposure to 0.2 cGy of 1000 MeV/u $^{56}$Fe ions.**

**Table 4-7: Fluence at the interface soda-lime glass /cell monolayer from different particles after exposure of the flaskettes to 0.2 cGy from 1 GeV/u $^{56}$Fe ions. When the standard deviation is < 0.0001 cGy, as it can represent a high deviation, it is expressed and noted in %.**

| | Surface between soda-lime glass and cell culture | |
|---|---|---|
| | **Fluence ± standard deviation** *particle/cm$^2$/0.0021 primary* | **Fluence** *particle/cm$^2$/primary* |
| **Total heavy ions** | 0.0022 ± 0.29 % | 1.0147 |
| **$^{56}$Fe** | 0.0021 ± 0.27 % | 1.0000 |
| **Electrons** | 0.0273 ± 0.71 % | 12.7185 |
| **Photons** | 0.0013 ± 1.59 % | 0.5956 |
| **Protons** | 0.0006 ± 2.84 % | 0.2613 |
| **Alpha** | 4.6166 x 10$^{-5}$ ± 4.16 % | 0.0215 |

**Table 4-8: Fluence at the interface soda-lime glass/cell monolayer from different particles after exposure of the flaskettes to 0.2 cGy from 600 MeV/u $^{28}$Si ions. When the standard deviation is < 0.0001 cGy, as it can represent a high deviation, it is expressed and noted in %.**

| | Surface between soda-lime glass and cell culture | |
|---|---|---|
| | **Fluence ± standard deviation** *particle/cm$^2$/0.0022 primary* | **Fluence** *particle/cm$^2$/primary* |
| **Total heavy ions** | 0.0022 ± 0.49 % | 1.0071 |
| **$^{28}$Si** | 0.0022 ± 0.48 % | 1.0000 |
| **Electrons** | 0.0042 ± 1.22 % | 1.9606 |
| **Photons** | 0.0002 ± 4.73 % | 0.1064 |
| **Protons** | 0.0003 ± 3.99 % | 0.1345 |
| **Alpha** | 2.1128 x 10$^{-5}$ ± 6.23 % | 0.0098 |

In both cases, after exposure of the flaskette to 0.2 cGy from 1 GeV/u $^{56}$Fe or 600 MeV/u $^{28}$Si ions, the number of electrons at the interface soda-lime glass/cell culture represents typically the double of the number of heavy ions but their energy are of course much less and the associated biological effect are different. The ionization cross-section for electrons that slow down in water, peaks around 100 eV (Plante and Cucinotta 2009). At high

electron energies, electrons loose more and more of their energy through Bremsstrahlung radiation (the critical energy for electrons in water is ~100 MeV; beyond this energy, the Bremsstrahlung component becomes the main energy loss process for electrons). Those later Bremsstrahlung photons are taken into account in the photon component of the presented calculations. In other words, this means that electrons produce the most dramatic effects at low energy (i.e. where the energy deposition is very local). In order to visualize the electron energy deposition in the whole flaskette, a computation was performed scaling the dose due to electrons. Figure 4-12 presents the results obtained with iron ions as well as silicon ions and shows clearly that most of the energy deposited by electrons is deposited outside of the cell layer (one order of magnitude higher in the medium), which confirms the above suggestion.
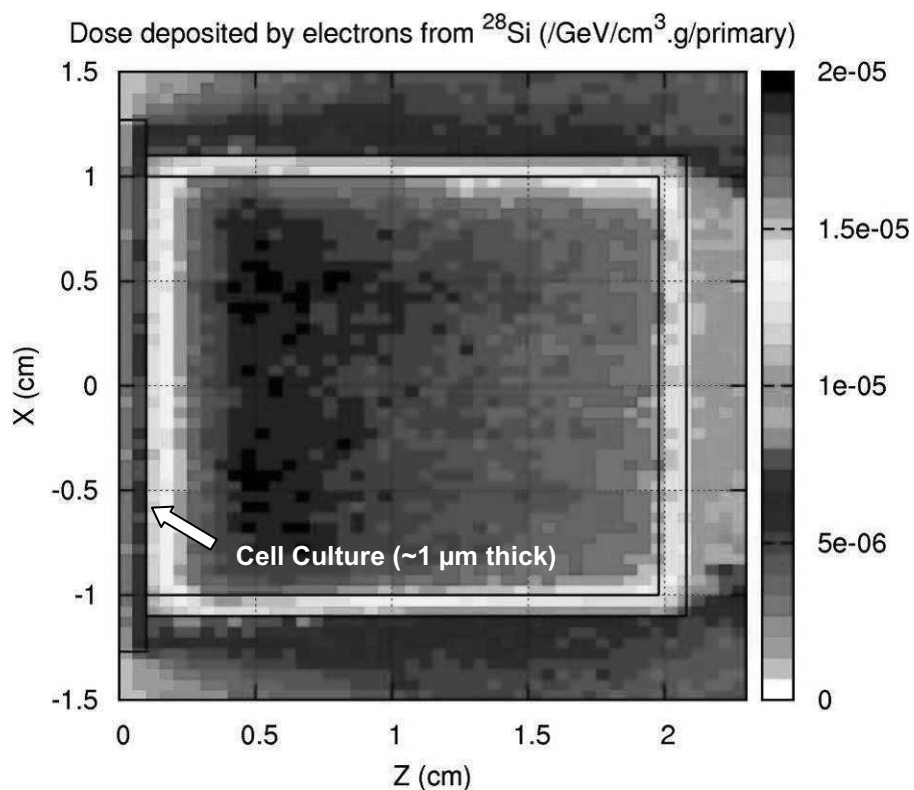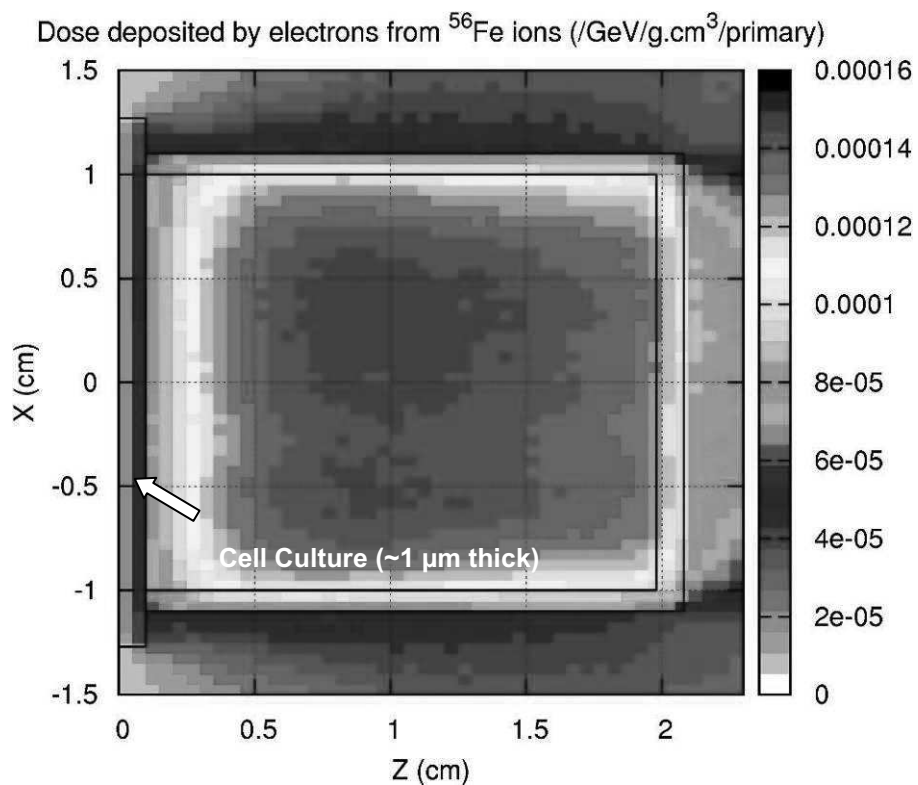
Figure 4-12: Cartography of dose deposited by electrons in soda-lime glass, cell culture and medium when flaskette is exposed to 0.2 cGy from 1 GeV/u $^{56}$Fe or 600 MeV/u $^{28}$Si ions.

## 4.3.4 Fragmentation

Figure 4-13, Figure 4-14 and Figure 4-15 represent the fragment yield integrated over $2\pi$ steradian in function of the charge of the ions when the flaskette is exposed to 0.2 cGy from 1000 MeV/u $^{56}$Fe ions, 600 MeV/u $^{28}$Si or 290 MeV/u $^{12}$C ions, respectively. The majority of the ions consists of the primary ions 1000 MeV/u $^{56}$Fe ions (Z=26), 600 MeV/u $^{28}$C ions (Z=14) or 290 MeV/u $^{12}$C ions (Z=6) in Figure 4-13 Figure 4-14 and Figure 4-15, respectively. For carbon ions, there is a peak at Z=8 that does not originate from fragmentation of carbon ions as only lower Z than Z of the primary ions are considered; they originate from recoil oxygen nuclei on which carbon ions did elastically diffuse in the soda-lime glass (Figure 4-15).
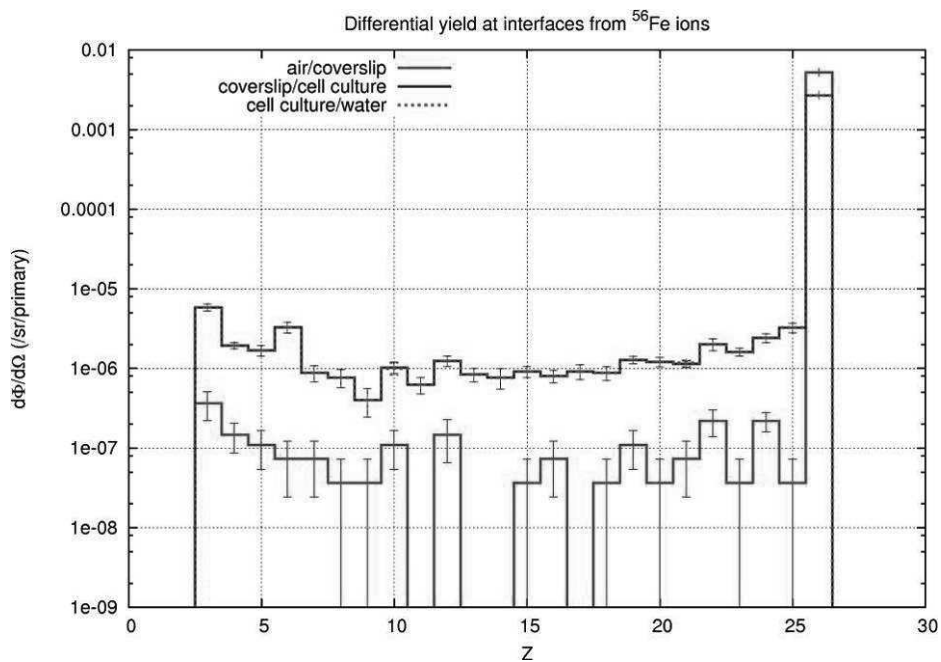


**Figure 4-13: Fluences in function of the charge of the heavy ions at the interface coverslip/cell culture (red) and interface cell culture/medium (blue) integrated over on $2\pi$ steradian after exposure to 0.2 cGy of 1000 MeV/u $^{56}$Fe ions.**
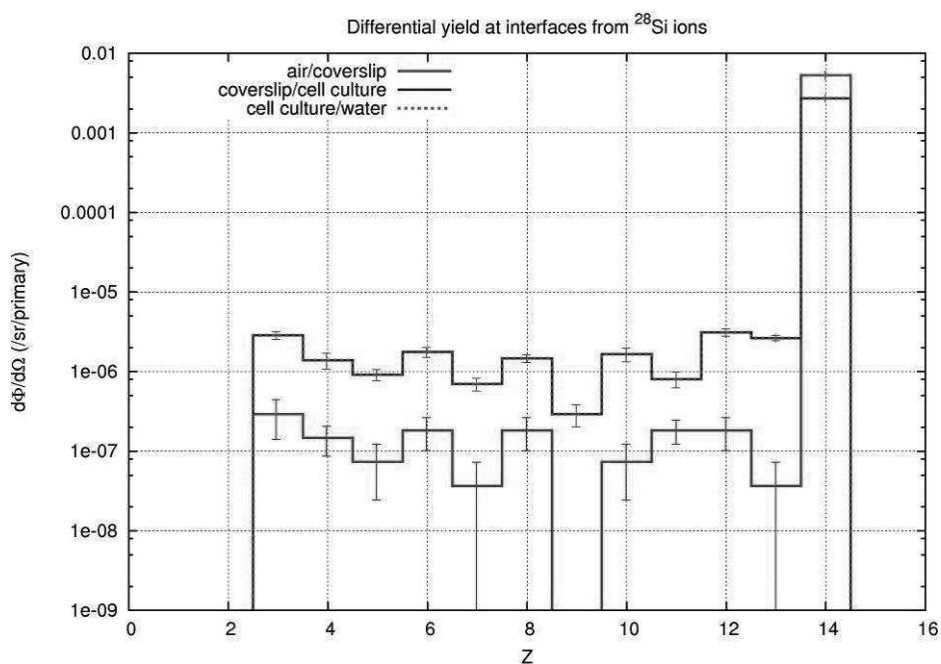
**Figure 4-14: Fluences in function of the charge of the heavy ions at the interface coverslip/cell culture (red) and interface cell culture/medium (blue) integrated over on $2\pi$ steradian after exposure to 0.2 cGy of 600 MeV/u $^{28}$Si ions.**
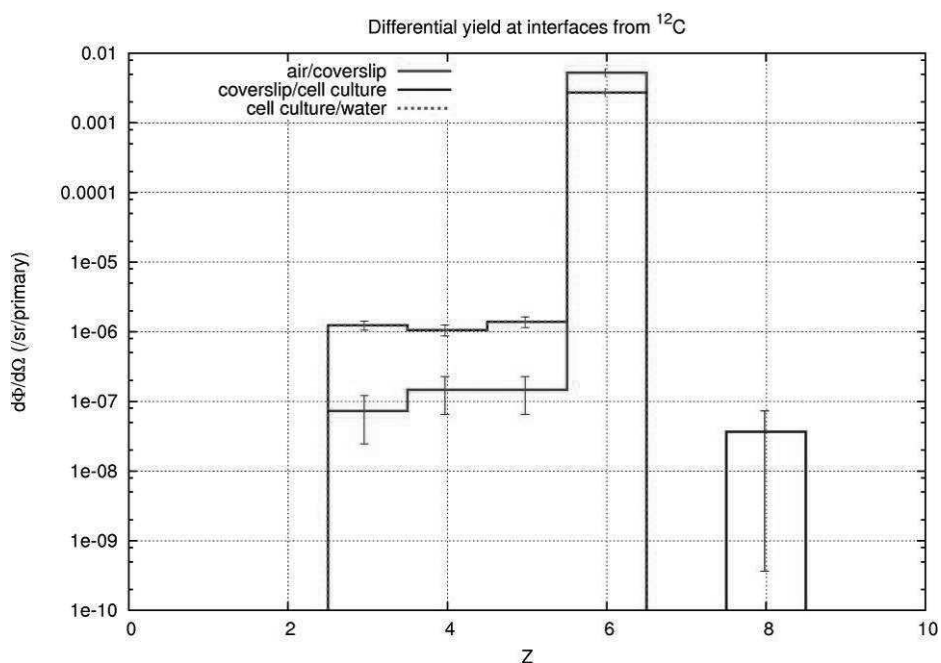


**Figure 4-15: Fluences in function of the charge of the heavy ions at the interface coverslip/cell culture (red) and interface cell culture/medium (blue) integrated over on $2\pi$ steradian after exposure to 0.2 cGy of 290 MeV/u $^{12}$C ions.**

## 4.4 Discussion

The beam delivered to samples can generate several components in addition to the nominal particles' beam which may be important when accounting for a better understanding of biological endpoints, in particular when considering low doses of radiation. Here, we consider the participation of different secondary particles such as fragments, electrons, photons, protons and α particles.

Those results highlight the weakness of the dose deposited by the fragments as compared to the dose deposited by the primary beam. However, the angular distributions and the production of fragments are all the higher so the charge is low. Indeed, in case of 95 MeV/u $^{12}$C, it has been shown that the more the fragments are heavy, the more they will be focused forward and centred on the primary ion's trajectory (Braunn 2010) as a result of linear momentum transfer from the beam. In our case, using a glass-bottomed flaskette, the angular dispersion of heavy-ion-fragments does not exceed 7° in case of 600 MeV/u $^{28}$Si and 1GeV/u $^{56}$Fe ions. Moreover, considering their low fluence, the probability that fragments affect surrounding cell nuclei is low and their contribution in bystander effect observed after heavy ions is negligible. In contrast, the electrons can be spread all around the primary ion's trajectory with ranges up to several hundred micrometers (Metting, Rossi et al. 1988). In our experiments where thin confluent cell monolayers are used, it is very unlikely that long range secondaries such as high energy δ rays do not escape out of the cellular culture and therefore they should rather deposit their energy outside of the living medium. Conversely, it should be noticed that the FLUKA computer code uses cut-off energy of 1 keV; thus, low-energy electrons as well as soft X rays are not taken into account although their effects on molecular structures are well known to be deleterious and very localized.

The results presented in this chapter do not take account of other components delivered in the NSRL beam room in addition to the nominal beam particles such as secondary particles

and scattered particles that may also irradiate the samples placed on top of or close to a table or any other massive surface.

Nevertheless, those results give a partial answer to the contribution of secondary particles in the observed bystander effect. Expanded FLUKA experiments and additional studies using other multi-particle transport code such as GEANT IV or Penelope adapted to lower energies and pushing the energy cut-off lower than 1 keV, particularly for electrons, would help answer more clearly the contribution of secondary radiations to the HZE-induced bystander effect.

# Chapter 5 <u>Specific Aim 3</u>: To examine mechanisms involved in the propagation of bystander effects in confluent normal human diploid cell cultures exposed to low fluence of HZE particles

## 5.1 Hypothesis

Several mechanisms have been implicated in the propagation of radiation-induced bystander effects. They include oxidative metabolism (Narayanan, Goodwin et al. 1997; Azzam, De Toledo et al. 2002), indirect and direct modes of intercellular communication (Mothersill and Seymour 1997; Azzam, de Toledo et al. 1998; Bishayee, Rao et al. 1999; Zhou, Randers-Pehrson et al. 2000; Azzam, de Toledo et al. 2001), physical contact (Gerashchenko and Howell 2005; Hei, Zhou et al. 2008), and membrane- (Nagasawa, Cremesti et al. 2002; Hanot, Hoarau et al. 2009), and cytoplasm-originating effects (Shao, Folkard et al. 2004). In these studies, the focus has been mainly on either γ ray or α particle-induced bystander effects (Mothersill and Seymour 2004). In contrast, our knowledge of mechanisms underlying bystander effects induced by HZE particles is unclear and is only emerging.

We hypothesize that gap junction intercellular communication and DNA repair have significant effects in the propagation of stressful effects from low fluence HZE-particle-irradiated cells to neighboring bystander cells. To test this hypothesis, AG1522 fibroblasts cultures were exposed to low fluences of 1000 MeV/u $^{56}$Fe or 600 MeV/u $^{28}$Si ions in presence or absence of chemical inhibitors of gap junction intercellular communication or DNA repair. The results were compared with those obtained in cultures exposed in parallel to low fluences of 3.7 MeV α particles.

We also hypothesize that the concentration of environmental oxygen during cell growth and at the time of irradiation modulates the magnitude of stressful effects induced in bystander cells in cultures exposed to low fluences of α particles. The latter studies extend our understanding of mechanisms underlying α-particle-induced non-targeted effects and mimic *in vivo* conditions wherein the oxygen concentration is much lower than ambient.

Micronucleus formation, 53BP1 foci formation and changes in levels of stress-responsive proteins were used as endpoints in these mechanistic studies.

## *5.2 Role of intercellular communication*

### 5.2.1 Rationale

Trosko et al. postulated that intercellular communication plays a major role in the response to ionizing radiation (Trosko, Chang et al. 1990). Subsequent studies with chemical inhibitors and genetic approaches have shown that gap junction intercellular communication indeed plays an important role in propagation of α-particle-induced bystander effect (Azzam, de Toledo et al. 1998; Zhou, Randers-Pehrson et al. 2000). Its role in the propagation of β-particle-induced bystander effects was also demonstrated in studies involving Chinese hamster V79 cells labeled with tritiated thymidine ([$^{3}$H]dThd) and mixed with non-labeled cells (Bishayee, Rao et al. 1999). The short range of the β particles emanating from tritium allows only self-irradiation of labeled cells and effectively no cross-irradiation of unlabeled cells. Similarly, the maximum range of the delta rays produced by a 3.7 MeV alpha particle is only about 0.1 μm (Hamm, Turner et al. 1985); therefore, bystander cells do not receive any cross dose. However, the physical characteristics of HZE particle irradiation are more complex, and evaluation of the contribution of junctional communication to bystander effects that HZE particles may induce could be complicated by the secondary radiations generated

during interactions of the incident particles with the target materials (i.e. cells and their surrounding substrates).

The AG1522 normal human fibroblasts used in this project are gap junction intercellular communication-competent (Azzam, de Toledo et al. 2001). Using the scrape-loading technique (el-Fouly, Trosko et al. 1987), the fluorescent dye Lucifer yellow diffused to adjacent cells in density-inhibited cultures (left panel of Figure 5-1). In contrast, the dye was confined to the damaged cells when the culture was incubated with 50 $\mu M$ 18-$\alpha$-glycyrrhetinic acid (AGA), a gap junction inhibitor (right panel of Figure 5-1) (Gaillard, Pusset et al. 2009).
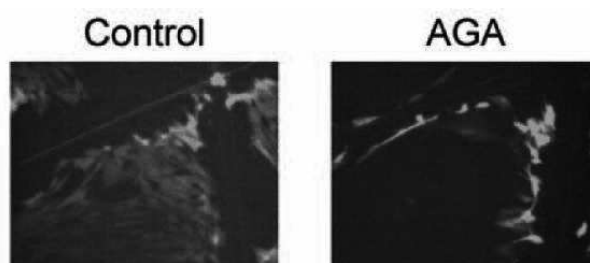


**Figure 5-1: Transfer of the fluorescent dye Lucifer yellow through gap junctions in AG1522 confluent, density inhibited cultures (left panel) and inhibition of its transfer to adjacent cells by 50 $\mu M$ AGA (right panel) (Gaillard, Pusset et al. 2009)**

To investigate the role of gap junction intercellular communication in the propagation of signaling events that lead to HZE-particle-induced bystander effects, we evaluated different stressful effects in confluent AG1522 cell cultures exposed to low fluences of energetic iron or silicon ions. We examined micronucleus and 53BP1 foci formation, and analyzed the level of p-TP53ser15, p21$^{Wafl}$, p-ERK1/2 and connexin 43 (cx 43) proteins by western blot analyses in cell cultures that were irradiated in presence or absence of AGA. The results were compared with those obtained in cell cultures exposed in parallel to low fluences of 3.7 MeV $\alpha$ particles.

## 5.2.2 Results

Three hours after exposure to 0, 0.2 or 1 cGy from 3.7 MeV α particles, the cell populations were harvested and assayed for micronucleus formation and *in situ* analyses of 53BP1 foci formation. Consistent with previous results, cell cultures exposed to 0.2 or 1 cGy from α particles showed significant increases ($p < 0.05$ and $p < 0.01$, respectively) in binucleated cells with micronuclei (Figure 5-2). Consistent with this induction of DNA damage, they also showed, relative to control, greater increases than expected in 53BP1 foci formation whether when the fraction of cell with 53BP1 foci or the mean number of 53BP1 foci per cell ($p < 0.001$) (Figure 5-3) were considered. Those increases are much higher than the percentage (1.4 % or 7.2 % for 0.2 and 1 cGy, respectively) of cells that would have been traversed by a particle track through the nucleus, which suggests the involvement of cells other than those initially irradiated in the response of the exposed cultures to α particles.
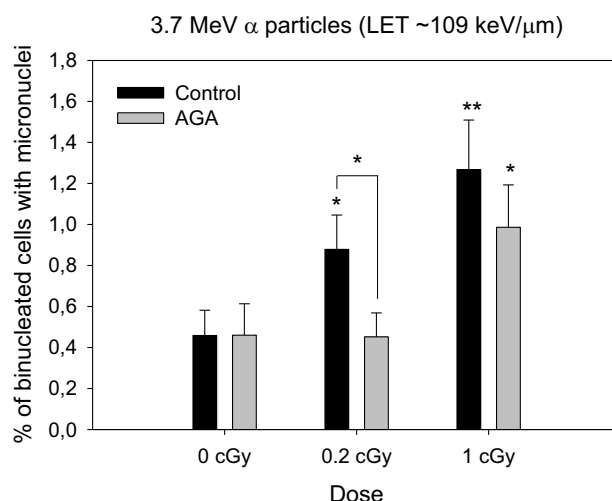


**Figure 5-2: Percentage of micronucleated cells in confluent AG1522 cell cultures after exposure to a mean dose of 0, 0.2 or 1 cGy from 3.7 MeV α particles in presence or absence of AGA. The cell cultures were subcultured, 3 h after exposure, and grown in presence of cytochalasin B for 72 hours. The graph is representative of 2 experiments. (\*: *p* <0.05 and \*\*: *p* <0.01)**

When the cell cultures were exposed to α particles in presence of 50 μ$M$ AGA, the increase in micronucleus formation observed at 3 h after exposure to mean absorbed dose of 0.2 cGy was significantly inhibited ($p$ <0.05) and the fraction of micronucleated cells was similar to that observed in control cell cultures (Figure 5-2). In cell cultures exposed to 1 cGy in presence of AGA, the micronucleus formation was attenuated but not completely inhibited.

In presence of AGA, the percent excess of cells with 53BP1 foci and the mean number of 53BP1 foci per cell (Figure 5-3, Panels A and B) also decreased by 3 h after exposure to a mean absorbed dose of 0.2 cGy ($p$ <0.05 and $p$ <0.01, respectively). Inhibition of junctional communication by AGA seems to limit the increases in 53BP1 foci formation without eliminating them entirely. However, in these experiments, incubation with AGA significantly induced an increase in the fraction of control cells with foci. These data are different from those described in Figure 5-2 where incubation of control cells with AGA did not increase micronucleus formation. Interestingly however, the 53BP1 data suggest that intercellular communication under homeostatic conditions is essential in controlling the level of DNA damage due to metabolic activity (i.e. DNA damage in the absence of irradiation). DNA damage due to metabolic activity is continuously generated and is readily repaired (Weinberg 2007).
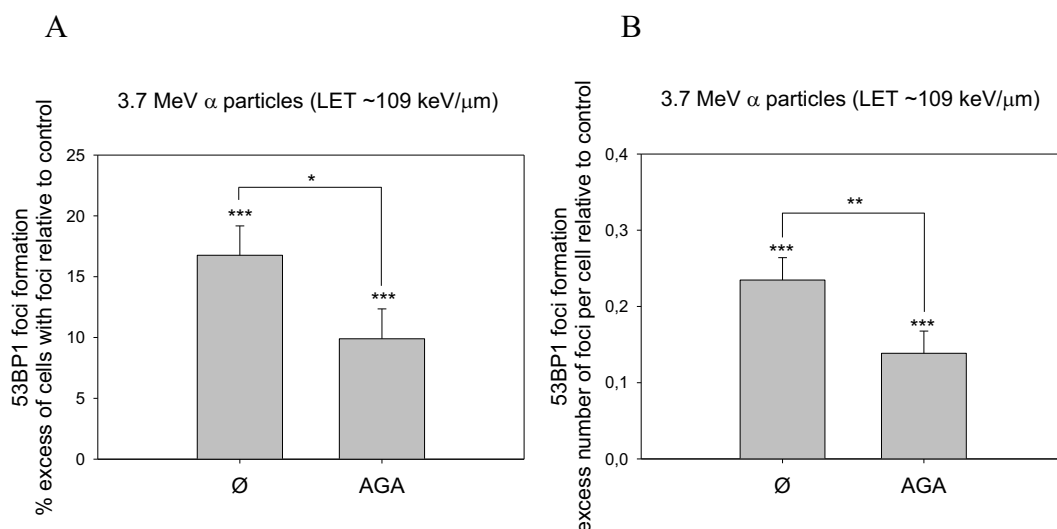
**Figure 5-3: (A) Percent excess of cells with 53BP1 foci and (B) Excess of mean number of 53BP1 foci per cell in confluent AG1522 cell cultures 3 h after exposure to 0.2 cGy from 3.7 MeV α particles in presence or absence of AGA (\*: $p < 0.05$, \*\*: $p < 0.01$ and \*\*\*: $p < 0.001$)**

The data in Figure 5-2 and Figure 5-3 support the role of junctional communication as a mediator of the induction of stressful non-targeted effects after α-particles-irradiation as was previously described (Azzam, de Toledo et al. 1998; Zhou, Randers-Pehrson et al. 2000).

To evaluate the contribution of intercellular communication in the propagation of bystander effect following HZE-particle-irradiation, confluent cultures were exposed to 0.2 cGy from 1000 MeV/u $^{56}$Fe or 600 MeV/u $^{28}$Si ions, and assayed for 53BP1 foci formation *in situ*. In irradiations with both $^{56}$Fe (Figure 5-4, Panel A) and $^{28}$Si ions (Figure 5-4, Panel B), the significant increases in the percent of cells with 53BP1 foci over what would be expected ($p < 0.001$) based on the fraction of cells irradiated through the nucleus (1.2 % and 3.5 %, respectively) support the participation of non-targeted cells as was shown before (Figure 3-2 and Figure 3-3). In presence of AGA, those increases were clearly attenuated in case of $^{56}$Fe ions ($p < 0.01$) (Figure 5-4, Panel A) and inhibited in case of $^{28}$Si ions (Figure 5-4, Panel B). These data strongly support the role of gap junction intercellular communication in mediating non-targeted effects not only after α-particles-irradiation but

also after exposure to low fluences of 1000 MeV/u $^{56}$Fe (LET ~151 keV/μm) or 600 MeV/u $^{28}$Si (LET ~50 keV/μm) ions.

A             B
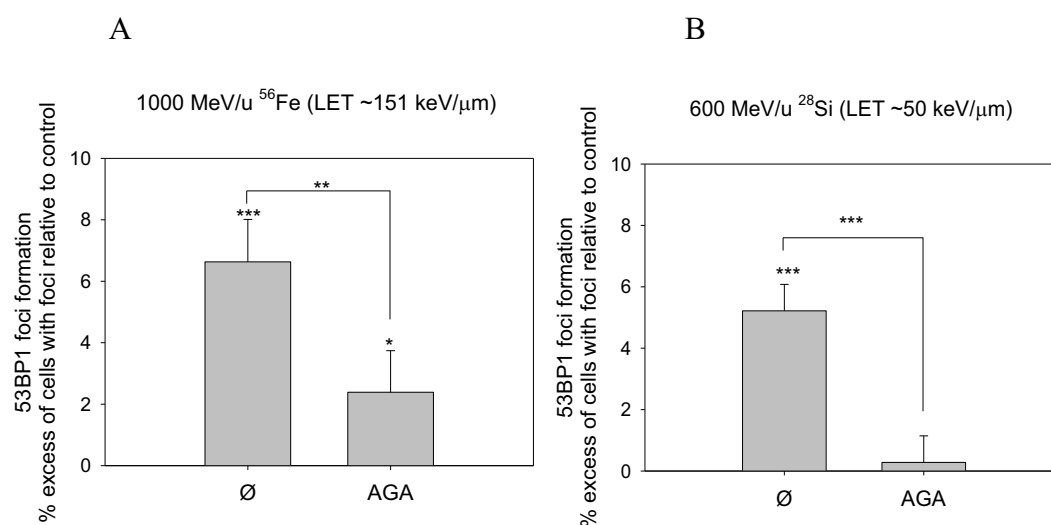


**Figure 5-4: Percent excess of cells with 53BP1 foci in confluent AG1522 cell cultures 3 h after exposure to 0.2 cGy from (A) 1000 MeV/u $^{56}$Fe ions or (B) 600 MeV/u $^{28}$Si ions in presence or absence of AGA (\*: $p$ <0.05, \*\*: $p$ <0.01 and \*\*\*: $p$ <0.001)**

The involvement of gap junction intercellular communication in high LET-induced bystander effects was further supported by attenuation of the increases in p21$^{Waf1}$ induction when cell cultures were exposed to low doses of α particles in presence of AGA (Figure 5-5).
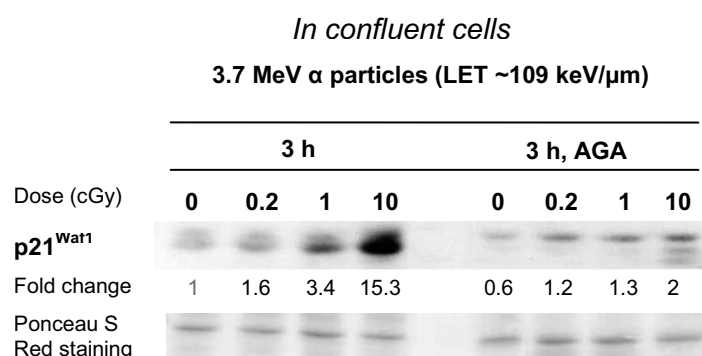


**Figure 5-5: Western Blot analysis of p21$^{Waf1}$ level in AG1522 cells population 3 h after exposure to a mean dose of 0, 0.2, 1 or 10 cGy from 3.7 MeV α particles in presence or absence of 50 μ$M$ AGA. Staining with Ponceau S Red was used as loading control. Fold change represents relative change compared to the control at 3 h without the drug.**

In AG1522 cell cultures exposed to doses of α particles by which a very small fraction of cell nuclei is traversed by a particle track, the extent of the increase in p21$^{Wafl}$ level suggests participation of a greater proportion of cells in the response than expected based on physical dosimetry calculations (Figure 5-5). For doses of 0.2, 1 or 10 cGy of α particles, the percentages of cells traversed through the nucleus are 1.4 %, 7.2 %, and 35.8 %, respectively. Chemical inhibition of gap junctions by AGA attenuated these increases in cultures exposed to doses in the range of 0.2 to 10 cGy.

The p21$^{Wafl}$ protein is, in part, induced in a p53-dependent manner in cells that have sustained DNA damage (el-Deiry, Tokino et al. 1993). The data in Figure 5-5 are thus consistent with those in Figure 5-2 showing that exposure of AG1522 cell cultures to absorbed doses as low as 0.2 cGy induces micronuclei in a greater fraction of cells than expected. They suggest that DNA damage may be the signal for the bystander induction of p21$^{Wafl}$ in these cultures as was previously shown (Azzam, de Toledo et al. 1998).

In case of HZE-particle-irradiation, sparse and confluent AG1522 cell cultures were exposed to 0, 0.2, 1 or 10 cGy of 1000 MeV/u $^{56}$Fe ions and the induction of p21$^{Wafl}$ was analyzed in cell populations harvested 3 h after exposure (Figure 5-6).

**1000 MeV/u $^{56}$Fe (LET ~151 keV/µm)**

**3h**

| | Sparse cultures | | | | Confluent cultures | | | |
|---|---|---|---|---|---|---|---|---|
| Dose (cGy) | 0 | 0.2 | 1 | 10 | 0 | 0.2 | 1 | 10 |
| p21$^{Waf1}$ | | | | | | | | |
| Fold change | 0.2 | 0.2 | 0.3 | 0.4 | 1 | 1.6 | 1.6 | 1.8 |
| Ponceau S Red staining | | | | | | | | |
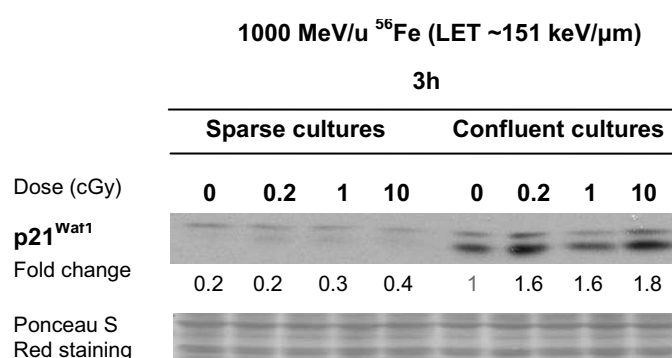
**Figure 5-6: Western Blot analysis of p21$^{Wafl}$ level in sparse and confluent AG1522 cells population 3 h after exposure to a mean absorbed dose of 0, 0.2, 1 or 10 cGy from 1000 MeV/u $^{56}$Fe ions. Staining with Ponceau S Red was used as loading control. Fold change represents relative change compared to the control in confluent cell culture. This experiment has been performed once.**

The data in Figure 5-6 indicate no or slight increase in p21$^{Wafl}$ level following exposure of sparse AG1522 cell cultures to low fluence of $^{56}$Fe ions. Importantly however, with sparse cell cultures, the fraction of cells traversed in the nucleus by a HZE particle is much less than expected by Poisson distribution as highlighted in Materials and Methods. Together, the results showed that physical contact between cells play an important role in propagation of signaling events that lead to p21$^{Wafl}$ induction in low fluence HZE-particle-irradiated cell cultures.

To examine if gap junction intercellular communication participates in propagation of stressful effects from HZE-particle-irradiated to non-irradiated cells, AG1522 cell cultures were incubated in presence or absence of 50 µ$M$ AGA and exposed to low doses of 1000 MeV/u $^{56}$Fe (Figure 5-7, Panel A) or 600 MeV/u $^{28}$Si ions (Figure 5-7, Panel. B), and harvested for analyses 3 h later. The data in Figure 5-7 describe western blot analyses of stress-responsive p21$^{Wafl}$, p-TP53ser15, p-ERK1/2, and connexin 43 (cx 43) after exposure to 0, 0.2, 1, 5, or 10 cGy from $^{56}$Fe (Figure 5-7, Panel A) or $^{28}$Si ions (Figure 5-7, Panel. B).

*In confluent cells*

**(A)** 1000 MeV/u $^{56}$Fe (LET ~151 keV/µm)

| | 3 h | | | | 3 h, AGA | | | |
|---|---|---|---|---|---|---|---|---|
| Dose (cGy) | 0 | 0.2 | 1 | 5 | 0 | 0.2 | 1 | 5 |
| p21$^{Waf1}$ | | | | | | | | |
| Fold change | 1 | 1.4 | 1.5 | 1.4 | 0.6 | 0.7 | 0.9 | 0.7 |
| cx 43 | | | | | | | | |
| Fold change | 1 | 1.4 | 1.4 | 1.2 | 1 | 0.6 | 0.5 | 0.3 |
| Loading control | | | | | | | | |

| | 3 h | | | | 3 h, AGA | | | |
|---|---|---|---|---|---|---|---|---|
| Dose (cGy) | 0 | 0.2 | 1 | 10 | 0 | 0.2 | 1 | 10 |
| p-ERK1/2 | | | | | | | | |
| Fold change | 1 | 3.6 | 4.2 | 5 | 0.7 | 1.3 | 1.3 | 1.9 |
| Ponceau S Red staining | | | | | | | | |

**(B)** 600 MeV/u $^{28}$Si (LET ~50 keV/µm)

| | 3 h | | | | 3 h, AGA | | | |
|---|---|---|---|---|---|---|---|---|
| Dose (cGy) | 0 | 0.2 | 1 | 10 | 0 | 0.2 | 1 | 10 |
| p21$^{Waf1}$ | | | | | | | | |
| Fold change | 1 | 1.6 | 2.4 | 12.0 | 0.7 | 1.2 | 1.5 | 2.3 |
| p-TP53ser15 | | | | | | | | |
| Fold change | 1 | 2 | 2.7 | 7.0 | 0.8 | 1.1 | 1.2 | 6.0 |
| Ponceau S Red staining | | | | | | | | |

**Figure 5-7: Western Blot analyses of p21$^{Waf1}$, cx 43, p-ERK1/2 or p-TP53ser15 in AG1522 confluent cells 3 h after exposure to a mean dose of 0, 0.2, 1, 5 or 10 cGy from 1000 MeV/u $^{56}$Fe ions or 600 MeV/u $^{28}$Si ions. Reaction of goat anti-rabbit immunoglobulin G with a protein of ~30 kDa or staining with Ponceau S Red was used as loading control. Fold change represents relative change compared to the control in absence of AGA.**

Similar to results obtained following α-particle-irradiation, the induction of p21$^{Waf1}$ 3 h after exposure to 0.2, 1 or 5 cGy of 1000 MeV/u $^{56}$Fe or 600 MeV/u $^{28}$Si ions was inhibited in presence of AGA (Figure 5-7, Panels A and B). At higher mean doses (e.g.

10 cGy from 600 MeV/u $^{28}$Si) where most cell nuclei in the exposed culture are traversed by a particle track, AGA did not have a clear attenuating effect on the p21$^{\text{Waf1}}$ response.

We also measured the levels of phosphorylation of Ser-15 in TP53 following exposure to low fluence of $^{28}$Si ions (Figure 5-7, Panel B) in presence and absence of AGA. Several studies have indicated that p-TP53-ser15 is a suitable marker of DNA damage; it occurs in an ATM-dependent manner shortly after irradiation (Canman, Lim et al. 1998). Whereas the data in Figure 5-7 (Panel B) indicate an increase in TP53 phosphorylation 3 h after exposure of confluent AG1522 cells to mean absorbed doses of 0.2 or 1 cGy, these increases were attenuated in presence of 50 µ$M$ AGA. This is not the case however after exposure to 10 cGy, when every single cell nucleus has been traversed by one or more particle(s); TP53 was phophorylated in the majority of cells whether AGA was present or absent.

Similarly, at 3 h after exposure to 1000 MeV/u $^{56}$Fe ions, the levels of stress responsive and pro-survival extracellular signal-related p-ERK1/2 were also inhibited in presence of AGA.

Concerning cx 43, a major constituent of gap junctions in AG1522 cells, relative to respective controls, the up-regulation observed at absorbed mean dose of 0.2 cGy from $^{56}$Fe ions was inhibited in presence of 50 µ$M$ AGA. As with α particle-induced bystander effect, these results are consistent with participation of cx 43-gap junctions in the HZE particle-induced bystander response. Modulation of cx 43 levels by low fluence HZE particles may also affect other responses to ionizing radiation.

Gap junctions are constituted of different connexins (at least 20 are known to exist in human cells). Each type of connexin forms channels with specific permeability, and it would be interesting to investigate the role of specific channel permeabilities on low fluence HZE-particle-induced bystander effects. Those results would help identify the different molecules

propagated between irradiated and bystander cells. Identification of such molecules would be useful in formulating countermeasures to the harmful effects of space radiation. It may also have implications to radiotherapy.

## 5.3  DNA repair and cellular responses to low fluence HZE particles

### 5.3.1  Rationale

Proper functioning of a cell, and especially faithful transmission of genetic information to its descendants, depends on maintaining the structural integrity of its DNA. The DNA molecule may undergo permanent damage due, mainly, to oxidative metabolism and other endogenous stresses (e.g. replication errors, higher than normal body temperature), as well as due to occasional exposure to exogenous stresses (e.g. UV radiation, chemicals, ionizing radiation from occupational or diagnostic procedures). The direct and indirect effects of ionizing radiation can lead to four main types of DNA modifications. Base damage is the most predominant type of DNA damage, followed (in decreasing order of incidence) by single-strand breaks, DNA-protein cross-links, and double-strand breaks. The latter is the most harmful as it can lead to cell death, genomic rearrangement and neoplastic transformation. Following exposure to ionizing radiation, several signaling pathways involved in DNA-damage sensing and repair are triggered, often in a manner that is dependent on the type of damage, position in the cell cycle and other factors. Considerable overlap and interactions between these pathways exist.

Earlier work by Nagasawa et *al*. indicated a link between α-particle-induced bystander effects and DNA repair mechanisms (Nagasawa, Peng et al. 2005). We hypothesize that the propagation of bystander effects is facilitated when certain components of DNA repair are inhibited. For this study, we used chemical inhibitors of key components of DNA

damage sensing and repair, namely KU55933 as Ataxia Telangectasia Mutated (ATM) inhibitor, and PJ34 as poly(ADP-ribose) polymerase (PARP-1) inhibitor

Among many types of lesions, ionizing radiation induces DNA strand breaks, with the proportion, per unit dose, of induced single to double-strand breaks being dependent on the LET of the radiation. DNA strand breaks and other oxidizing types of damage activate ATM kinase, a cell cycle checkpoint protein that is a member of the phosphatidyl inositol 3-kinase-like kinases (PIKKs) family (Bakkenist and Kastan 2003). This family includes also ATM and Rad3-related protein (ATR), the catalytic subunit of DNA-dependent protein kinase (DNA-PKcs), hSMG1, and mammalian target of rapamycin (mTOR) kinases (Lempiainen and Halazonetis 2009). ATM is a critical player in the early detection and repair of ionizing radiation-induced DNA damage (Shiloh 2003). Although a fraction of ATM is cytoplasmic and is involved in pathways related to metabolic processes, the majority of ATM is nuclear (Alexander, Cai et al. 2010; Alexander and Walker 2010). Following DNA damage, nuclear ATM is rapidly recruited to sites of DNA double-strand breaks and contributes to phosphorylation of the histone variant H2AX producing γ-H2AX on serine 139 (Burma, Chen et al. 2001). In turn, the ubiquitination of γ-H2AX by RNF8 stabilizes the recruitment of 53BP1 and BRCA1, both of which are also phosphorylated by ATM (Lavin 2008). Shortly after induction of DNA damage, ATM autophosphorylates on serine 1981 and releases an active monomer that can directly phosphorylate p53 and murine double minute 2 (MDM2, known in human cells as HDM2) as well as checkpoint kinase Chk2 that phosphorylates, in turn, p53 and MDM2. Phosphorylation of both p53 and MDM2 results in stabilization of p53 (de Toledo, Azzam et al. 2000). Activated p53 enhances transcription of *WAF1*, the gene that codes for the cyclin-CDK inhibitor p21$^{Waf1}$, which results in a $G_1$ cell cycle delay (Little 1968). The second mechanism is rapid but transient, and involves phosphorylation of the checkpoint kinases Chk1 and Chk2 by ATM/ATR complex. In late $G_1$/early S phase, ATM

phosphorylates Chk2 that, in turn, phosphorylates and inactivates Cdc25A phosphatase leading to inhibition of cyclinE/A-Cdk2 activity (reviewed in Bensimon, Aebersold et al. 2011). Recently, it has been also shown that ATM is an important sensor of ROS in human cells (Shiloh 2003; Guo, Deshpande et al. 2010; Guo, Kozlov et al. 2010). Studies in our laboratory have shown that inhibition of ROS generation by NAD(P)H-oxidase induces a pronounced $G_1$ arrest in an ATM-dependent manner (Venkatachalam, de Toledo et al. 2008).

Poly(ADP-ribose) polymerase-l (PARP-l) is a molecular sensor of DNA breaks (Malanga and Althaus 2005); it also plays an important role in DNA repair, cell death and proliferation (Huang, Xiong et al. 2008). PARP-1 binds to both single- and double-strand breaks (Eustermann, Videler et al. 2011). It is however mainly involved in repair of single-strand break and base damage. It recruits the X ray cross complementing factor 1 (XRCC1) protein to the site of DNA damage, which acts as a scaffold to coordinate the repair of damaged bases. Inhibition of PARP-1 induces accumulation of large numbers of unrepaired single strand breaks, which leads to the collapse of replication fork during S phase with consequent generation of DNA double strand breaks (Peralta-Leal, Rodriguez-Vargas et al. 2009). Moreover, PARP-1 interacts with ATM and therefore may influence growth arrest cascades particularly in $G_2$/M phase. (Madison, Stauffer et al. 2011).

Here, micronucleus formation and 53BP1 foci formation reflecting DNA damage were analysed in confluent AG1522 cell cultures exposed to 0, 0.2 or 1 cGy from 3.7 MeV α particles, 1000 MeV/u [56]Fe or 600 MeV/u [28]Si ions in presence or absence of the ATM inhibitor KU55933 or the PARP-1 inhibitor PJ34.

## 5.3.2 Results

*Role of ATM*

Confluent AG1522 cell cultures were incubated in presence or absence of 10 $\mu M$ KU55933 30 min before exposure to 0.2 cGy from 3.7 MeV $\alpha$ particles. The cell cultures were processed for *in situ* evaluation of 53BP1 foci 3 h later. Consistent with the data in previous figures, the percent excess of cells with 53BP1 foci increased significantly after exposure to a mean absorbed dose of 0.2 cGy ($p < 0.001$) (Figure 5-8). In presence of KU55933, the percentage of cells with 53BP1 foci in control (sham-irradiated) cell cultures was reduced ($p < 0.001$) and the increase due to low fluence of $\alpha$ particles was suppressed (Figure 5-8).
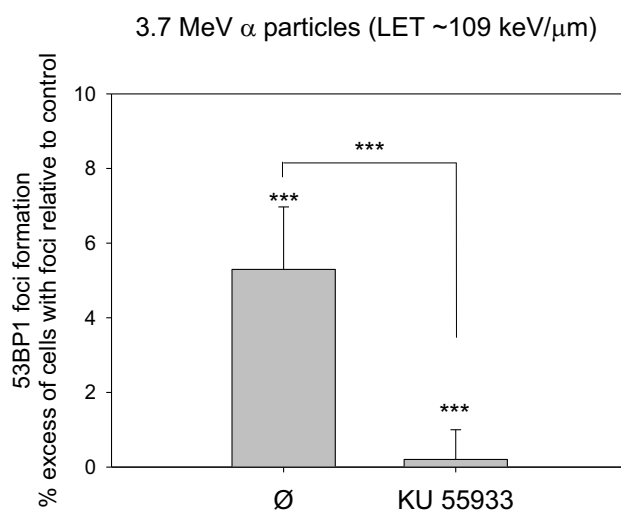


**Figure 5-8: Percent excess cells with 53BP1 foci in confluent AG1522 cell cultures 3 h after exposure to a mean absorbed dose of 0.2 cGy from 3.7 MeV $\alpha$ particles in presence or absence of KU55933 (\*\*\*: $p < 0.001$)**

Following exposure to a similar mean dose (0.2 cGy) of 1000 MeV $^{56}$Fe or 600 MeV $^{28}$Si ions, the increases in 53BP1 foci were also greater than expected based on the fraction of nuclei traversed by an energetic ion (1.2 % and 3.5 %, respectively). In presence of 10 $\mu M$ KU55933, both the sham-irradiated cultures ($p < 0.001$) and 1000 MeV/u $^{56}$Fe- (Figure 5-9,

Panel A) or 600 MeV/u $^{28}$Si-irradiated cultures (Figure 5-9, Panel B) had notably reduced fractions of cells with 53BP1 foci ($p$ <0.001).

A                                                B
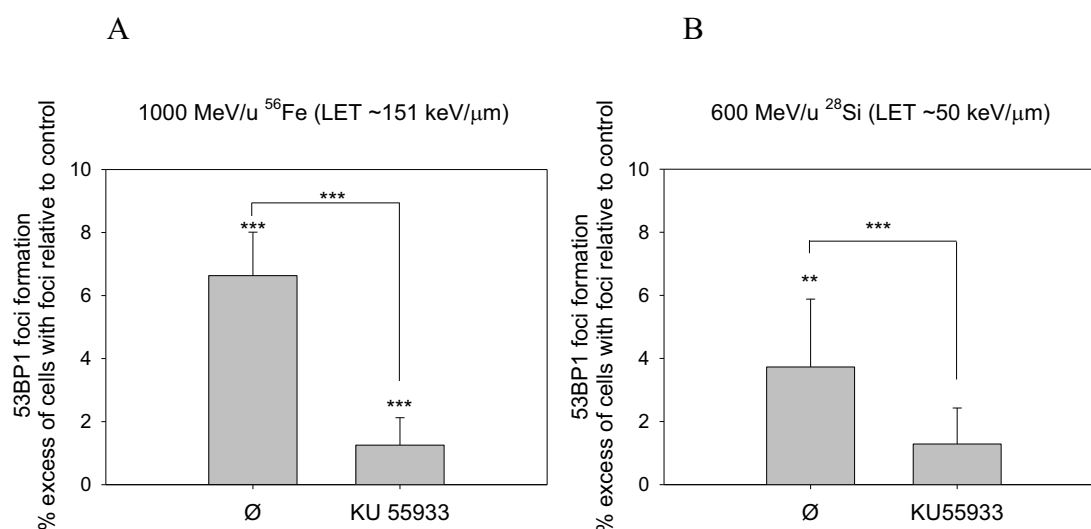


**Figure 5-9: Percent excess of cells with 53BP1 foci in confluent AG1522 cell cultures 3 h after exposure to 0.2 cGy from (A) 1000 MeV/u $^{56}$Fe ions or (B) 600 MeV/u $^{28}$Si ions in presence or absence of KU55933 (*: $p$ <0.05, **: $p$ <0.01 and ***: $p$ <0.001)**

These results support the involvement of ATM signaling in mediating the propagation of events leading to DNA damage in bystander cells. Whether ATM mediates bystander effects at the level of the irradiated or the bystander cells remains to be investigated.

*Role of DNA repair*

To gain insight into the role of DNA repair in the biological effects of low fluence particulate radiations, confluent AG1522 cell cultures were incubated in presence or absence of 10 µ$M$ PJ34, a PARP-1 inhibitor 24 h before exposure. They were then irradiated with 0.2 cGy from 3.7 MeV α particles, 1000 MeV/u $^{56}$Fe ions or 600 MeV/u $^{28}$Si ions and fixed *in situ* for analyses of 53BP1 foci or subcultured for analyses of micronuclei formation, 3 h later.

In cell cultures exposed to 3.7 MeV α particles, significant increases in micronucleus formation were observed after exposure to mean absorbed doses of 0.2 or 1 cGy ($p$ <0.05 and

*p* <0.01, respectively) (Figure 5-10, Panel A). Similarly, increases in percent excess of cells with 53BP1 foci were detected after exposure to 0.2 cGy of α particles (*p* <0.001) (Figure 5-10, Panel B). Following similar radiation treatments, in presence of PJ34, the increases in the percentage of cells with micronuclei (*p* <0.05 and *p* <0.01) (Figure 5-10, Panel A) or 53BP1 foci (*p* <0.001) (Figure 5-10, Panel B) were enhanced.
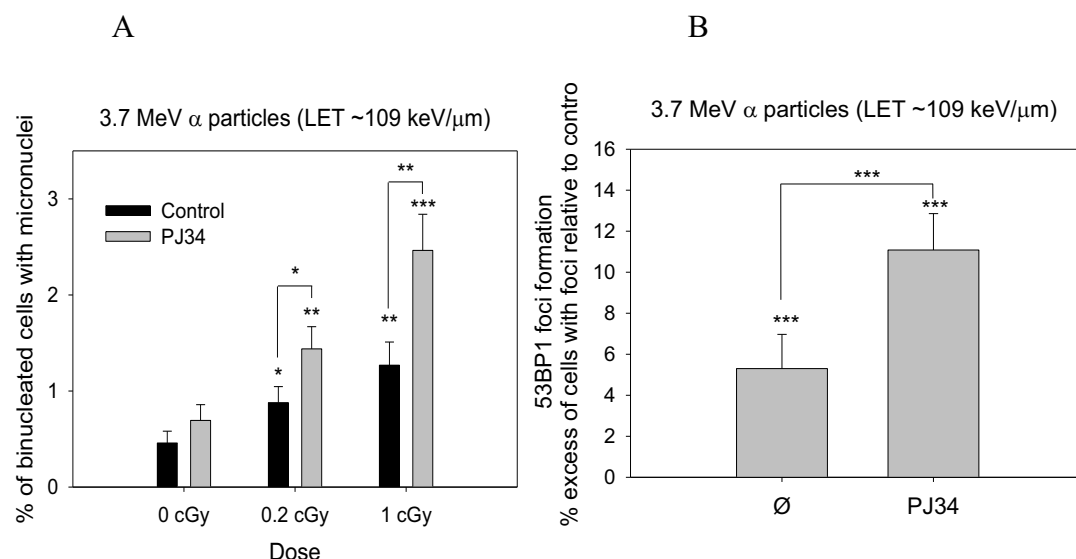


**Figure 5-10: (A) Percentage of micronucleated cells and (B) Percent excess of cells with 53BP1 foci in confluent AG1522 cell cultures 3 h after exposure to mean absorbed doses of 0, 0.2 or 1 cGy from 3.7 MeV α particles in presence or absence of PJ34 (\*: *p* <0.05, \*\*: *p* <0.01 and \*\*\*: *p* <0.001)**

Similarly, after exposure to mean absorbed dose of 0.2 cGy from 1000 MeV/u $^{56}$Fe ions or 600 MeV/u $^{28}$Si ions, the percent excess of cells with 53BP1 foci were increased (*p* <0.01 and *p* <0.001, respectively). In presence of PJ34, those increases were also enhanced (*p* <0.001) (Figure 5-11, Panels A and B).
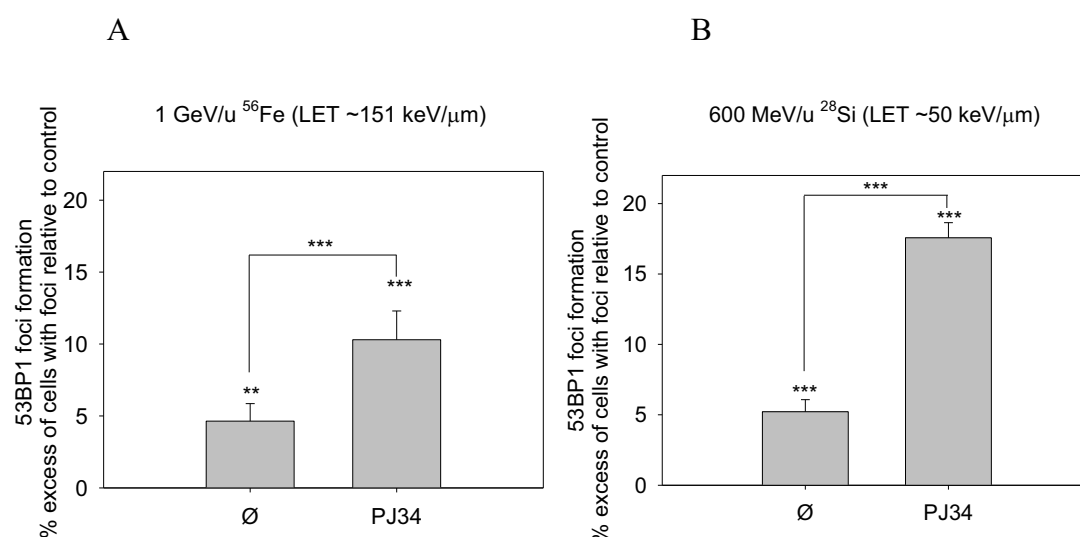
**Figure 5-11: Percent excess of cells with 53BP1 foci in confluent AG1522 cell cultures 3 h after exposure to 0.2 cGy from (A) 1000 MeV/u $^{56}$Fe ions or (B) 600 MeV/u $^{28}$Si ions in presence or absence of 10 μ$M$ PJ34 (\*\*: $p$ <0.01 and \*\*\*: $p$ <0.001)**

Unrepaired oxidative base damage and single strand breaks were reported to cause clustered DNA damage, in particular when they occur in close proximity to each other, which can lead to double strand breaks (Sutherland, Bennett et al. 2000). Therefore, the increases in micronucleus formation and 53BP1 foci, a reflection of DNA double strand breaks, upon inhibition of PARP-1 by PJ34 may result from DNA single strand breaks and base damage in bystander cells. The latter types of DNA damage may arise from oxidative stress resulting from perturbations in oxidative metabolism in the bystander cells as was previously shown (Narayanan, Goodwin et al. 1997; Azzam, De Toledo et al. 2002; Shao, Stewart et al. 2003).

## *5.4 Implication of partial tension of oxygen*

### 5.4.1 Rationale

All forms of aerobic life have developed sophisticated antioxidant defenses to cope with the threat of oxidation from molecular oxygen (Haddad 2002). Currently, cell cultures

performed in "classic" incubators with 5 % $CO_2$ are under an oxygen atmospheric pressure of ~160 mm Hg ($\approx$ 21 % $O_2$). *In vivo*, the partial tension of oxygen ($Po_2$) in tissues never reaches ambient conditions (i.e. 160 mm Hg). For example, the $Po_2$ of arterial blood is 95 $\pm$ 5 mm Hg and of venous blood is ~40 mm Hg; in most tissues, the $Po_2$ varies between 6 and 34 mm Hg (1-5 % $O_2$) (Wion, Dematteis et al. 2008). Thus, classical *in vitro* method of culturing cells derived from human tissue imposes an artificial "hyperoxia" with consequences that have not been entirely characterized. Although cells can adapt their physiological functions to ambient $Po_2$, the activity of their oxygen and redox-sensitive signaling molecules could be altered. Such variations in the activity of signaling molecules (e.g. transcription factors) could affect cell fate; in the context of this project, these variations could modulate the extent of propagation of radiation-induced bystander effects.

While acutely hypoxic cells are more resistant to the effects of ionizing radiation than their normoxic counterparts (Russo, Mitchell et al. 1985; Brown and Giaccia 1994), a controversy exists as to whether an increase or a decrease in the metabolic production of ROS is involved in hypoxic signaling (Bunn and Poyton 1996; Chandel, Maltepe et al. 1998; Chandel and Schumacker 2000). According to Clanton (Clanton 2007), ROS are more likely to be produced in hypoxia when there is both a high reductive capacity (e.g., high $NADH/NAD^+$) and sufficient $O_2$ available for reaction (Figure 5-12). Regardless, it is well established that decreased $Po_2$ in cells results in reduced cytotoxicity, mutagenicity and DNA breaks (Hall and Giaccia 2012). Further, under hypoxic condition, the rate of cell growth (Bedford and Mitchell 1974), expression of specific genes (Wilson and Sutherland 1989; Graeber, Peterson et al. 1994; Semenza 2000), and ion channels activity may be modulated (Lopez-Barneo, Lopez-Lopez et al. 1988).
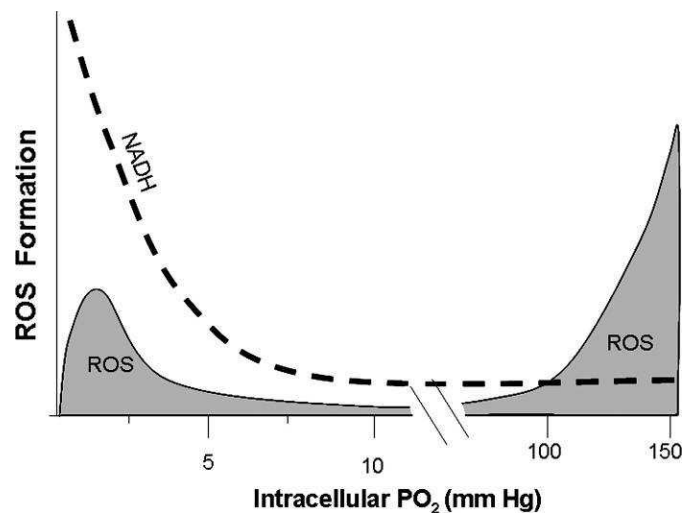
**Figure 5-12: Depiction of the proposed bimodal distribution of reactive oxygen species formation as a function of $Po_2$ in which hypoxia and hyperoxia support elevations in ROS formation (Clanton 2007).**

The role of the different effects of hypoxia (i.e. $Po_2$ lower than ambient) on the expression of bystander responses in cell cultures exposed to low doses/low fluences of radiation at physiological $Po_2$ has not been studied. Standard protocols for cell culture at ambient $Po_2$ may or may not accurately simulate *in vivo* physiological responses to ionizing radiation. The characterization of the bystander effect under conditions that mimic *in vivo* conditions is important for our understanding of intercellular communication and their implications for radiation protection and radiation therapy.

We hypothesize that varying the oxygen tension at which cells are cultured and irradiated results in variable effects on the propagation of the bystander effect in confluent AG1522 cell cultures exposed to low fluence of 3.7 MeV α particles. To test this hypothesis, confluent cell cultures were incubated in a 5 % $CO_2$ and 0.5 % oxygen in air atmosphere for 48 h before exposure to 0.2 cGy. At different times after exposure, the cells were processed for analyses of different biological endpoints.

In addition to the above, we also hypothesize that inherent oxidative status of cells affects the propagation of stressful effects from α-particle-irradiated to neighboring non-irradiated cells. To this end, AG1522 cells were pretreated with $0.5\,\mu M$ *tert*-butyl hydroperoxide (*t*-BOOH) prior to exposure to low fluences of 3.7 MeV α particles in a 5 % $CO_2$ in ambient air atmosphere. *t*-butyl hydroperoxide is a pharmacological compound that induces oxidative stress. Similar to other organic peroxides, it decomposes into alkoxyl and peroxyl radicals in the presence of metal ions; the net result is generation of ROS, including $H_2O_2$ (Woodbine, Brunton et al. 2011). Decomposition of *t*-BOOH accelerates lipid peroxidation, damages DNA, and causes depletion of glutathione (GSH) (Sandstrom 1991; Guidarelli, Cattabeni et al. 1997; Kim, Kang et al. 1998). Incubation of cells in $0.5\,\mu M$, for periods of time extending to 4 h did not alter clonogenic survival (our data, not shown).

### 5.4.2 Results

*Effect of $Po_2$ on DNA damage induced by low mean doses of α particles*

Three hours after exposure to 0, 0.2, 1 or 10 cGy from 3.7 MeV α particles, cells population were harvested and assayed for micronucleus formation and *in situ* detection of 53BP1 foci. Under culture and irradiation atmosphere of 21 % $O_2$, relative to control, significant increases in micronuclei formation occurred after exposure to 0.2, 1 or 10 cGy ($p < 0.01$, $p < 0.001$ and $p < 0.001$, respectively) (Figure 5-13). When cells were cultured and irradiated at 0.5 % $O_2$ in air atmosphere, these increases were attenuated but remained significantly greater than control ($p < 0.05$, $p < 0.001$ and $p < 0.001$ for 0.2, 1 and 10 cGy respectively). The difference in induction of micronuclei observed at 0.5 and 21 % oxygen atmosphere was significant only after irradiation of the cultures with 10 cGy ($p < 0.05$) (Figure 5-13).

*Effect of t-BOOH on DNA damage induced by low mean doses of α particles*

When cell cultures were incubated in an atmosphere of 21 % $O_2$ in the presence of 0.5 $\mu M$ t-BOOH dissolved in 48 h-conditioned medium and added to cell cultures 1 h before irradiation and maintained in its presence until they were harvested 3 h later, increases in micronuclei formation were higher than in absence of the drug. The difference was significant after exposure to 1 cGy from α particles ($p < 0.05$) (Figure 5-13).
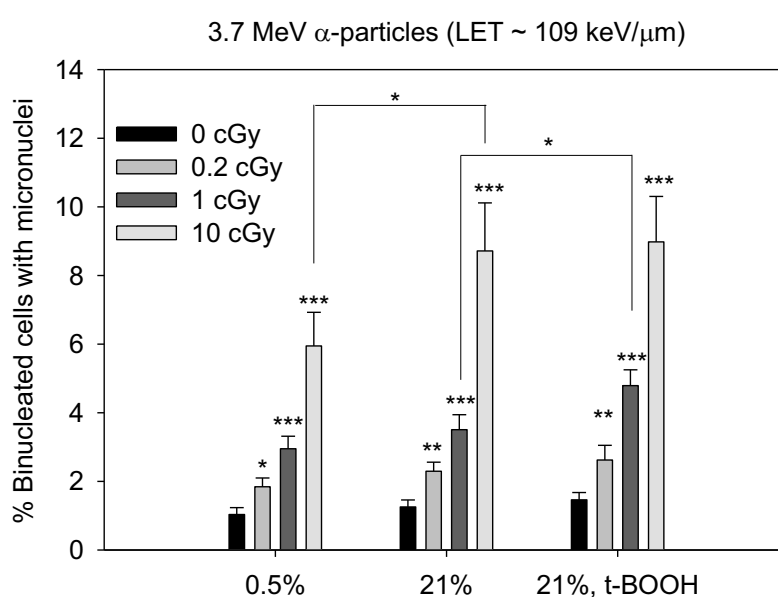


**Figure 5-13: Percentage of micronucleated cells in confluent AG1522 cell cultures after exposure to a mean absorbed dose of 0, 0.2, 1 or 10 cGy from 3.7 MeV α particles at different oxygen tensions and cells maintained at 21 % oxygen atmosphere in presence or absence of 0.5 $\mu M$ t-butyl hydroperoxide at the time of irradiation. The cell cultures were subcultured in presence of cytochalasin B 3 h after exposure. (\*: $p < 0.05$, \*\*: $p < 0.01$ and \*\*\*: $p < 0.001$)**

Similarly, in low mean dose irradiated cells, 53BP1 foci formation was reduced at 0.5 % of $O_2$ compared to 21 % of $O_2$ even in non-irradiated cell cultures ($p < 0.001$), and enhanced in presence of 0.5 $\mu M$ t-BOOH ($p < 0.001$) (Figure 5-14).
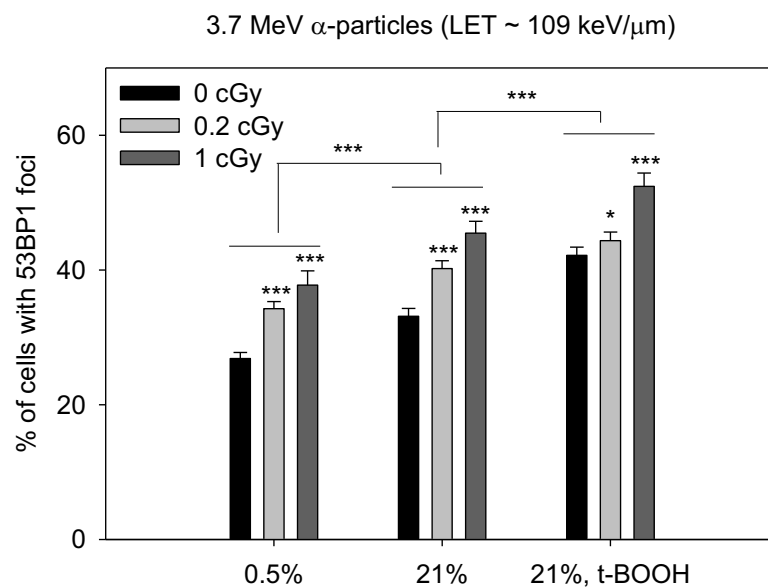
**Figure 5-14: Fraction of cell with 53BP1 foci in confluent AG1522 cell cultures after exposure to a mean dose of 0, 0.2 or 1 cGy from 3.7 MeV α particles at different oxygen tensions and in presence or absence of 0.5 µ*M* *t*-butyl hydroperoxide (*: $p < 0.05$, **: $p < 0.01$ and ***: $p < 0.001$)**

Whereas at low oxygen concentrations (0.5 % or ~4 mm Hg), the cellular level of ROS may be less than that at 21 % of $O_2$ (~160 mm Hg) (Figure 5-12), emerging data from our laboratory suggests that enhanced DNA repair activity may occur at *in vivo*-like $Po_2$, which may explain the differences in induced DNA damage at low $Po_2$ and ambient $Po_2$. However, the presence of 0.5 µ*M* t-BOOH in confluent cell cultures enhanced the effect of ionizing radiation at inducing DNA damage.

*Effect of $Po_2$ on stress-responsive protein levels in cell cultures exposed to low doses of*
*α particles*

Normal human fibroblast sense oxygen levels and respond to hypoxic conditions through the regulation of multiple signaling pathways. We investigated responses of confluent AG1522 fibroblasts under low (0.5 %) or ambient (21 %) oxygen atmosphere. AG1522 cell cultures were exposed to absorbed doses of 0, 0.2, 1 or 10 cGy of 3.7 MeV α particles and harvested for western blot analyses 3 h later.

The levels of p-TP53ser15, p21$^{Wafl}$, and p-ERK1/2 were examined. In the representative data shown in Figure 5-15, the relative change in protein levels was compared to non-irradiated samples maintained at 21 % $O_2$. Consistent with previous data, exposure to 0.2, 1 or 10 cGy from 3.7 MeV α particles increased p-TP53ser15, p21$^{Wafl}$ and p-ERK1/2 levels when cell cultures were maintained and irradiated at normal $Po_2$ (21 % $O_2$) (Figure 5-15). Under reduced $O_2$ concentration in the incubation atmosphere, the basal level of p-TP53ser15 and p21$^{Wafl}$ were lower than in normoxia (note that the data in Figure 5-15 are from samples electrophoresed in the same gel). In irradiated samples, the increases in protein levels relative to control were also less than under normoxia. These differences were particularly noticeable at 10 cGy where 60 % of cells were presumably traversed by a particle through the nucleus. In case of p-ERK1/2, greater increase occurred under hypoxia than at 21 % $O_2$ in irradiated samples (a factor of 2 at 0.2 cGy) (Figure 5-15).

*In confluent cells*



| | | | | | | | | |
|---|---|---|---|---|---|---|---|---|
| **3.7 MeV α particles (LET ~109 keV/μm)** | | | | | | | | |
| $Po_2$ | **0.5** | | | | **21 %** | | | |
| Dose (cGy) | **0** | **0.2** | **1** | **10** | **0** | **0.2** | **1** | **10** |
| **p21$^{Waf1}$** | | | | | | | | |
| Fold change | 0.4 | 0.4 | 0.6 | 0.7 | 1 | 1.1 | 1 | 3.5 |
| **p-TP53ser15** | | | | | | | | |
| Fold change | 0.4 | 0.5 | 1.2 | 5.4 | 1 | 1.4 | 1.4 | 7.1 |
| **p-ERK1/2** | | | | | | | | |
| Fold change | 0.9 | 2.1 | 1.8 | 2.2 | 1 | 1.2 | 1.5 | 1.4 |
| Ponceau S Red staining | | | | | | | | |
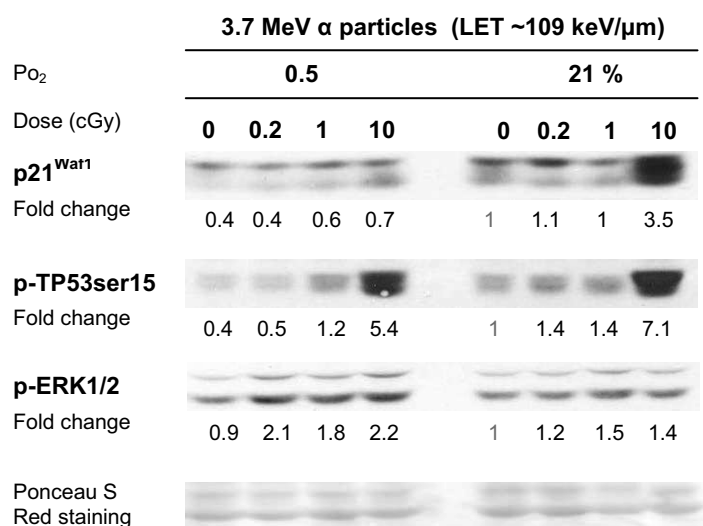
**Figure 5-15: Western blot analyses of p21$^{Wafl}$, p-TP53ser15 or p-ERK1/2 in AG1522 confluent cells 3 h after exposure to a mean absorbed dose of 0, 0.2, 1 or 10 cGy from 3.7 MeV α particles. Staining with Ponceau S Red was used as loading control. Fold change represents relative change compared to control at 21 % of $O_2$**

Together, the data suggest that under reduced oxygen tension, the magnitude of stressful effects in bystander cells is reduced. The significance of enhanced phosphorylation of ERK1/2 remains to be understood.


## 5.5  Discussion

Although radiation-induced bystander effects have been well documented and the mechanisms underlying their expression are increasingly being understood, the spectrum of signaling events involved and their induction at *in vivo*-like conditions is not yet clear. Several pathways are involved in the bystander phenomenon, and different cell types respond differently to bystander signaling. In this project, using human fibroblasts exposed to α or HZE particles, we have shown that several mechanisms are implicated in the propagation of high-LET radiation-induced bystander effects. Gap junction intercellular communication, DNA repair, and partial tension of oxygen have an effect in the propagation of the bystander effect. This list is non-exhaustive and others factors likely play a role in an inter-connected manner with other mechanisms.

Gap junctions are dynamic structures that are critical for diverse physiological functions (Harris 2001; Mehta 2007). Evidence for the involvement of GJIC in propagation of bystander effects has been derived from studies with high- and low-LET radiations (Azzam, de Toledo et al. 1998; Bishayee, Rao et al. 1999; Vance and Wiley 1999; Zhou, Randers-Pehrson et al. 2000). The intercellular channels that comprise gap junctions are formed by connexin proteins (Harris 2001). Manipulation (↓↑) of connexin expression/gap-junction gating by chemical agents, forced connexin expression by transfection, and connexin gene knockout studies provide substantial evidence for the participation of gap junctions in radiation-induced bystander effects (Azzam, de Toledo et al. 2003; Hall and Hei 2003). This is supported by stabilization and up-regulation of connexin mRNA and protein by ionizing

radiation (Azzam, de Toledo et al. 2003). Disruption of cholesterol rich areas of the plasma membrane where gap-junction channels partition (Schubert, Schubert et al. 2002) attenuated propagation of IR effects to bystander cells (Nagasawa, Cremesti et al. 2002; Hanot, Hoarau et al. 2009).

Connexins are an extensive family of proteins comprising several members (20 isoforms) (Harris 2001) that are expressed in different tissues and have different selectivity related to the size and charge of the communicated molecules (Kumar and Gilula 1996; Veenstra 1996). By allowing direct intercellular transfer of ions and low-molecular-weight molecules, gap junctions provide a powerful pathway for molecular signaling between cells. Though the properties of channels formed by each isoform differ, in general, connexin pores are considered to allow permeation of small molecules (reviewed in Harris 2001). Previous work from our laboratory has shown that cx 43, a major constituent of gap junctions in AG1522 cells has a prominent role in the propagation of bystander effect after exposure to low fluences of α particles (Azzam, de Toledo et al. 2001; Azzam, de Toledo et al. 2003). In this project, using the same type of cells, evidence was presented that suggests that junctional communication also plays a role in HZE-particle-induced bystander effects. This was supported by reduced induction of p-TP53ser15, p21$^{Wafl}$, p-ERK1/2 and cx 43 levels in confluent cells treated with the gap-junction inhibitor AGA (Figure 5-7), and when low density cell populations were exposed HZE particles (Figure 5-6). Significantly, exposure to HZE particles up-regulates cx 43 (Figure 5-7), an effect that was associated with functional gap junction intercellular communication (GJIC) (Gaillard, Pusset et al. 2009).

Effective repair systems (Base Excision Repair, Nucleotide Excision Repair, Non Homologous End Joining, and Homologous Recombination) explain how cells maintain integrity of their genetic information. Defective DNA repair, particularly failure to repair double strand breaks, may result in chromosomal rearrangements (deletions, translocation)

which in turn may promote neoplastic transformation. It would be intriguing, in the context of radiation-induced bystander effects, to investigate whether it is the initial induced DNA damage in bystander cells or the capacity to repair it (Joubert and Foray 2007) that determines the extent of long-term consequences of the bystander effect in progeny cells. Additional mechanisms affecting the source of events leading to DNA damage in bystander cells and their progeny (e.g. epigenetic events) may activate ROS-generating oxidases or silence genes coding for antioxidants among other effects. Nevertheless, the capacity to repair the induced damage remains the critical factor that determines the nature and amount of residual DNA damage. Apoptosis and immune responses may act to eliminate damaged cells and promote healthy survival (Averbeck 2009; Tubiana, Feinendegen et al. 2009).

Using a chemical inhibitor, the data in Figure 5-9 confirm that expression of 53BP1 foci in control, irradiated and bystander cells is dependent on ATM function. However, genetic approaches would be necessary to dissect the exact role of ATM in the bystander response. Other studies with energetic helium ions have shown that ATM activation in bystander cells is dependent on ATR function (Burdak-Rothkamm, Rothkamm et al. 2008). Furthermore, the induction and co-localization of ATR, 53BP1, p-ATM-S1981, p21$^{Waf1}$ and BRCA1 foci in non-targeted cells was demonstrated, suggesting their involvement in bystander DNA-damage signaling and providing additional potential targets for modulation of bystander responses. Compared to our studies with $G_0/G_1$-phase cells, 53BP1 bystander foci were induced in an ATR dependent manner predominantly in S-phase cells (Burdak-Rothkamm, Short et al. 2007; Burdak-Rothkamm, Rothkamm et al. 2008).

Highlighting the role of DNA repair in expression of high LET-radiation-induced bystander effects, incubation of cell cultures with an inhibitor of PARP-1 resulted in higher magnitude of 53BP1 foci formation after exposure to low fluences of α or HZE particles. Inhibitors of PARP-1 have been shown to enhance the cytotoxic effects of ionizing radiation

and chemotherapy agents. Strategies whereby PARP-1 is down-regulated, specifically in tumor cells, may therefore potentiate lethal effects of certain types of radiotherapy such as radio-immunotherapy whereby non all tumor cells uptake radiolabeled antibodies (Akudugu and Howell 2011).

Recent work in our laboratory has indicated that bystander effects are not only a low fluence phenomenon; cells exposed to $\alpha$ or HZE particles communicate with each other (via gap junctions) to enhance the cytotoxic effects of such energetic particles (Autsavapromporn, de Toledo et al. 2011). Down-regulation of PARP-1 in such cells would yet further enhance cytotoxic effects and result in greater benefit. This will broaden the rationale of using PARP inhibitors as radio-sensitizers. A net benefit may be a lowering of the radiation dose delivered to the patient.

This project shows that the concentration of molecular oxygen significantly modulates the magnitude of stressful effects in cell cultures exposed to low fluences of particulate high-LET radiation ($\alpha$ particles). Whereas, stressful bystander effects were still expressed under hypoxia (0.5 % $O_2$) (Figure 5-13, Figure 5-14 and Figure 5-15), they were attenuated compared to effects observed under ambient atmosphere of 21 % $O_2$. Interestingly, ERK1/2 phosphorylation was stimulated under reduced oxygen tension. Expansion of these studies to investigate global changes in gene expression (e.g. at mRNA, protein levels) and epigenetic events (e.g. methylation patterns, level of different microRNAs) following irradiation under reduced or ambient oxygen levels would enhance our understanding of mechanisms. It is relevant to radiotherapy, and may contribute to formulation of adequate models to assessing the health effects of exposure to low fluences of energetic radiations with high LET character.

# Chapter 6     Conclusion

Using *in vitro* tissue culture approach, this thesis project has provided evidence for the existence of HZE-particle-induced bystander effects. Using different biological endpoints, exposure of confluent normal human diploid AG1522 fibroblasts to low fluences of energetic iron (1000 MeV/u $^{56}$Fe, LET ~151 keV/μm) or silicon (600 MeV/u $^{28}$Si, LET ~50 keV/μm) ions indicated that a greater fraction of cells participate in the stress response than predicted by microdosimetric considerations. The percentage of micronucleated cells and nuclei with 53BP1 foci in cultures exposed to a dose of 0.2 cGy of either iron or silicon ions were significantly greater ($0.05<p<0.001$) than the 1.2 or 3.5 % of nuclei that would have been traversed, respectively, by a particle track. The data suggested that the fraction of cells sustaining DNA damage increases with time up to 3 h after the initial exposure, following which it decreased and returned to near basal levels by 24 h. The results were supported by extensive modulation of stress-responsive proteins. The levels of p21$^{Waf1}$ and HDM2 that control the $G_1$ cell cycle checkpoint were elevated whether the irradiated cells were maintained in confluence or subcultured to lower density. Similar increases in these proteins following γ-irradiation were detected when AG1522 cultures were exposed to 50 cGy or greater dose (Azzam, de Toledo et al. 1998). Consistent with persistent stressful effects, extensive protein oxidation and lipid peroxidation were detected 24 h after exposure of confluent AG1522 cells to low mean absorbed doses of HZE particles. Together, the results were similar to effects observed using similar endpoints in cell cultures exposed, in parallel, to low fluences of 3.7 MeV α particles (LET ~109 keV/μm). Interestingly, they were not observed following exposure to 290 MeV/u $^{12}$C ions (LET ~13 keV/μm). However, biological changes measured by other endpoints may be induced. Carbon ions of 300 MeV/u are used clinically to treat cancer, and the absence of propagation of stressful effects from

cells exposed to such ions to their normal neighboring bystanders would reduce the risk of second malignancy in these bystanders. Alternatively, a therapeutic gain of propagating events that lead to lethal effects in adjacent bystander tumor cells would be lost.

Mechanistic studies have shown that gap-junction intercellular communication is an important mediator of the HZE-particle-induced bystander effect. Its inhibition with 18-α-glycerretinic acid (AGA) greatly attenuated the level of stress in low fluence iron-irradiated cell cultures. Direct interactions between cells are fundamental to the development and function of multicellular organisms. This thesis has demonstrated that intercellular communication plays an important role in the response to ionizing radiation. It showed that cell populations respond as a whole to HZE and α particles of high-LET characteristics (50 to 150 keV/μm). It indicated that the response is not restricted to that of the individual traversed cells but involves the non-traversed cells also. Similar to earlier observations with α-particle-irradiated cell cultures (Gaillard, Pusset et al. 2009), the use of CR-39 nuclear track detector fused to tissue culture dishes has greatly supported the participation of bystander cells in the response to low fluence iron ion irradiation (1000 MeV/u). The modulation of the expression of genes related to cell cycle regulation and/or DNA damage sensing and repair in bystander cells could alter not only their growth characteristics but also their response to endogenous DNA damage.

In addition to the role of gap-junction intercellular communication in mediating HZE-particle-induced bystander effects, this thesis shows the involvement of DNA repair processes. The results with 53BP1 foci formation showed that by 24 h after exposure to 1000 MeV/u $^{56}$Fe ions (Figure 3-2), the excess formation of foci returned to near basal level. This may suggest that the induction of DNA damage in bystander cells is transient and is repairable; however, accumulating data with HZE-particle-irradiated cell cultures show that bystander cells experience genomic instability that manifests in persistent induction of

chromosomal damage in progeny of the bystander cells (Buonanno, de Toledo et al. 2011; Ponnaiya, Suzuki et al. 2011). The latter effect was associated with perturbations in biochemical processes associated with oxidative metabolism (Buonanno, de Toledo et al. 2011; Ponnaiya, Suzuki et al. 2011).

Both junctional communication and DNA repair may be also impacted by cellular partial oxygen tension. Our results show that maintenance and irradiation of cells at lower than ambient oxygen atmosphere attenuates the HZE-particle-induced bystander effect assessed by micronucleus formation and 53BP1 foci induction. The effect was associated with enhanced phosphorylation of ERK1/2 proteins. Cellular $P_{O_2}$ is expected to modulate the cellular redox-environment and may affect long-term effects on oxidative metabolism. It is therefore likely that multiple mechanisms act in concert to mediate the propagation of signaling events from irradiated to non-irradiated cells. The mechanisms may involve, in particular secreted factors that render even cells that are not in direct physical contact in communication with each other (Shao, Stewart et al. 2003; reviewed in Mothersill and Seymour 2004; Shao, Folkard et al. 2008).

Although, the expression of bystander effects has been considered a low dose ionizing radiation phenomenon, in case of cells traversed even by a single HZE particle track, the traversed cell receives a massive dose concentrated in the center of the track where the local dose may reach thousands of Gy while a few microns away it may be close to zero (Cucinotta, Nikjoo et al. 2000). In addition, charged particles undergo nuclear reactions to produce secondary particles (i.e. heavy ion fragments, electrons, photons, protons, neutrons, and $\alpha$ particles) that create their own tracks of molecular damage, and may therefore extend the range of damage beyond that of the primary particle track (Nelson 2003). In this project, FLUKA calculations showed that the dose deposited by secondary particles due to the fragmentation of the 1000 MeV/u $^{56}$Fe, 600 MeV/u $^{28}$Si or 290 MeV/u $^{12}$C HZE primary ions

through the flaskettes do not appreciably contribute to the total dose. Moreover, the fragments are projected in a direction close to incident ions; thus the probability that fragments affect surrounding cell nuclei is low. Only electrons can spread everywhere with some being even perpendicular to the incident beam and thus may affect adjacent cells. However, under different culture conditions, fragmentation products may induce signaling pathways that can enhance or attenuate the induced bystander effects in a manner that depends on the LET of the secondary products (Elmore, Lao et al. 2009).

Together, the studies in this project may contribute to the efforts by NASA, other space agencies around the world, and in particular regulatory organizations to develop risk based radiation exposure guidelines, and may be pertinent to radiotherapy with particulate radiations. Identifying the propagated factors that promote stressful effects in bystander cells would have obvious translational applications; it would increase our understanding of radiation-induced signaling pathways in particular intercellular communication under stress conditions.

# References

Aiginger, H., V. Andersen, et al. (2005). "The FLUKA code: new developments and application to 1 GeV/n iron beams." Adv Space Res **35**(2): 214-222.

Akudugu, J. M. and R. W. Howell (2011). "Flow Cytometry-Assisted Monte Carlo Simulation Predicts Clonogenic Survival of Cell Populations with Lognormal Distributions of Radiopharmaceuticals and Anticancer Drugs." Int J Radiat Biol.

Alexander, A., S. L. Cai, et al. (2010). "ATM signals to TSC2 in the cytoplasm to regulate mTORC1 in response to ROS." Proc Natl Acad Sci U S A **107**(9): 4153-4158.

Alexander, A. and C. L. Walker (2010). "Differential localization of ATM is correlated with activation of distinct downstream signaling pathways." Cell Cycle **9**(18): 3685-3686.

Allen, R. G. and M. Tresini (2000). "Oxidative stress and gene regulation." Free Radic Biol Med **28**(3): 463-499.

Asaithamby, A., N. Uematsu, et al. (2008). "Repair of HZE-particle-induced DNA double-strand breaks in normal human fibroblasts." Radiat Res **169**(4): 437-446.

Aurengo, A., D. Averbeck, et al. (2005). Dose-effect relationships and estimation of the carcinogenic effects of low doses of ionizing radiation, Académie des Sciences & Académie nationale de Médecine.

Autsavapromporn, N., S. M. de Toledo, et al. (2011). "Intercellular Communication Amplifies Stressful Effects in High-Charge, High-Energy (HZE) Particle-Irradiated Human Cells." J Radiat Res (Tokyo) **52**(4): 408-414.

Autsavapromporn, N., S. M. de Toledo, et al. (2011). "The role of gap junction communication and oxidative stress in the propagation of toxic effects among high-dose alpha-particle-irradiated human cells." Radiat Res **175**(3): 347-357.

Averbeck, D. (2009). "Does scientific evidence support a change from the LNT model for low-dose radiation risk extrapolation?" Health Phys **97**(5): 493-504.

Azzam, E. I., S. M. de Toledo, et al. (1992). Radiation-induced radioresistance in a normal human skin fibroblast cell line. Low Dose Irradiation and Biological Defense Mechanisms. T. Suguhara, L. A. Sagan and T. Aoyama. Amsterdam, Elsevier**:** 291–294.

Azzam, E. I., S. M. de Toledo, et al. (1998). "Intercellular communication is involved in the bystander regulation of gene expression in human cells exposed to very low fluences of alpha particles." Radiat Res **150**(5): 497-504.

Azzam, E. I., S. M. de Toledo, et al. (2001). "Direct evidence for the participation of gap junction-mediated intercellular communication in the transmission of damage signals from alpha -particle irradiated to nonirradiated cells." <u>Proc Natl Acad Sci U S A</u> **98**(2): 473-478.

Azzam, E. I., S. M. de Toledo, et al. (2003). "Expression of CONNEXIN43 is highly sensitive to ionizing radiation and other environmental stresses." <u>Cancer Res</u> **63**(21): 7128-7135.

Azzam, E. I., S. M. de Toledo, et al. (2003). "Oxidative metabolism, gap junctions and the ionizing radiation-induced bystander effect." <u>Oncogene</u> **22**(45): 7050-7057.

Azzam, E. I., S. M. de Toledo, et al. (2007). "Mechanisms underlying the expression and propagation of low dose/low fluence ionizing radiation effects." <u>International Journal of Low Radiation</u> **4**(1): 61-68.

Azzam, E. I., S. M. de Toledo, et al. (1996). "Low-dose ionizing radiation decreases the frequency of neoplastic transformation to a level below the spontaneous rate in C3H 10T1/2 cells." <u>Radiat Res</u> **146**(4): 369-373.

Azzam, E. I., S. M. De Toledo, et al. (2002). "Oxidative metabolism modulates signal transduction and micronucleus formation in bystander cells from alpha-particle-irradiated normal human fibroblast cultures." <u>Cancer Res</u> **62**(19): 5436-5442.

Azzam, E. I., J. P. Jay-Gerin, et al. (2011). "Ionizing radiation-induced metabolic oxidative stress and prolonged cell injury." <u>Cancer Letters</u>.

Azzam, E. I., G. P. Raaphorst, et al. (1994). "Radiation-induced adaptive response for protection against micronucleus formation and neoplastic transformation in C3H 10T1/2 mouse embryo cells." <u>Radiat Res</u> **138**(1 Suppl): S28-31.

Bakkenist, C. J. and M. B. Kastan (2003). "DNA damage activates ATM through intermolecular autophosphorylation and dimer dissociation." <u>Nature</u> **421**(6922): 499-506.

Bao-An, B., Z. Feng-Shou, et al. (2008). "Fragmentation Cross Sections of 12 C on Different Targets at Beam Energies from 50 to 100MeV/Nucleon." <u>Chinese Physics Letters</u> **25**(2): 451.

Barcellos-Hoff, M. H. and A. L. Brooks (2001). "Extracellular signaling through the microenvironment: a hypothesis relating carcinogenesis, bystander effects, and genomic instability." <u>Radiat Res</u> **156**(5 Pt 2): 618-627.

Battistoni, G., F. Broggi, et al. (2011). "Applications of FLUKA Monte Carlo code for nuclear and accelerator physics." <u>Nucl.Instrum.Meth.</u> **B269**: 2850-2856.

Battistoni, G., S. Muraro, et al. (2007). <u>The FLUKA code: Description and benchmarking</u>. Proceedings of the Hadronic Shower Simulation Workshop 2006, Fermilab AIP Conference Proceeding.

Bedford, J. S. and J. B. Mitchell (1974). "The effect of hypoxia on the growth and radiation response of mammalian cells in culture." <u>Br J Radiol</u> **47**(562): 687-696.

Bedner, P., H. Niessen, et al. (2006). "Selective permeability of different connexin channels to the second messenger cyclic AMP." <u>J Biol Chem</u> **281**(10): 6673-6681.

Beilajew, A. F. (2001). Fundamentals of the Monte Carlo method for neutral and charged particle transport, Ann Arbor Michigan.

BEIR VI (1998). Health Effects of Exposure to Radon (BEIR VI). Washington, DC, National Research Council, Committee on the Biological Effects of Ionizing Radiations.

BEIR VII (2006). Health risks from exposure to low levels of ionizing radiation: BEIR VII Phase 2. Washington, DC, Committee to assess health risks from exposure to low levels of ionizing radiation, Nuclear and radiation studies board, National research council of the national academies.

Belyakov, O. V., M. Folkard, et al. (2006). "Bystander-induced differentiation: a major response to targeted irradiation of a urothelial explant model." <u>Mutat Res</u> **597**(1-2): 43-49.

Belyakov, O. V., A. M. Malcolmson, et al. (2001). "Direct evidence for a bystander effect of ionizing radiation in primary human fibroblasts." <u>Br J Cancer</u> **84**(5): 674-679.

Belyakov, O. V., S. A. Mitchell, et al. (2005). "Biological effects in unirradiated human tissue induced by radiation damage up to 1 mm away." <u>Proc Natl Acad Sci U S A</u> **102**(40): 14203-14208.

Belyakov, O. V., K. M. Prise, et al. (1999). "Delayed lethality, apoptosis and micronucleus formation in human fibroblasts irradiated with X-rays or alpha-particles." <u>Int J Radiat Biol</u> **75**(8): 985-993.

Bensimon, A., R. Aebersold, et al. (2011). "Beyond ATM: the protein kinase landscape of the DNA damage response." <u>FEBS Lett</u> **585**(11): 1625-1639.

Berlett, B. S. and E. R. Stadtman (1997). "Protein oxidation in aging, disease, and oxidative stress." <u>J Biol Chem</u> **272**(33): 20313-20316.

Bertram, J. S. (2004). "Induction of connexin 43 by carotenoids: functional consequences." <u>Arch Biochem Biophys</u> **430**(1): 120-126.

Bishayee, A., H. Z. Hill, et al. (2001). "Free radical-initiated and gap junction-mediated bystander effect due to nonuniform distribution of incorporated radioactivity in a three-dimensional tissue culture model." Radiat Res **155**(2): 335-344.

Bishayee, A., D. V. Rao, et al. (1999). "Evidence for pronounced bystander effects caused by nonuniform distributions of radioactivity using a novel three-dimensional tissue culture model." Radiat Res **152**(1): 88-97.

Blakely, E. A. and A. Kronenberg (1998). "Heavy-ion radiobiology: new approaches to delineate mechanisms underlying enhanced biological effectiveness." Radiat Res **150**(5 Suppl): S126-145.

Bosi, A., A. Micheli, et al. (1991). "Effect of pH shifts on radiosensitivity of human lymphocytes irradiated in the G2 stage." Mutat Res **250**(1-2): 325-329.

Bottollier-Depois, J. F., Q. Chau, et al. (2000). "Assessing exposure to cosmic radiation during long-haul flights." Radiat Res **153**(5 Pt 1): 526-532.

Braunn, B. (2010). La fragmentation du 12C à 95 MeV par nucléon appliquée au domaine de la hadronthérapie - Etude expérimentale et simulations sur cibles épaisses de PMMA - . Doctorate, UNIVERSITE de CAEN.

Brenner, D. J., R. Doll, et al. (2003). "Cancer risks attributable to low doses of ionizing radiation: assessing what we really know." Proc Natl Acad Sci U S A **100**(24): 13761-13766.

Brown, J. M. and A. J. Giaccia (1994). "Tumour hypoxia: the picture has changed in the 1990s." Int J Radiat Biol **65**(1): 95-102.

Browne. E and R. B. Firestone (1986). Table of radioactive isotopes, Wiley, 1986.

Bunn, H. F. and R. O. Poyton (1996). "Oxygen sensing and molecular adaptation to hypoxia." Physiol Rev **76**(3): 839-885.

Buonanno, M., S. M. de Toledo, et al. (2011). "Increased frequency of spontaneous neoplastic transformation in progeny of bystander cells from cultures exposed to densely ionizing radiation." PLoS One **6**(6): e21540.

Buonanno, M., S. M. de Toledo, et al. (2011). "Long-term consequences of radiation-induced bystander effects depend on radiation quality and dose and correlate with oxidative stress." Radiat Res **175**(4): 405-415.

Burdak-Rothkamm, S., K. Rothkamm, et al. (2008). "ATM acts downstream of ATR in the DNA damage response signaling of bystander cells." Cancer Res **68**(17): 7059-7065.

Burdak-Rothkamm, S., S. C. Short, et al. (2007). "ATR-dependent radiation-induced gamma H2AX foci in bystander primary human astrocytes and glioma cells." Oncogene 26(7): 993-1002.

Burma, S., B. P. Chen, et al. (2001). "ATM phosphorylates histone H2AX in response to DNA double-strand breaks." J Biol Chem 276(45): 42462-42467.

Cai, L. and S. Z. Liu (1990). "Induction of cytogenetic adaptive response of somatic and germ cells in vivo and in vitro by low-dose X-irradiation." Int J Radiat Biol 58(1): 187-194.

Campa, A., F. Ballarini, et al. (2005). "DNA DSB induced in human cells by charged particles and gamma rays: experimental results and theoretical approaches." Int J Radiat Biol 81(11): 841-854.

Canman, C. E., D. S. Lim, et al. (1998). "Activation of the ATM kinase by ionizing radiation and phosphorylation of p53." Science 281(5383): 1677-1679.

Catelinois, O., A. Rogel, et al. (2006). "Lung cancer attributable to indoor radon exposure in france: impact of the risk models and uncertainty analysis." Environ Health Perspect 114(9): 1361-1366.

Cember, H. (1996). Introduction to health physics. New York, McGraw-Hill, Health Professions Division.

Chandel, N. S., E. Maltepe, et al. (1998). "Mitochondrial reactive oxygen species trigger hypoxia-induced transcription." Proc Natl Acad Sci U S A 95(20): 11715-11720.

Chandel, N. S. and P. T. Schumacker (2000). "Cellular oxygen sensing by mitochondria: old questions, new insight." J Appl Physiol 88(5): 1880-1889.

Chang, W. P. and J. B. Little (1991). "Delayed reproductive death in X-irradiated Chinese hamster ovary cells." Int J Radiat Biol 60(3): 483-496.

Charlton, D. E. and R. Sephton (1991). "A relationship between microdosimetric spectra and cell survival for high-LET irradiation." Int J Radiat Biol 59(2): 447-457.

Clanton, T. L. (2007). "Hypoxia-induced reactive oxygen species formation in skeletal muscle." J Appl Physiol 102(6): 2379-2388.

Clapham, D. E. (1995). "Intracellular calcium. Replenishing the stores." Nature 375(6533): 634-635.

Cornforth, M. N., M. E. Schillaci, et al. (1989). "Radiobiology of ultrasoft X rays. III. Normal human fibroblasts and the significance of terminal track structure in cell inactivation." Radiat Res 119(3): 511-522.

Cucinotta, F. A. and L. J. Chappell (2010). "Non-targeted effects and the dose response for heavy ion tumor induction." Mutat Res.

Cucinotta, F. A. and M. Durante (2006). "Cancer risk from exposure to galactic cosmic rays: implications for space exploration by human beings." Lancet Oncol **7**(5): 431-435.

Cucinotta, F. A., R. Katz, et al. (1998). "Radial distribution of electron spectra from high-energy ions." Radiat Environ Biophys **37**(4): 259-265.

Cucinotta, F. A., H. Nikjoo, et al. (1998). "The effects of delta rays on the number of particle-track traversals per cell in laboratory and space exposures." Radiat Res **150**(1): 115-119.

Cucinotta, F. A., H. Nikjoo, et al. (2000). "Model for radial dependence of frequency distributions for energy imparted in nanometer volumes from HZE particles." Radiat Res **153**(4): 459-468.

Davidson, J. S., I. M. Baumgarten, et al. (1986). "Reversible inhibition of intercellular junctional communication by glycyrrhetinic acid." Biochem Biophys Res Commun **134**(1): 29-36.

de Toledo, S. M., N. Asaad, et al. (2006). "Adaptive responses to low-dose/low-dose-rate gamma rays in normal human fibroblasts: the role of growth architecture and oxidative metabolism." Radiat Res **166**(6): 849-857.

de Toledo, S. M. and E. I. Azzam (2006). "Adaptive and Bystander Responses in Human and Rodent Cell Cultures Exposed to Low Level Ionizing Radiation: The Impact of Linear Energy Transfer." Dose-Response **4**: 291-301.

de Toledo, S. M., E. I. Azzam, et al. (2000). "ATM complexes with HDM2 and promotes its rapid phosphorylation in a p53-independent manner in normal and tumor human cells exposed to ionizing radiation." Oncogene **19**(54): 6185-6193.

de Toledo, S. M., M. Buonanno, et al. (2011). "The impact of adaptive and non-targeted effects in the biological responses to low dose/low fluence ionizing radiation: the modulating effect of linear energy transfer." Health Phys **100**(3): 290-292.

Deshpande, A., E. H. Goodwin, et al. (1996). "Alpha-particle-induced sister chromatid exchange in normal human lung fibroblasts: evidence for an extranuclear target." Radiat Res **145**(3): 260-267.

Droge, W. (2002). "Free radicals in the physiological control of cell function." Physiol Rev **82**(1): 47-95.

Durante, M. and A. Kronenberg (2005). "Ground-based research with heavy ions for space radiation protection." Adv Space Res **35**(2): 180-184.

Durante, M. and J. S. Loeffler (2010). "Charged particles in radiation oncology." <u>Nat Rev Clin Oncol</u> **7**(1): 37-43.

el-Deiry, W. S., T. Tokino, et al. (1993). "WAF1, a potential mediator of p53 tumor suppression." <u>Cell</u> **75**(4): 817-825.

el-Fouly, M. H., J. E. Trosko, et al. (1987). "Scrape-loading and dye transfer. A rapid and simple technique to study gap junctional intercellular communication." <u>Exp Cell Res</u> **168**(2): 422-430.

Elmore, E., X. Y. Lao, et al. (2009). "Threshold-type dose response for induction of neoplastic transformation by 1 GeV/nucleon iron ions." <u>Radiat Res</u> **171**(6): 764-770.

Eustermann, S., H. Videler, et al. (2011). "The DNA-binding domain of human PARP-1 interacts with DNA single-strand breaks as a monomer through its second zinc finger." <u>Journal of molecular biology</u> **407**(1): 149-170.

Facoetti, A., F. Ballarini, et al. (2006). "Gamma ray-induced bystander effect in tumour glioblastoma cells: a specific study on cell survival, cytokine release and cytokine receptors." <u>Radiat Prot Dosimetry</u> **122**(1-4): 271-274.

Fenech, M. (2008). The Micronucleus Assay Determination of Chromosomal Level DNA Damage
Environmental Genomics. C. C. Martin, Humana Press. **410:** 185-216.

Fenech, M. and A. A. Morley (1986). "Cytokinesis-block micronucleus method in human lymphocytes: effect of in vivo ageing and low dose X-irradiation." <u>Mutat Res</u> **161**(2): 193-198.

Ferradini, C. (1979). "Actions chimiques des radiations ionisantes." <u>J. Phys. Chim.</u> **76**: 636-644.

Ferrari, A., P. R. Sala, et al. (2005). FLUKA: A Multi-Particle Transport Code. Geneva, CERN European organization for nuclear research.

Fick, J., F. G. Barker, 2nd, et al. (1995). "The extent of heterocellular communication mediated by gap junctions is predictive of bystander tumor cytotoxicity in vitro." <u>Proc Natl Acad Sci U S A</u> **92**(24): 11071-11075.

Finkel, T. and N. J. Holbrook (2000). "Oxidants, oxidative stress and the biology of ageing." <u>Nature</u> **408**(6809): 239-247.

Fournier, C., P. Barberet, et al. (2009). "No evidence for DNA and early cytogenetic damage in bystander cells after heavy-ion microirradiation at two facilities." <u>Radiat Res</u> **171**(5): 530-540.

Fournier, C., D. Becker, et al. (2007). "Cell cycle-related bystander responses are not increased with LET after heavy-ion irradiation." Radiat Res **167**(2): 194-206.

Freeman, S. M., C. N. Abboud, et al. (1993). "The "bystander effect": tumor regression when a fraction of the tumor mass is genetically modified." Cancer Res **53**(21): 5274-5283.

Gaillard, S., D. Pusset, et al. (2009). "Propagation distance of the alpha-particle-induced bystander effect: the role of nuclear traversal and gap junction communication." Radiat Res **171**(5): 513-520.

Gerashchenko, B. I. and R. W. Howell (2005). "Bystander cell proliferation is modulated by the number of adjacent cells that were exposed to ionizing radiation." Cytometry A **66**(1): 62-70.

Goldberg, G. S., A. P. Moreno, et al. (2002). "Gap junctions between cells expressing connexin 43 or 32 show inverse permselectivity to adenosine and ATP." J Biol Chem **277**(39): 36725-36730.

Goodenough, D. A. and D. L. Paul (2009). "Gap junctions." Cold Spring Harb Perspect Biol **1**(1): a002576.

Goodhead, D. T. (1989). "The initial physical damage produced by ionizing radiations." Int J Radiat Biol **56**(5): 623-634.

Goodhead, D. T. (1994). "Initial events in the cellular effects of ionizing radiations: clustered damage in DNA." Int J Radiat Biol **65**(1): 7-17.

Goodhead, D. T., J. Thacker, et al. (1993). "Weiss Lecture. Effects of radiations of different qualities on cells: molecular mechanisms of damage and repair." Int J Radiat Biol **63**(5): 543-556.

Graeber, T. G., J. F. Peterson, et al. (1994). "Hypoxia induces accumulation of p53 protein, but activation of a G1-phase checkpoint by low-oxygen conditions is independent of p53 status." Mol Cell Biol **14**(9): 6264-6277.

Gray, L. H., A. D. Conger, et al. (1953). "The concentration of oxygen dissolved in tissues at the time of irradiation as a factor in radiotherapy." Br J Radiol **26**(312): 638-648.

Groesser, T., B. Cooper, et al. (2008). "Lack of bystander effects from high-LET radiation for early cytogenetic end points." Radiat Res **170**(6): 794-802.

Guidarelli, A., F. Cattabeni, et al. (1997). "Alternative mechanisms for hydroperoxide-induced DNA single strand breakage." Free Radic Res **26**(6): 537-547.

Guo, Z., R. Deshpande, et al. (2010). "ATM activation in the presence of oxidative stress." Cell Cycle **9**(24): 4805-4811.

Guo, Z., S. Kozlov, et al. (2010). "ATM activation by oxidative stress." Science **330**(6003): 517-521.

Haddad, J. J. (2002). "Science review: Redox and oxygen-sensitive transcription factors in the regulation of oxidant-mediated lung injury: role for nuclear factor-kappaB." Crit Care **6**(6): 481-490.

Hall, E. J. and A. J. Giaccia (2006). Radiobiology for the radiologist. Philadelphia, Lippincott Williams & Wilkins.

Hall, E. J. and A. J. Giaccia (2012). Radiobiology for the radiologist. Philadelphia, Wolters Kluwer Health/Lippincott Williams & Wilkins.

Hall, E. J. and T. K. Hei (2003). "Genomic instability and bystander effects induced by high-LET radiation." Oncogene **22**(45): 7034-7042.

Halliwell, B. (1996). "Free radicals, proteins and DNA: oxidative damage versus redox regulation." Biochem Soc Trans **24**(4): 1023-1027.

Hamada, N., M. Maeda, et al. (2011). "Signaling pathways underpinning the manifestations of ionizing radiation-induced bystander effects." Curr Mol Pharmacol **4**(2): 79-95.

Hamada, N., M. Ni, et al. (2008). "Temporally distinct response of irradiated normal human fibroblasts and their bystander cells to energetic heavy ions." Mutation Research/Fundamental and Molecular Mechanisms of Mutagenesis **639**(1-2): 35-44.

Hamm, R. N., J. E. Turner, et al. (1985). "Calculation of heavy-ion tracks in liquid water." Radiat Res Suppl **8**: S20-26.

Hanot, M., J. Hoarau, et al. (2009). "Membrane-dependent bystander effect contributes to amplification of the response to alpha-particle irradiation in targeted and nontargeted cells." Int J Radiat Oncol Biol Phys **75**(4): 1247-1253.

Harada, K., T. Nonaka, et al. (2009). "Heavy-ion-induced bystander killing of human lung cancer cells: role of gap junctional intercellular communication." Cancer Sci **100**(4): 684-688.

Harris, A. L. (2001). "Emerging issues of connexin channels: biophysics fills the gap." Q Rev Biophys **34**(3): 325-472.

Harris, A. L. (2007). "Connexin channel permeability to cytoplasmic molecules." Prog Biophys Mol Biol **94**(1-2): 120-143.

Hei, T. K., H. Zhou, et al. (2008). "Mechanism of radiation-induced bystander effects: a unifying model." J Pharm Pharmacol **60**(8): 943-950.

Held, K. D. (2009). "Effects of low fluences of radiations found in space on cellular systems." Int J Radiat Biol **85**(5): 379-390.

Herrlich, P. and F. D. Bohmer (2000). "Redox regulation of signal transduction in mammalian cells." Biochem Pharmacol **59**(1): 35-41.

Huang, S. H., M. Xiong, et al. (2008). "PJ34, an inhibitor of PARP-1, suppresses cell growth and enhances the suppressive effects of cisplatin in liver cancer cells." Oncol Rep **20**(3): 567-572.

Huber, A., P. Bai, et al. (2004). "PARP-1, PARP-2 and ATM in the DNA damage response: functional synergy in mouse development." DNA Repair (Amst) **3**(8-9): 1103-1108.

Huo, Q. and Q. Yang (2011). "P53-binding protein 1: a new player for tumorigenesis and a new target for breast cancer treatment." Med Hypotheses **77**(3): 359-363.

ICRP, Ed. (1991). Recommendations of the International Commission on Radiological Protection. , Elsevier Science Pub Co.

Ikushima, T. (1987). "Chromosomal responses to ionizing radiation reminiscent of an adaptive response in cultured Chinese hamster cells." Mutat Res **180**(2): 215-221.

Iliakis, G. (1991). "The role of DNA double strand breaks in ionizing radiation-induced killing of eukaryotic cells." Bioessays **13**(12): 641-648.

Iyer, R. and B. E. Lehnert (2000). "Effects of ionizing radiation in targeted and nontargeted cells." Arch Biochem Biophys **376**(1): 14-25.

Iyer, R., B. E. Lehnert, et al. (2000). "Factors underlying the cell growth-related bystander responses to alpha particles." Cancer Res **60**(5): 1290-1298.

Jain, M. R., M. Li, et al. (2011). "In vivo space radiation-induced non-targeted responses: late effects on molecular signaling in mitochondria." Curr Mol Pharmacol **4**(2): 106-114.

Jay-Gerin, J. P. and C. Ferradini (2000). "Are there protective enzymatic pathways to regulate high local nitric oxide (NO) concentrations in cells under stress conditions?" Biochimie **82**(2): 161-166.

Jensen, R. and P. M. Glazer (2004). "Cell-interdependent cisplatin killing by Ku/DNA-dependent protein kinase signaling transduced through gap junctions." Proc Natl Acad Sci U S A **101**(16): 6134-6139.

Jermann, M. (2010). Hadron Therapy Patient Statistics, Particle Therapy Co-Operative Group (PTCOG).

Joubert, A. and N. Foray (2007). "[Intrinsic radiosensitivity and DNA double-strand breaks in human cells]." <u>Cancer Radiother</u> **11**(3): 129-142.

Kadhim, M. A., D. A. Macdonald, et al. (1992). "Transmission of chromosomal instability after plutonium alpha-particle irradiation." <u>Nature</u> **355**(6362): 738-740.

Kalvelyte, A., A. Imbrasaite, et al. (2003). "Connexins and apoptotic transformation." <u>Biochem Pharmacol</u> **66**(8): 1661-1672.

Kashino, G., K. Suzuki, et al. (2007). "Radiation induced bystander signals are independent of DNA damage and DNA repair capacity of the irradiated cells." <u>Mutat Res</u> **619**(1-2): 134-138.

Katz, R. and F. A. Cucinotta (1999). "Tracks to therapy." <u>Radiat Meas</u> **31**(1-6): 379-388.

Kelsey, K. T., A. Memisoglu, et al. (1991). "Human lymphocytes exposed to low doses of X-rays are less susceptible to radiation-induced mutagenesis." <u>Mutat Res</u> **263**(4): 197-201.

Khan, M. A., R. P. Hill, et al. (1998). "Partial volume rat lung irradiation: an evaluation of early DNA damage." <u>Int J Radiat Oncol Biol Phys</u> **40**(2): 467-476.

Khandogina, E. K., G. R. Mutovin, et al. (1991). "Adaptive response in irradiated human lymphocytes: radiobiological and genetical aspects." <u>Mutat Res</u> **251**(2): 181-186.

Kim, J. A., Y. S. Kang, et al. (1998). "Role of Ca2+ influx in the tert-butyl hydroperoxide-induced apoptosis of HepG2 human hepatoblastoma cells." <u>Exp Mol Med</u> **30**(3): 137-144.

Koturbash, I., K. Kutanzi, et al. (2008). "Radiation-induced bystander effects in vivo are sex specific." <u>Mutat Res</u> **642**(1-2): 28-36.

Kronenberg, A. and J. B. Little (1989). "Locus specificity for mutation induction in human cells exposed to accelerated heavy ions." <u>Int J Radiat Biol</u> **55**(6): 913-924.

Kumar, N. M. and N. B. Gilula (1996). "The gap junction communication channel." <u>Cell</u> **84**(3): 381-388.

Kuriyama, S., T. Nakatani, et al. (1995). "Bystander effect caused by suicide gene expression indicates the feasibility of gene therapy for hepatocellular carcinoma." <u>Hepatology</u> **22**(6): 1838-1846.

LaVerne, J. A. (2000). "Track effects of heavy ions in liquid water." <u>Radiat Res</u> **153**(5 Pt 1): 487-496.

LaVerne, J. A. (2004). Radiation chemical effects of heavy ions. <u>Charged Particle and Photon Interactions with Matter. Chemical, Physicochemical, and Biological Consequences with Applications</u>. A. Mozumder and Y. Hatano. New York, Marcel Dekker**:** 403-429.

Lavin, M. F. (2008). "Ataxia-telangiectasia: from a rare disorder to a paradigm for cell signalling and cancer." <u>Nat Rev Mol Cell Biol</u> **9**(10): 759-769.

Lehnert, B. E., E. H. Goodwin, et al. (1997). "Extracellular factor(s) following exposure to alpha particles can cause sister chromatid exchanges in normal human cells." <u>Cancer Res</u> **57**(11): 2164-2171.

Lehnert, S. (2008). <u>Biomolecular action of ionizing radiation</u>. New York, Taylor & Francis.

Lempiainen, H. and T. D. Halazonetis (2009). "Emerging common themes in regulation of PIKKs and PI3Ks." <u>EMBO J</u> **28**(20): 3067-3073.

Little, J. B. (1968). "Delayed initiation of DNA synthesis in irradiated human diploid cells." <u>Nature</u> **218**(5146): 1064-1065.

Little, J. B. (2000). "Radiation carcinogenesis." <u>Carcinogenesis</u> **21**(3): 397-404.

Little, J. B. (2003). "Genomic instability and bystander effects: a historical perspective." <u>Oncogene</u> **22**(45): 6978-6987.

Little, J. B. (2006). "Lauriston S. Taylor lecture: nontargeted effects of radiation: implications for low-dose exposures." <u>Health Phys</u> **91**(5): 416-426.

Loeb, K. R. and L. A. Loeb (1999). "Genetic instability and the mutator phenotype. Studies in ulcerative colitis." <u>The American journal of pathology</u> **154**(6): 1621-1626.

Loeb, L. A. (2001). "A mutator phenotype in cancer." <u>Cancer research</u> **61**(8): 3230-3239.

Lopez-Barneo, J., J. R. Lopez-Lopez, et al. (1988). "Chemotransduction in the carotid body: K+ current modulated by PO2 in type I chemoreceptor cells." <u>Science</u> **241**(4865): 580-582.

Lorimore, S. A., P. J. Coates, et al. (2003). "Radiation-induced genomic instability and bystander effects: inter-related nontargeted effects of exposure to ionizing radiation." <u>Oncogene</u> **22**(45): 7058-7069.

Lyng, F. M., C. B. Seymour, et al. (2001). "Oxidative stress in cells exposed to low levels of ionizing radiation." <u>Biochem Soc Trans</u> **29**(Pt 2): 350-353.

Lyng, F. M., C. B. Seymour, et al. (2002). "Early events in the apoptotic cascade initiated in cells treated with medium from the progeny of irradiated cells." Radiat Prot Dosimetry **99**(1-4): 169-172.

Madison, D. L., D. Stauffer, et al. (2011). "The PARP inhibitor PJ34 causes a PARP1-independent, p21 dependent mitotic arrest." DNA Repair (Amst) **10**(10): 1003-1013.

Magee, J. L. and A. Chatterjee (1980). "Radiation chemistry of heavy-particle tracks. 1. Gene¬ral considerations." J. Phys. Chem. **84**: 3529-3536.

Malanga, M. and F. R. Althaus (2005). "The role of poly(ADP-ribose) in the DNA damage signaling network." Biochem Cell Biol **83**(3): 354-364.

Matsumoto, H., N. Hamada, et al. (2007). "Vanguards of paradigm shift in radiation biology: radiation-induced adaptive and bystander responses." J Radiat Res (Tokyo) **48**(2): 97-106.

Matsumoto, H., S. Hayashi, et al. (2001). "Induction of radioresistance by a nitric oxide-mediated bystander effect." Radiat Res **155**(3): 387-396.

Meesungnoen, J., M. Benrahmoune, et al. (2001). "Monte Carlo calculation of the primary radical and molecular yields of liquid water radiolysis in the linear energy transfer range 0.3-6.5 keV/micrometer: application to 137Cs gamma rays." Radiat Res **155**(2): 269-278.

Meesungnoen, J. and J. P. Jay-Gerin (2011). Radiation chemistry of liquid water with heavy ions: Monte Carlo simulation studies. Charged Particle and Photon Interactions with Matter. Recent Advances, Applications, and Interfaces. Y. Hatano, Y. Katsumura and A. Mozumder. Boca Raton, FL, Taylor and Francis**:** 355-400.

Meesungnoen, J., J. P. Jay-Gerin, et al. (2002). "Low-energy electron penetration range in liquid water." Radiat Res **158**(5): 657-660.

Mehta, P. P. (2007). "Introduction: a tribute to cell-to-cell channels." J Membr Biol **217**(1-3): 5-12.

Meplan, C., M. J. Richard, et al. (2000). "Redox signalling and transition metals in the control of the p53 pathway." Biochem Pharmacol **59**(1): 25-33.

Mesnil, M., C. Piccoli, et al. (1996). "Bystander killing of cancer cells by herpes simplex virus thymidine kinase gene is mediated by connexins." Proc Natl Acad Sci U S A **93**(5): 1831-1835.

Metting, N. F., H. H. Rossi, et al. (1988). "Microdosimetry near the trajectory of high-energy heavy ions." Radiat Res **116**(2): 183-195.

Mitchel, R. E., J. S. Jackson, et al. (1999). "The adaptive response modifies latency for radiation-induced myeloid leukemia in CBA/H mice." Radiat Res **152**(3): 273-279.

Morgan, W. F. (2003). "Is there a common mechanism underlying genomic instability, bystander effects and other nontargeted effects of exposure to ionizing radiation?" Oncogene **22**(45): 7094-7099.

Mothersill, C. and C. Seymour (1997). "Medium from irradiated human epithelial cells but not human fibroblasts reduces the clonogenic survival of unirradiated cells." Int J Radiat Biol **71**(4): 421-427.

Mothersill, C. and C. B. Seymour (1998). "Cell-cell contact during gamma irradiation is not required to induce a bystander effect in normal human keratinocytes: evidence for release during irradiation of a signal controlling survival into the medium." Radiat Res **149**(3): 256-262.

Mothersill, C. and C. B. Seymour (2004). "Radiation-induced bystander effects--implications for cancer." Nat Rev Cancer **4**(2): 158-164.

Mothersill, C., R. W. Smith, et al. (2007). "Characterization of a radiation-induced stress response communicated in vivo between zebrafish." Environ Sci Technol **41**(9): 3382-3387.

Mozumder, A. and J. L. Magee (1966). "Model of tracks of ionizing radiations for radical reaction mechanisms." Radiat Res **28**(2): 203-214.

Muroya, Y., I. Plante, et al. (2006). "High-LET ion radiolysis of water: visualization of the formation and evolution of ion tracks and relevance to the radiation-induced bystander effect." Radiat Res **165**(4): 485-491.

Nagasawa, H., A. Cremesti, et al. (2002). "Involvement of membrane signaling in the bystander effect in irradiated cells." Cancer Res **62**(9): 2531-2534.

Nagasawa, H. and J. B. Little (1992). "Induction of sister chromatid exchanges by extremely low doses of alpha-particles." Cancer Res **52**(22): 6394-6396.

Nagasawa, H. and J. B. Little (1999). "Unexpected sensitivity to the induction of mutations by very low doses of alpha-particle radiation: evidence for a bystander effect." Radiat Res **152**(5): 552-557.

Nagasawa, H., Y. Peng, et al. (2005). "Role of homologous recombination in the alpha-particle-induced bystander effect for sister chromatid exchanges and chromosomal aberrations." Radiat Res **164**(2): 141-147.

Naidu, R., Y. C. Har, et al. (2011). "Genetic polymorphisms of TP53-binding protein 1 (TP53BP1) gene and association with breast cancer risk." APMIS **119**(7): 460-467.

Narayanan, P. K., E. H. Goodwin, et al. (1997). "Alpha particles initiate biological production of superoxide anions and hydrogen peroxide in human cells." Cancer Res **57**(18): 3963-3971.

Narayanan, P. K., K. E. LaRue, et al. (1999). "Alpha particles induce the production of interleukin-8 by human cells." Radiat Res **152**(1): 57-63.

NASA (1998). Strategic Program Plan for Space Radiation Health Research. Washington, DC, NASA.

National Research Council (U.S.). Committee on the Evaluation of Radiation Shielding for Space Exploration. and ebrary Inc. (2008). Managing space radiation risk in the new era of space exploration. Washington, D.C., National Academies Press.

Naus, C. C. and D. W. Laird (2010). "Implications and challenges of connexin connections to cancer." Nat Rev Cancer **10**(6): 435-441.

NCRP (2011). Potential impact of individual genetic susceptibility and previous radiation exposure on radiation risk for astronauts. Bethesda, Md., National Council on Radiation Protection and Measurements.

Nelson, G. A. (2003). "Fundamental space radiobiology." Gravit Space Biol Bull **16**(2): 29-36.

Neti, P. V., S. M. de Toledo, et al. (2004). "A multi-port low-fluence alpha-particle irradiator: fabrication, testing and benchmark radiobiological studies." Radiat Res **161**(6): 732-738.

Niessen, H., H. Harz, et al. (2000). "Selective permeability of different connexin channels to the second messenger inositol 1,4,5-trisphosphate." J Cell Sci **113 ( Pt 8)**: 1365-1372.

O'Neill, P. and P. Wardman (2009). "Radiation chemistry comes before radiation biology." Int J Radiat Biol **85**(1): 9-25.

Okayasu, R., K. Suetomi, et al. (2000). "A deficiency in DNA repair and DNA-PKcs expression in the radiosensitive BALB/c mouse." Cancer Res **60**(16): 4342-4345.

Olivieri, G., J. Bodycote, et al. (1984). "Adaptive response of human lymphocytes to low concentrations of radioactive thymidine." Science **223**(4636): 594-597.

Ottolenghi, A., M. Merzagora, et al. (1997). "DNA complex lesions induced by protons and alpha-particles: track structure characteristics determining linear energy transfer and particle type dependence." Radiat Environ Biophys **36**(2): 97-103.

Parsons, W. B., Jr., C. H. Watkins, et al. (1954). "Changes in sternal marrow following roentgen-ray therapy to the spleen in chronic granulocytic leukemia." Cancer **7**(1): 179-189.

Peralta-Leal, A., J. M. Rodriguez-Vargas, et al. (2009). "PARP inhibitors: new partners in the therapy of cancer and inflammatory diseases." Free Radic Biol Med **47**(1): 13-26.

Petkau, A. (1987). "Role of superoxide dismutase in modification of radiation injury." Br J Cancer Suppl **8**: 87-95.

Plante, I. and F. A. Cucinotta (2008). "Ionization and excitation cross sections for the interaction of HZE particles in liquid water and application to Monte Carlo simulation of radiation tracks." New Journal of Physics **10**.

Plante, I. and F. A. Cucinotta (2009). "Cross sections for the interactions of 1 eV–100 MeV electrons in liquid water and application to Monte-Carlo simulation of HZE radiation tracks." New Journal of Physics **11**(6): 063047.

Platzman, R. (1958). The physical and chemical basis of mechanisms in radiation biology. Radiation Biology and Medicine. Selected Reviews in the Life Sciences. E. W. Claus. Reading, MA, Addison-Wesley**:** 15-72.

Podgorsak, E. B. (2005). Radiation oncology physics: a handbook for teachers and students, International Atomic Energy Agency.

Ponnaiya, B., M. Suzuki, et al. (2011). "Detection of Chromosomal Instability in Bystander Cells after Si490-Ion Irradiation." Radiat Res.

Ponomarev, A. L. and F. A. Cucinotta (2006). "Nuclear fragmentation and the number of particle tracks in tissue." Radiat Prot Dosimetry **122**(1-4): 354-361.

Preston, R. J. (2003). "The LNT model is the best we can do--today." J Radiol Prot **23**(3): 263-268.

Price, B. D. and S. K. Calderwood (1992). "Gadd45 and Gadd153 messenger RNA levels are increased during hypoxia and after exposure of cells to agents which elevate the levels of the glucose-regulated proteins." Cancer Res **52**(13): 3814-3817.

Rappold, I., K. Iwabuchi, et al. (2001). "Tumor suppressor p53 binding protein 1 (53BP1) is involved in DNA damage-signaling pathways." J Cell Biol **153**(3): 613-620.

Redpath, J. L., D. Liang, et al. (2001). "The shape of the dose-response curve for radiation-induced neoplastic transformation in vitro: evidence for an adaptive response against neoplastic transformation at low doses of low-LET radiation." Radiat Res **156**(6): 700-707.

Rigaud, O., D. Papadopoulo, et al. (1993). "Decreased deletion mutation in radioadapted human lymphoblasts." Radiat Res **133**(1): 94-101.

Romero-Calvo, I., B. Ocon, et al. (2010). "Reversible Ponceau staining as a loading control alternative to actin in Western blots." Anal Biochem **401**(2): 318-320.

Rossi, H. H. (1959). "Specification of radiation quality." Radiat Res **10**(5): 522-531.

Rueckert, R. R. and G. C. Mueller (1960). "Effect of oxygen tension on HeLa cell growth." Cancer Res **20**: 944-949.

Russo, A., J. Mitchell, et al. (1985). "Determinants of radiosensitivity." Semin Oncol **12**(3): 332-349.

Ryan, L. A., R. W. Smith, et al. (2008). "Dilution of irradiated cell conditioned medium and the bystander effect." Radiat Res **169**(2): 188-196.

Samson, L. and J. Cairns (1977). "A new pathway for DNA repair in Escherichia coli." Nature **267**(5608): 281-283.

Sanderson, B. J. and A. A. Morley (1986). "Exposure of human lymphocytes to ionizing radiation reduces mutagenesis by subsequent ionizing radiation." Mutat Res **164**(6): 347-351.

Sandstrom, B. E. (1991). "Induction and rejoining of DNA single-strand breaks in relation to cellular growth in human cells exposed to three hydroperoxides at 0 degrees C and 37 degrees C." Free Radic Res Commun **15**(2): 79-89.

Schubert, A. L., W. Schubert, et al. (2002). "Connexin family members target to lipid raft domains and interact with caveolin-1." Biochemistry **41**(18): 5754-5764.

Schultz, L. B., N. H. Chehab, et al. (2000). "p53 binding protein 1 (53BP1) is an early participant in the cellular response to DNA double-strand breaks." J Cell Biol **151**(7): 1381-1390.

Schulze-Osthoff, K., M. Baur, et al. (1997). Reactive oxygen intermediates as primary signals and second messengers in the activation of transcription factors. Oxidative stress and signal transduction. H. J. Forman and E. Cadenas. New York, Chapman & Hall**:** 239-259.

Semenza, G. L. (2000). "HIF-1: mediator of physiological and pathophysiological responses to hypoxia." J Appl Physiol **88**(4): 1474-1480.

Seymour, C. B., C. Mothersill, et al. (1986). "High yields of lethal mutations in somatic mammalian cells that survive ionizing radiation." Int J Radiat Biol Relat Stud Phys Chem Med **50**(1): 167-179.

Shadley, J. D. (1994). "Chromosomal adaptive response in human lymphocytes." Radiat Res **138**(1 Suppl): S9-12.

Shadley, J. D., V. Afzal, et al. (1987). "Characterization of the adaptive response to ionizing radiation induced by low doses of X rays to human lymphocytes." Radiat Res **111**(3): 511-517.

Shadley, J. D. and J. K. Wiencke (1989). "Induction of the adaptive response by X-rays is dependent on radiation intensity." Int J Radiat Biol **56**(1): 107-118.

Shadley, J. D. and S. Wolff (1987). "Very low doses of X-rays can cause human lymphocytes to become less susceptible to ionizing radiation." Mutagenesis **2**(2): 95-96.

Shao, C., M. Folkard, et al. (2004). "Targeted cytoplasmic irradiation induces bystander responses." Proc Natl Acad Sci U S A **101**(37): 13495-13500.

Shao, C., M. Folkard, et al. (2008). "Role of TGF-beta1 and nitric oxide in the bystander response of irradiated glioma cells." Oncogene **27**(4): 434-440.

Shao, C., Y. Furusawa, et al. (2006). "Involvement of gap junctional intercellular communication in the bystander effect induced by broad-beam or microbeam heavy ions." Nuclear Instruments and Methods in Physics Research Section B: Beam Interactions with Materials and Atoms **251**(1): 177-181.

Shao, C., Y. Furusawa, et al. (2003). "Bystander effect induced by counted high-LET particles in confluent human fibroblasts: a mechanistic study." FASEB J **17**(11): 1422-1427.

Shao, C., K. M. Prise, et al. (2008). "Signaling factors for irradiated glioma cells induced bystander responses in fibroblasts." Mutat Res **638**(1-2): 139-145.

Shao, C., V. Stewart, et al. (2003). "Nitric oxide-mediated signaling in the bystander response of individually targeted glioma cells." Cancer Res **63**(23): 8437-8442.

Shareef, M. M., N. Cui, et al. (2007). "Role of tumor necrosis factor-alpha and TRAIL in high-dose radiation-induced bystander signaling in lung adenocarcinoma." Cancer Res **67**(24): 11811-11820.

Shiloh, Y. (2003). "ATM and related protein kinases: safeguarding genome integrity." Nat Rev Cancer **3**(3): 155-168.

Siliciano, J. D., C. E. Canman, et al. (1997). "DNA damage induces phosphorylation of the amino terminus of p53." Genes & development **11**(24): 3471-3481.

Sowa, M. B., W. Goetz, et al. (2010). "Lack of evidence for low-LET radiation induced bystander response in normal human fibroblasts and colon carcinoma cells." Int J Radiat Biol **86**(2): 102-113.

Spitz, D. R., E. I. Azzam, et al. (2004). "Metabolic oxidation/reduction reactions and cellular responses to ionizing radiation: a unifying concept in stress response biology." Cancer Metastasis Rev **23**(3-4): 311-322.

Stadtman, E. R. (1993). "Oxidation of free amino acids and amino acid residues in proteins by radiolysis and by metal-catalyzed reactions." Annu Rev Biochem **62**: 797-821.

Stewart, W. W. (1978). "Functional connections between cells as revealed by dye-coupling with a highly fluorescent naphthalimide tracer." Cell **14**(3): 741-759.

Sutherland, B. M., P. V. Bennett, et al. (2000). "Clustered DNA damages induced in isolated DNA and in human cells by low doses of ionizing radiation." Proc Natl Acad Sci U S A **97**(1): 103-108.

Tartier, L., S. Gilchrist, et al. (2007). "Cytoplasmic irradiation induces mitochondrial-dependent 53BP1 protein relocalization in irradiated and bystander cells." Cancer Res **67**(12): 5872-5879.

Terasima, T. and L. J. Tolmach (1961). "Changes in x-ray sensitivity of HeLa cells during the division cycle." Nature **190**: 1210-1211.

Tobias, C. A., E. A. Blakely, et al. (1982). "Molecular and cellular radiobiology of heavy ions." Int J Radiat Oncol Biol Phys **8**(12): 2109-2120.

Torres, M. (2003). "Mitogen-activated protein kinase pathways in redox signaling." Front Biosci **8**: d369-391.

Trosko, J. E. and C. C. Chang (2001). "Mechanism of up-regulated gap junctional intercellular communication during chemoprevention and chemotherapy of cancer." Mutat Res **480-481**: 219-229.

Trosko, J. E., C. C. Chang, et al. (1990). "Modulation of intercellular communication during radiation and chemical carcinogenesis." Radiat Res **123**(3): 241-251.

Tsoupas, N., A. Ahrens, et al. (2007). Uniform beam distributions at the target of the NSRL beam transfer line. 22nd Particle Accelerator Conference (PAC). Albuquerque, New Mexico.

Tubiana, M. and A. Aurengo (2005). La relation dose-effet et l'estimation des effets cancérogènes des faibles doses de rayonnements ionisants, Rapport commun de l'Académie Nationale de Médecine et de l'Académie des Sciences.

Tubiana, M., L. E. Feinendegen, et al. (2009). "The linear no-threshold relationship is inconsistent with radiation biologic and experimental data." Radiology **251**(1): 13-22.

Ugenskiene, R., K. Prise, et al. (2009). "Dose response and kinetics of foci disappearance following exposure to high- and low-LET ionizing radiation." Int J Radiat Biol **85**(10): 872-882.

UNSCEAR (2000). Sources and effects of ionizing radiation: Sources. Report to the General Assembly. New York, United Nations Scientific Committee on the Effects of Atomic Radiation **REPORT Vol. I**.

Valerie, K., A. Yacoub, et al. (2007). "Radiation-induced cell signaling: inside-out and outside-in." Mol Cancer Ther **6**(3): 789-801.

van Dillen, I. J., N. H. Mulder, et al. (2002). "Influence of the bystander effect on HSV-tk/GCV gene therapy. A review." Curr Gene Ther **2**(3): 307-322.

Vance, M. M. and L. M. Wiley (1999). "Gap junction intercellular communication mediates the competitive cell proliferation disadvantage of irradiated mouse preimplantation embryos in aggregation chimeras." Radiat Res **152**(5): 544-551.

Veenstra, R. D. (1996). "Size and selectivity of gap junction channels formed from different connexins." J Bioenerg Biomembr **28**(4): 327-337.

Venkatachalam, P., S. M. de Toledo, et al. (2008). "Regulation of normal cell cycle progression by flavin-containing oxidases." Oncogene **27**(1): 20-31.

Voulgaridou, G. P., I. Anestopoulos, et al. (2011). "DNA damage induced by endogenous aldehydes: current state of knowledge." Mutat Res **711**(1-2): 13-27.

Ward, J. F. (1994). "The complexity of DNA damage: relevance to biological consequences." Int J Radiat Biol **66**(5): 427-432.

Watt, D. E. (1996). Quantities for dosimetry of ionizing radiations in liquid water. London ; Bristol, PA, Taylor & Francis.

Weinberg, R. A. (2007). The biology of cancer. New York, Garland Science.

Wilson, P. F., P. B. Nham, et al. (2010). "Inter-individual variation in DNA double-strand break repair in human fibroblasts before and after exposure to low doses of ionizing radiation." Mutat Res **683**(1-2): 91-97.

Wilson, R. E. and R. M. Sutherland (1989). "Enhanced synthesis of specific proteins, RNA, and DNA caused by hypoxia and reoxygenation." Int J Radiat Oncol Biol Phys **16**(4): 957-961.

Wion, D., M. Dematteis, et al. (2008). "Pression partielle en oxygène et culture de cellules cancéreuses." Medecine/Sciences **24**(12): 1093-1095.

Wolff, S. (1998). "The adaptive response in radiobiology: evolving insights and implications." Environ Health Perspect **106 Suppl 1**: 277-283.

Wolvetang, E. J., M. F. Pera, et al. (2007). "Gap junction mediated transport of shRNA between human embryonic stem cells." Biochemical and Biophysical Research Communications **363**(3): 610-615.

Woodard, H. Q. and D. R. White (1986). "The composition of body tissues." Br J Radiol **59**(708): 1209-1218.

Woodbine, L., H. Brunton, et al. (2011). "Endogenously induced DNA double strand breaks arise in heterochromatic DNA regions and require ataxia telangiectasia mutated and Artemis for their repair." Nucleic Acids Res **39**(16): 6986-6997.

Wu, L. J., G. Randers-Pehrson, et al. (1999). "Targeted cytoplasmic irradiation with alpha particles induces mutations in mammalian cells." Proc Natl Acad Sci U S A **96**(9): 4959-4964.

Wygoda, M. R., M. R. Wilson, et al. (1997). "Protection of herpes simplex virus thymidine kinase-transduced cells from ganciclovir-mediated cytotoxicity by bystander cells: the Good Samaritan effect." Cancer Res **57**(9): 1699-1703.

Yang, H., V. Anzenberg, et al. (2007). "Effects of heavy ions and energetic protons on normal human fibroblasts." Radiats Biol Radioecol **47**(3): 302-306.

Yang, H., V. Anzenberg, et al. (2007). "The time dependence of bystander responses induced by iron-ion radiation in normal human skin fibroblasts." Radiat Res **168**(3): 292-298.

Yang, H., N. Asaad, et al. (2005). "Medium-mediated intercellular communication is involved in bystander responses of X-ray-irradiated normal human fibroblasts." Oncogene **24**(12): 2096-2103.

Zeitlin, C., A. Fukumura, et al. (2006). Fragmentation cross sections of 28Si at beam energies from 290A MeV to 1200A MeV.

Zhou, H., V. N. Ivanov, et al. (2005). "Mechanism of radiation-induced bystander effect: role of the cyclooxygenase-2 signaling pathway." Proc Natl Acad Sci U S A **102**(41): 14641-14646.

Zhou, H., G. Randers-Pehrson, et al. (2000). "Induction of a bystander mutagenic effect of alpha particles in mammalian cells." Proc Natl Acad Sci U S A **97**(5): 2099-2104.

Zhou, H., M. Suzuki, et al. (2002). "Effects of irradiated medium with or without cells on bystander cell responses." <u>Mutat Res</u> **499**(2): 135-141.

Zhou, H., M. Suzuki, et al. (2001). "Radiation risk to low fluences of alpha particles may be greater than we thought." <u>Proc Natl Acad Sci U S A</u> **98**(25): 14410-14415.

Ziegler, J. F. "Particle interaction with matter, SRIM (Stopping and Range of Ions in Matter) " <u>http://www.srim.org/</u>.

Zirkle, R. E. and W. Bloom (1953). "Irradiation of parts of individual cells." <u>Science</u> **117**(3045): 487-493.